CCFE
CULHAM CENTRE FOR FUSION ENERGY

UK Atomic Energy Authority

UKAEA-CCFE-PR(23)185

Yao Ren, Robert Skilton

A Review of Pipe Cutting, Welding, and NDT Technologies for Use in Fusion Devices

A Review of Pipe Cutting, Welding, and NDT Technologies for Use in Fusion Devices

Yao Ren, Robert Skilton

This is a preprint of a paper submitted for publication in
Fusion Engineering and Design

A Review of Pipe Cutting, Welding, and NDT Technologies for Use in Fusion Devices

Yao Ren, Robert Skilton

UK Atomic Energy Authority, Culham Science Centre, Abingdon, OX14 3DB, Oxfordshire, UK

Abstract

Piping systems that transport coolant and breeding fluid are naturally an essential part of the support system of the nuclear fusion power plants. Following a campaign of operations, the reactor is required to be shut down and maintained entirely. Pipes connected to the reactor components are to be cut, re-welded or re-joined, and inspected non-destructively, using Remote Handling (RH) equipment and tools. This paper outlines the candidate structural materials and their weldability in fusion reactor pipework, reviews investigated welding, cutting and NDE technologies, developed tooling prototypes and processes for remote pipe maintenance, summarizes the existing and emerging technological challenges that to be tackled as the results of the environmental constraints, material selections and the requirement of engineering designs, and highlights the exploration of the unknown and areas to further research in the future. The urge of developing tools with RH compatibility and high tolerance to environmental constraints, such as in-pipe robotics with miniaturized end effectors and sensors for operations and inspections under hazardous condition, is also addressed.

Keywords: Fusion, maintenance, robotics, welding, cutting, NDE

1 Introduction

Nuclear Fusion powers the sun and stars as hydrogen atoms fuse together to form helium, and matter is converted into energy. It offers an almost inexhaustible source of energy and could be one of a very few sustainable options to replace fossil fuels for future generations [1], [2]. However, fusion is difficult to achieve on earth as the fusion fuel - different isotopes of hydrogen – must be heated to extreme temperatures, and must be kept steady under intense pressure, thus dense enough and confined for long enough to allow the nuclei to fuse. Currently, the most readily feasible reaction is between the nuclei of the two heavy forms (isotopes) of hydrogen – deuterium (D) and tritium (T): $d + t \rightarrow 4He\ (3.5\ MeV) + n\ (14.1\ MeV)$, where the reaction must take place in a magnetic confinement fusion machine such as tokamak. While the Joint European Torus (JET) [3] and International Thermonuclear Experimental Reactor (ITER) [4]'tokamaks' are both experimental fusion devices, European demonstration fusion power plant (DEMO) [5], [6] is the near-term reactor design aims to produce electricity and operation with a closed fuel-cycle. Deuterium can be sourced naturally from seawater, whereas tritium has limited quantity therefore it must be bred in a fusion system from lithium.

In a fusion reactor, D-T reaction generated high-energy neutrons will bombard the lithium in the breeding zone of the blanket to produce tritium and back fuel the reactor. In the meantime, blanket will be heated up as a result of the absorption of the kinetic energy from the neutrons and the coolant flowing through it will collect the heat for energy conversion. This presents the major design trade-offs between tritium self-sufficiency and power generation. Intense neutron bombardment rapidly degrades the plasma facing components, which are the cassettes that from the divertor and breeding blanket modules, requiring frequent replacement of significant amounts of reactor hardware. Although fusion energy promises zero fuel waste, there will be component waste. Hence using the right materials in a nuclear fusion reactor will have an environmental dimension and is also going to come down to striking the right balance between the performance and cost.

Neutron flux also activates isotopes within the components and surrounding structures, causing materials to become radioactive, requires specifically developed technologies that with safe and reliable remote maintainability, as no direct human intervention is possible inside the vacuum vessel and other peripheral areas of the reactor [7]. The design complexity of the fusion power plant includes the large numbers of coils, the in-vessel components, ex-vessel components such as heating and diagnostics plugs, the Neutral Beam injectors and hot cell, and tokamak building, etc., all lead to the result of a compromise between operational and maintenance needs.

In-vessel maintenance of fusion devices (both experimental and future power plants) involves the regular replacement of plasma-facing components with cooling and fuelling interfaces, and therefore requires the cutting, joining, and qualification of pipe interfaces. These are the locations under higher radioactivity but lower accessibility and visibility. Tooling is required to be deployed through entry ports and carry out maintenance tasks in space-constrained environment. In addition, joints at such locations are subjected to elevated temperature and

cyclic thermal loads, leak tightness is key to protect the tokamak vacuum during operation [8]. It is also a critical aspect of fusion remote maintenance as it is anticipated that these activities constitute a large proportion of the overall maintenance duration[8]–[10], thus driving cost of electricity and therefore commercial viability, as well as being critical to plant operation and therefore requiring extremely high reliability. Many challenges remain outstanding in this field including relating to compatibility with the fusion environment, space and access constraints, and remote deployability.

The Joint European Torus (JET) was the first operating fusion device where Remote Handling (RH) techniques[11], [12] and associated tools have been developed and tested including on thin-walled cooling pipes [12]–[14]. Extensive experience such as orbital TIG (vacuum quality welding), MIG (structural quality welding) and orbital cutting that developed at JET, has been shared to inspire the development of Remote Maintenance (RM) strategies for ITER, DEMO and other future fusion machines around the world. The main operations carried out for cooling pipe maintenance during reactor shutdown include cutting and re-welding and then followed up with a series non-destructive inspection of the new joints. Activities must be conducted remotely, under different level of hazardous environmental impact, using bespoke tools. Depending on the design and maintenance requirements, pipes may be cut and post machined to meet the requirement of being ready to re-weld. To produce a compliant weld, a robust welding process procedure is required to be developed taking into the consideration all of, but not limited to, the material metallurgy, welding technique, joint design, pre- and post- process treatment, as well as service environmental constraints. Non-destructive inspection is mandatory, aiming to ensure the welds meet required levels of quality and are fit for purpose.

This review outlines the candidate structural materials and their weldability in fusion reactor pipework, summarizes the joining, cutting and inspection technologies have been investigated for pipe maintenance, as well as some of the tooling prototypes that have been developed, and identifies potential non-destructive evaluation (NDE) technologies worthy of exploration in the future.

2 Structural materials and their challenges

2.1 Development of candidate materials

Service pipes are an important part of the support system of a fusion reactor. Pipework associated with cooling functions are subjected to high temperature thus thermal degradations, high neutron energies and fluxes and strong magnetic fields inside the tokamak [15]. Service pipes may be made of structural materials such as stainless steels, Reduced-activation ferritic/martensitic (RAFM) steels or maybe even oxide dispersion strengthened (ODS) steels, depending on the design criteria for specific fusion operating environment, i.e., temperature, pressure, radiation doses, corrosive coolants, and stress conditions, etc., in various wall thickness and diameters. Selected pipe materials must meet the requirements of physical and mechanical properties, radiation resistance and coolant compatibility, for maintaining the structural integrity during reactor operation. RAFM steels are the most promising structural materials owning to their technology maturity such as qualified fabrication routes, welding technology and industrial experience [16].

The concept of low-activation material was introduced into the international fusion programs from mid-1980s in attempt to alleviate the generation of radioactive isotopes in the materials when exposed to the neutron environment of fusion. Since steels are limited by the decay of radioactive products from transmutation of atoms, reduced-activation materials were proposed based on the high Cr heat resistance steel - Grade 91 steel which is also known as modified 9Cr-1Mo steel or P91 steel with ferritic/martensitic (FM) [17], [18]

P91 steel was developed in late 1970s as a great candidate for steam generator components such as tubing, piping and headers. Due to its advantageous physical and mechanical properties, i.e., high strength, high resistance to corrosion, high thermal conductivity, low thermal expansion, and low oxidation rate [19], in the early 1980s, USA introduced tubing P91 steels to replace 300 series austenitic steels in steam boilers [20], [21]. Thereafter the material became the primary candidates for components for advanced fossil fuel power plants mid-1980s [22], [23]. It was also suggested that FM steels have higher swelling resistance in radiation environment as well as better thermal stress resistance and are thus less prone to thermal fatigue compared to austenitic stainless steels in fusion reactors [24]. FM steels were not considered as structural material candidates for nuclear reactors initially because of ferromagnetism, it was later confirmed the complication of the interaction with the magnetic fields could be managed by reactor design [25], [26].

Reduced-activation ferritic/martensitic steels (RAFM) with 7-9% Cr content were developed by replacing the common alloying elements molybdenum in conventional Cr-Mo steel with tungsten and/or vanadium and niobium

with tantalum. RAFM steels such as EUROFER (Fe–8.5Cr–1.0W–0.05Mn–0.25V–0.08Ta–.05N–0.005B–0.10C) and F82H (Fe–7.5Cr–2.0W–0.2V–0.04Ta–0.10C) have been considered as the primary candidates of fusion structural materials due to their good resistance to neutron irradiation [27]. A nominal 9wt percentage (wt%) Cr content was proved to be able to minimise the radiation-induced ductile-brittle transition temperature (DBTT) shift [28]. However, F82H and EUROFER97 exhibit lower creep compared to P91 steel, due to the low density of MX-type (M=Nb/Ta/V, X=C/N) precipitates which could not provide sufficient grain boundary pinning. Other concerns of baseline RAFM steels and proposed approaches are also summarised in early issue [29].

One of the approaches, claimed to have higher risk, as well as being time consuming and costly, but potentially with higher payoff, is to use powder metallurgy technique to manufacture high strength oxide dispersion strengthened (ODS) alloys, also named as nanostructured ferritic alloys (NFA) [29]. The processes includes the following steps: mechanically alloying followed by either by hot isothermal pressing (HIP) or hot extrusion and thermal-mechanical treatment [30]–[32].By adding in large amount of oxide nanoclusters to pin the sub-micrometre ferritic grains in the alloys, material exhibits superior creep resistance at high temperature. Besides, the oxide nanoclusters also act as trapping site for irradiation produced defects and helium atoms thus to provide superior radiation resistance compared to conventional RAFM steels [33]. A selection of 17 ODS steels and 6 traditional FM steels were summarised with their element compositions in Figure 1 [34].

	Material composition (wt.%)					
Alloy	**Cr**	**Al**	**Y_2O_3**	**C**	**W**	**Ti**
ODS steels						
MA956	18–21.7	4.5–5.8	0.5	0.018–0.06	–	0.32–0.4
MA957	13.7–14	–	0.5	<0.03	–	0.9–0.98
PM2000	19.2–20	5.5–5.7	0.5	0.01–0.013	–	<0.5
PM1000	20	0.3	0.6	0.05	–	0.5
12YWT	12	–	0.25	0.05	0.8	0.4
14YWT	14	–	0.25	0.05	0.6	0.3
9Cr-ODS	8.6–9.0	–	0.36	0.13–0.14	1.95–2	0.21
12Cr-ODS	12.0	–	0.24	0.024	2.01	0.3
K1	18.3	<0.01	0.368	0.05	0.29	0.28
K2	13.6	4.12	0.381	0.04	1.65	0.28
K3	16	4.59	0.368	0.08	1.82	0.28
K4	18.9	4.61	0.368	0.09	1.83	0.28
K5	22.0	4.55	0.356	0.1	1.8	0.27
K6	19.0	4.6	0.368	0.1	1.85	0.28
EUROFER97-ODS	9.1	–	0.3	–	1	–
J27	14	–	0.3	–	1	0.3
EFPL-E	14	–	0.3	–	2	0.3
FM steels						
F82H	7.5–8	–	–	0.09–0.093	1.96–2	<0.004
JLF-1	8.9–9.0	<0.003	–	0.097–0.1	1.97–1.99	<0.001
EUROFER97	8.8–9.0	–	–	0.12	1.15	–
HT-9	11.6	0.01	–	0.2	–	–
T91	9	0.02	–	0.1	0.4	0.01
EP-823	11.7	–	–	0.16	0.58	–

All alloys shown have a remaining balance of Fe

Figure 1 Comparison of ODS and non-ODS steels used in high temperature energy applications [34]

EUROFR97 is considered primary structural material for fusion reactor components, such as European ITER test blanket modules, the EU-DEMO breeding blankets and diverter cassette [35]–[38]. EUROFER97 is presently limited by a drop in mechanical strength at approximate 550 °C, which in comparison, ODS RAFM could be used for structural applications in fusion power reactors up to about 650 °C and the nano structured ODS RAFM are expected up to about 750 °C [39].

Conventional FM and RAFM steels also show poor thermal creep strength after 500°C -550°C, which limit their operating temperature. Future fusion power plants require structure material that can operate rate up to or even beyond 650°C, where ODS steels have a highly superior creep performance [29], [40]–[42]. Improvement of thermal creep property could be achieved by applying thermomechanical treatment with or without chemical modification such as boron addition and optimizing the chemical processing to nucleate a high density of MX particles in advanced alloys such as castable nanostructured alloy [43].

2.2 Irradiation degradation

In a fusion reactor, D-T fusion reaction produces 14MeV high energy neutrons that have sufficient kinetic energy to cause atomic vacancies and self-interstitial atoms over operating time in the structural materials. The main mechanisms of radiation damage which is quantified by dpa (displacements per atom) to structural materials vary at different operating temperatures and radiation levels [44].

For body-centred cubic (bcc) material such as FM materials at low temperature (below 0.3-0.4 T_M, where T_M is

the absolute melting temperature), radiation-induced defects clusters created by displacement cascades act as strong obstacles to dislocation motion which results in radiation hardening accompanied with reductions in material elongation and work hardening capacity and can induce loss of ductility and fracture toughness.

Neutron radiation can lead to large increases in the in the yield stress and DBTT shift with increased doses [33], [45]. EUFROFER97 and F82H tensile samples were prepared at irradiation temperatures between 300 and 335 °C up to 70 dpa and tested at 300 to 350 °C. Materials exhibit increases in yield strength and DBTT shift substantially below 10dpa, and low temperature hardening and embrittlement was indicated to be saturated at 70dpa. For bcc alloy, because radiation hardening emerges at relatively low temperatures and doses as low as 1pda, the radiation hardening and embrittlement phenomenon is often used to define the lower operating temperature in neutron irradiation environments.

At intermediate temperatures up to 0.6 T_M, and radiation does above 1-10 dpa, material performance may be affected by radiation induced segregation and precipitation that can lead to localised corrosion or mechanical degradation such as grain boundary embrittlement [44]. At this temperature regime, irradiation creep can cause dimensional expansion along directions of high stress or specific crystallographic directions. In addition to irradiation creep, void swelling which is caused by vacancy accumulation can also create unacceptable volumetric expansion though it is not anticipated to be significant in ferritic-martensitic steel up to damage levels in excess of 100dpa [46].

Changes in the spectrum of irradiation will change the properties of the materials. Four of the five key radiation degradation mechanisms for structural materials are strongly affected by the He/dpa ratio during irradiation [47], [48]. Investigations suggested hardening in the annealed irradiated F82H was contributed by helium bubbles. Though the barrier strength of helium bubbles with size 1-1.5nm is about 0.1 and small helium bubbles are weak obstacles, significant hardening can still be produced at very high-density 10^{23}-10^{24} m^3 [49].

Along with the neutron irradiation induced materials hardening and embrittlement, He generation rate may shift the BDTT even higher without taking into account attributable helium hardening effect. The maximum allowable operating temperature for a structural material may be defined by high temperature helium embrittlement along with thermal creep and chemical compatibility [46].

Future reactor designs call for structural materials with high radiation resistance, in excess of 100dpa, low residual activation and good compactivity with cooling media. RAFM steels (such as EUROFER97 and F82H), ODS RAFM and RAF steels are the most promising materials. Modifications have been made on EUROFER97 and F82H to improve the material performance [47], [50], for instance, through modified thermodynamical processing, BDTT of the material has been shifted ~100 °C lower than conventionally processed EUROFER97 [50]. Adding small amount of N element in conjunction with appropriate heat treatment has greatly increase creep lifetime of F82H [51].

2.3 Corrosion and tritium permeation

Liquid PbLi alloy is one of the candidate materials for tritium breeding in D-T fusion reactor. Key resulting issues with this to the pipe structural materials include corrosion and tritium permeation. Because of the direct contact, PbLi will cause corrosion of the materials due to the changes in the microstructure, composition and surface morphology [52]. Tests performed on RAFM steels at 550°C showed dissolution of Fe and Cr out of the steel matrix which leads to a corrosion rate at 400 μm/year and high risk of loop blockages by forming precipitates, which are freely transportable in the melt and deposited at positions with low flow rate or special magnetic field condition [53].

Tritium, a radioactive isotope of hydrogen, can migrate from the breeder region into the primary coolant due to the high tritium concentration, high temperature, and the large and thin metallic surface area, and then reach the working areas of the torus hall and the external environment through the steam generator by permeation and/or leaks [54]. To minimise the radiological hazards, the mitigation of tritium migration to the primary and secondary coolant loops can be achieved by applying dedicated coatings, such as anti-permeation barriers and/or natural oxide layers and by treating a certain fraction of the primary coolant flow rate inside the Coolant Purification System.]

The ITER water cooling systems comprise a variety of thin-walled austenitic stainless steel (SS) 316 pipes. Austenitic SSs are susceptible to irradiation assisted stress corrosion cracking (IASCC), which means materials have elevated susceptibility to stress corrosion cracking (SCC) in water-cooled reactors because of the exposure to high-energy neutron irradiation and high-temperature coolant. Although the mechanisms of IASCC are not fully

understood, the current consensus is that IASCC results from a synergistic effect of irradiation damage to the material as discussed above, water environment with possible radiolysis effects, and a stress state. In fusion reactors, tritium can permeate structural materials and affect the cooling water chemistry, forming tritiated water or as dissolved gaseous species in the coolant. SS316 was studied in Japan suggested SCC susceptibility of type 316L SS depends on test temperature and dissolved-hydrogen content, which higher dissolved-hydrogen content in water is necessary to trigger intergranular SCC rather than transgranular SCC at 613 K [55], [56].

Coatings on RAFM steels are one of the solutions to corrosion and tritium permeation issues. Aluminium (Al) based coating was investigated as its potential to work as a corrosion and tritium permeation barrier. To form a layer of dense and adherent Al_2O_3 film on the surface of a component i.e., blanket and cooling pipe, that has complex shape or specific geometry, various coating technologies have been studied. So-gel method fabricated coating failed due to mismatch between the thermal expansions of the sol-gel and substrate [57]. Chemical vapour deposition (CVD) and hot dipping aluminization (HDA) processes were also unsuccessful as coating separated from the substrate in different zones and cracks were observed in welded area of the specimens due to HDA process induced stresses [58]. In addition, inappropriate thermal treatment from HAD process can form Al rich phases in EUROFER97, which are less stable in Pb-17Li. Because of incomplete transformation of the Al scales material is sensitive to corrosive attack [59].

Very promising Al_2O_3 coatings on EUROFER97 disks have been obtained via pulsed layer deposition (PLD) and atomic laser deposition (ALD) techniques. However, the process may still limit the coating repair and fabrication in nuclear environment, which PLD requires the substrate housed in a vacuum chamber and the process involves high-power laser interaction and ALD uses reagents which directly interact onto the surface needs to be covered[54]. Other technologies such Al-based coating fabricated by electrochemical deposition method have shown excellent corrosion resistance to PbLi for RAFM steels [60] and Al-pack cementation to fabricated Al_2O_3 coatings on SS316 tubular specimens achieved a tritium permeation reduction factor of more than 3000 in gas-phase tests [61].

Coatings can also provide electrical insulation and reduce magnetohydrodynamic pressure drop in self-cooled lithium systems are correlated to vanadium-alloy structures [62]. Feasibility of coating with candidate materials of Er_2O_3 and Y_2O_3 have been demonstrated using various physical vapor deposition (PVD) methods, such as electron-beam assisted process [63], arc-source plasma deposition [64]–[66] and RF sputtering[66].

2.4 Welding techniques and weldability

EUROFER has been selected as the structural material for three concepts of DEMO breeding blanket (BB) [67]–[69]. Because of the complexity of the structure design, manufacturing of BB requires sophisticated joining strategy to maintain structural integrity. Considerable effort has been made to demonstrate the feasibility and reliability of different fusion joining technologies, such as tungsten inert gas (TIG) welding, electron beam (EB) welding, laser beam welding (LBW) and hybrid welding to fabricate test blanket module (TBM) mock-ups in the original multi-module segment blanket concept [70]–[72]. Investigated welding parameters and those used for manufacturing TBM mock-ups are listed in Table 1. For welding of EUROFER thicker than 8mm (in TBM structure), TIG welding is not recommended due to the introduction of inacceptable distortion levels. Single pass laser welding, instead, is superior and requires travel speeds greater than 1m/min in order to produce sound joints [70].

Table 1 Summary of the parameters investigated for welding of EUROFER using various welding technologies

Welding technique	EUROFER plate		Key parameter
TIG	8mm		Double sided 6-pass, two root passes and four filling passes
	11mm		130A, at 0.1m/min
	35mm		140-230A 0.1m/min
Laser	4kW	8mm	Double sided two-pass, twin spots
		11mm	0.3m/min
	8kW	8mm	Single pass at 0.5m/min
		11mm	Single pass at 0.35m/min
	10kW	11mm	Single pass at 2.5m/min
EB	40mm		-
	35mm		80mA at 10mm/s
MIG-Laser Hybrid	25mm		Multi-pass (including 14 filling passes for 18mm groove) at 1.3m/min
	35mm		YAG laser 4.5kW + MIG 21A at 1m/min

Although RAFM steels are considered having relatively good weldability, they still suffer property degradation, caused by phase transformation, from fusion processes. This is because the matrix of the steels comprises of tempered martensite with dispersed carbide, which the thermal cycle from welding process destroys such tailored microstructure, especially forming hard phases in the fusion zone due to uncontrolled martensite formation while softening in the HAZ due to over tempering [70], [73]. A laser welded EUROFER joint had hardness over 5GPa (over 500HV) in the fusion zone compared that of 2.75GPa (280HV) in the parent metal [74].

Post weld heat treatment (PWHT) is a common practice for restoring material microstructure and property. One method is to go through re-austenitisation followed by tempering in order to generate fully tempered martensitic structure with a homogeneous hardness profile. This procedure is especially unavoidable for high chromium FM steel, to soften the brittle as-quenched martensite of the weld and to reinforce the HAZ with hardening precipitation. Tempering is a heat treatment technique often conducted after welding process to reduce the excess hardness and relieve residual stresses in the weld. By heating up the weld to a temperature below the critical point and holding for a certain amount of time, welding included martensite will de-compose and carbides precipitate along the grain boundaries, achieving increases to the toughness. It was suggested heat treatment specification and acceptance values for RAFM steels are similar to those of conventional FM steels, at least in the case of the most mature ones, F82H and EUROFER97 [24].

Experimental results have proved that conducting one-step PWHT on F82H at the tempering temperature range coded in ASEM for P91, did improve toughness and inhomogeneity of strength without enhancing the weakness in softened HAZ [75]. Tempering EUROFER97 joints at 750°C allowed recovery of enough metallurgical and mechanical behaviour after 3 hours [70] and effective residual stress relief after 2 hours [74]. Cross sections and hardness tests on TIG and EB welded F82 joints after PWHT are shown in Figure 2. Both welds were subjected to PWHT at 720°C, below standard tempering temperature 750°C. Welding induced hardening still can be observed from the hardness test results. Multi-pass TIG welding had slower welding speed thus lower cooling rate, compared to single pass high speed EB welding, which results in wider joint with less hardened weld metal and obvious HAZ softening [76].

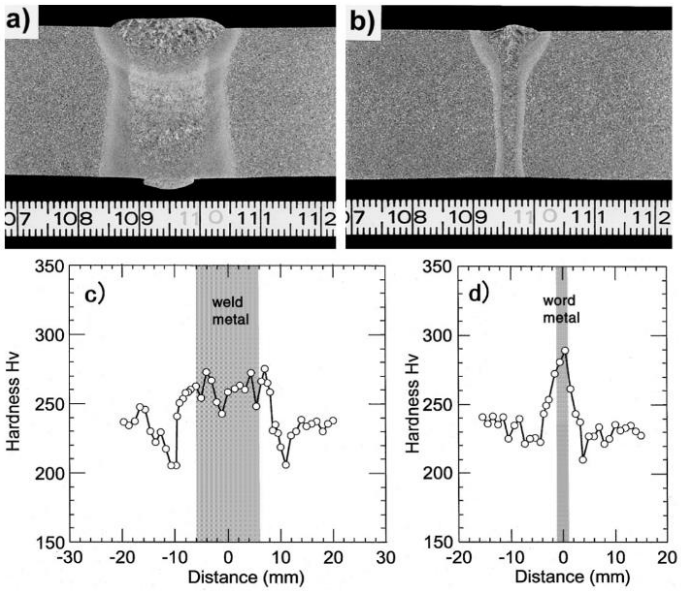

Figure 2 Cross sections of TIG(a) and EB(b) welded F82 plates and hardness distributions on TIG weld joint(c) and EB welded joint(d) [76]

Hybrid laser-arc welding performs arc welding (such as TIG, MIG or MIG welding) and laser welding simultaneously. In hybrid welding process, TIG welding provides higher heat input, ensuring proper high temperature residence time, with the aim of reducing the content of δ-ferrite which is detrimental to the toughness of the fusion zone in the joint, while laser welding guarantees increased penetration with high accuracy at high welding speed [70], [77]. A laser-laser hybrid welding process, where one laser was used in key-hole mode for joining of the metal while the other laser was used in conduction regime to provide additional heating and tailor the thermal history, was developed for RAFM steels [78]. This process is advantageous to keyhole only laser welding as it gives better weld profile, tolerance to fit-up and control of microstructure. It is also superior to standard laser-arc hybrid welding because it enables efficient addition of filler wire with better stability and control, but less spatter [79].

In addition to utilizing appropriate welding technology with optimized welding procedure and parameters, applying PWHT, the development of appropriate filler metal is also of importance to achieve good quality weldments. Though P91 is often used as substitute for welding trials to assist understanding of the weldability of RAFM, filler products for P91 have mainly been optimized for creep resistance in the frame of conventional power applications but not for toughness, which is a great concern in irradiation environments [24]. For RAFM, studies have been carried out on the adjustment of filler metal chemistries taking into account the low–activation requirement [24], [80], [81]. Early studies on optimizing of EUROFER filler wire have showed large tolerance in chemical composition, even wires out the standard selection window, porosity and crack free welds were achieved when butt joining 2mm EUROFER samples [70].

The development of joining methods for ODS FM steels is very challenging. This is mainly because traditional fusion welding methods cause nanoparticle coagulation in the melted region which is leading to a significant loss of strength [29]. Previous research work reported welds produced in simple structural geometries such as plates and pipes have demonstrated good strength and quality using diffusion bonding and friction-stir welding techniques [82]–[86]. Recently publications demonstrated feasibility using spark plasma sintering and pulsed laser beam welding methods to join the ODS steels [87]–[89].

In a nuclear reactor, dissimilar joints may be required in certain structures. Components are potentially manufactured by joining RAFM steel to stainless steel or to ODS steel. Electron beam welding and friction stir welding are candidate technologies defect-free similar and dissimilar welds filler [73], [90]–[92]. However, PWHT is always required, as re-precipitated carbides in the fusion zone soften the weld zone and the formation of the large oxide particles in weld zone results in mechanical property reduction.

3 Pipe welding and tooling development

ITER RH comprises seven core systems. Three of these, the Blanket RH system, Divertor RH system and Neutral Beam RH System involve significant maintenance activities involving cutting, re-welding and inspection of the cooling pipes [7]. All three systems are required to tackle the same environmental challenges such as operating in highly radioactive environment preventing human access, and in confined spaces with complex geometries, heavy components, and access limitations.

Radiation doses in the ITER Neutron Beam (NB) cell will be 10Gy/h during ITER operation and 1Gy/h during shutdown. An early concept on remote handling tools for pipe retraction, alignment, and clamping was reported in 2011 [93]. Three suites of tools, for DN200, DN80/100 and DN25/50 pipes, were identified and required to complete a series of maintenance activities, including bellows compression, pipe alignment, cutting, surface finish, welding, and inspection [94], [95]. An orbital TIG welding tool was developed and successfully demonstrated the feasibility of joining 3mm-walled 316LN stainless steel pipes without wire feed system. The tool comprised a small motor and a gear box to realise low welding speed required during the process. An off the shelf welding head, with electrode holder and gas lens that were commercially available were used for welding process (Figure 3). The experiments confirmed that a simple tool is feasible to achieve reliable operation, in which the cabling to the rotating drive was managed internally to avoid snags and the process did not require any additional active electrode height control system [96].

The ITER divertor, located at the bottom of the vacuum vessel and with a worst-case operational environment up to 300Gy/h, consists of 54 divertor cassettes and each is connected to two horizontal water-cooling pipes. These pipes are 316L Stainless steel in diameter of 71mm and 3mm wall thickness. Replacing the entire divertor requires cutting, rewelding and inspecting the 108 cooling pipes in the space with small clearance and limited viewing remotely [97]. TIG welding trials were performed using a commercial orbital welding tool (ESABA21 PRB33-90) [98]. Test pipes were mounted on a bespoke fixture which allowed controlled misalignment to be introduced six degree of freedom (Figure 4). A novel solution, to the problem of Marangoni effect induced undesired weld profile and gravitational weld sag, was to use 0.7mm filler ring that made of 316L stainless steel with a sulphur content of between 110 to 150 ppm tack-welded to the divertor cassette pipe with 0.4mm vertical offset prior to the welding process.

Significant effort has been made in bore tools systems (BTS) development for remote maintenance of cooling pipes during ITER engineering design phase. Before 1998, ITER diverter pipes were designed in 160mm diameter with straight configuration. A parametric study was carried out on a developed BTS system to assess the cutting, welding and NDT processes [97]. The welding tool head equipped with an internal alignment function that having a pulling capacity of 300kg to clamp the pipe ends and a continuous multi pass TIG weld could be performed automatically.

Figure 5 provides a general view of the divertor test platform (DTP) with the BTS not in alignment.

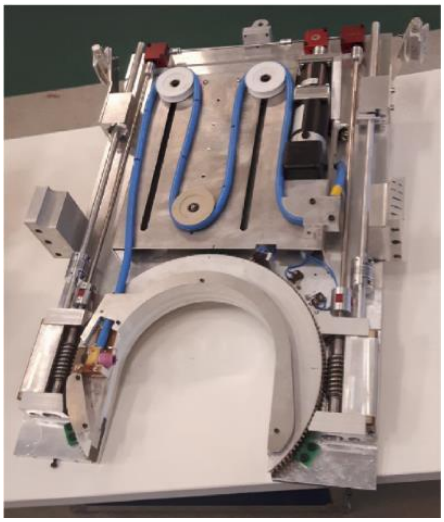

Figure 3 Welding tool developed for ITER Neutral Beam System [96]

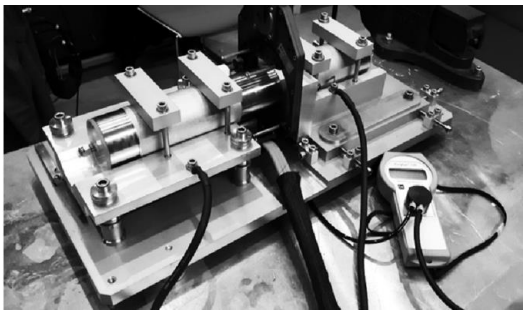

Figure 4 Fixture with controlled misalignment mechanism used for divertor cooling pipe welding trials [98]

The concept of modular bore tool was introduced in 1998, which a prototype was developed and tested to prove the concept of deploying a modular carrier with multiple sub-tooling systems, including milling, swaging, TIG tack-welding, TIG butt-welding, and inspection, to the 4-inch divertor cooling pipes with bending radius of 400mm [97], [99]. The carrier is designed with articulated configuration during the navigation through the pipes then to become a rigid configuration when reaching the working area (Figure 5).

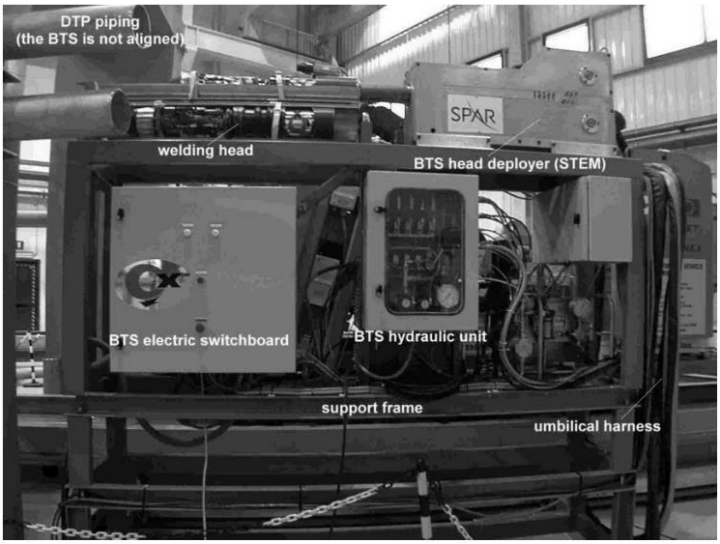

Figure 5 Overview of the 160 mm piping BTS on divertor test platform (DTP) [97]

In 2003, a modular laser BTS, comprised a laser module and pipe clamping and alignment modules (Figure 6), was designed and manufactured [100]. The total length of the carrier in the travelling configuration is approximately 1900mm. Functions of the modules as well as the system rigidification were verified in the operation testing, however, validation tests in a real situation showed significant limits in the design such as reliability of wiring, complexity of tool design, and suitability of using industrial laser connector and fibre.

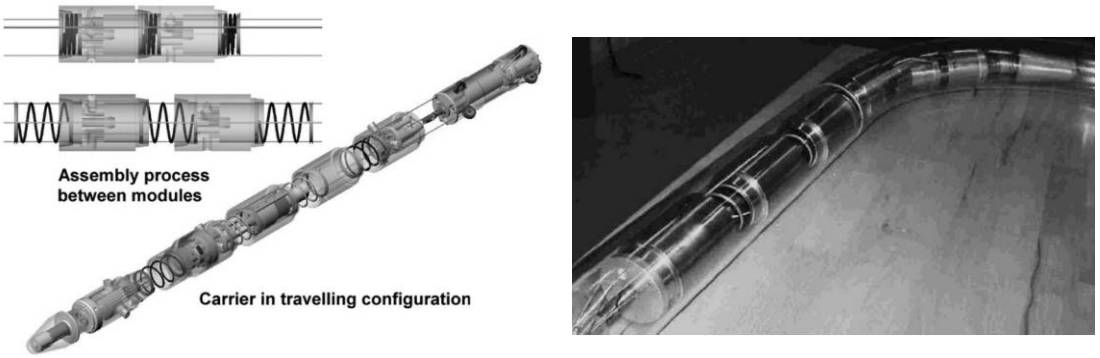

(a)

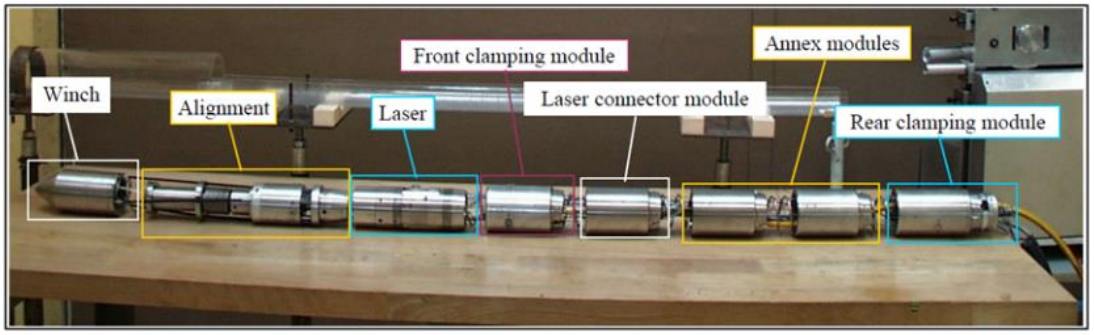

(b)

Figure 6 Modular BTS for ITER divertor cooling pipes (a) modular carrier in traveling configuration and the conical connection between the modules [97], [99]*, (b) modular laser BTS* [100]

Replacement of the ITER first wall requires deploying the tools from the surface side of the first wall and performing welding and cutting of the hydraulic pipes from in-bore. Those pipes, installed inside the blanket module, are made of SS316L with inner diameter of 42.72mm and wall thickness of 2.77m [101]. A comparative study of laser and TIG welding for ITER blanket hydraulic connection was carried out by JAEA (Japan Atomic Energy Agency) to assess various parameters such as allowable misalignment, the lifetime of the tools and amount of spatter and fumes in the welding processes [102]. Schematic drawings of the developed laser and TIG bore welding tools are shown in Figure 7. Table 2 lists the welding test results using both tools. Laser welding demonstrated improved tool life and reduced spatter by applying reduced power density. Much lower heat input from laser welding may be favoured for re-welding of neutron-irradiated helium-containing stainless-steel pipes and to use over long duration [103].

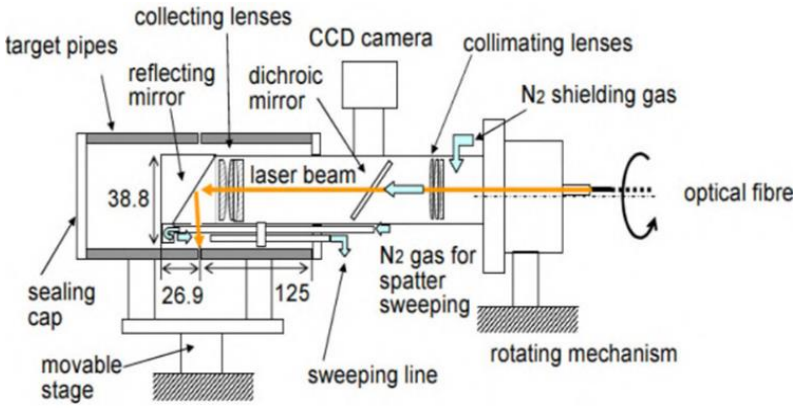

(a)

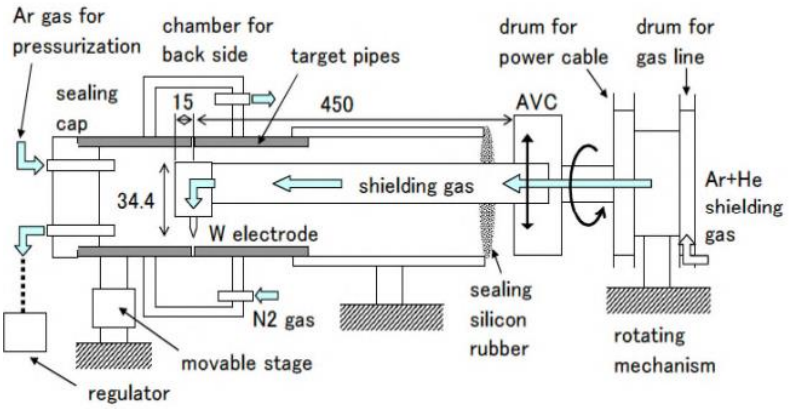

(b)

Figure 7 Schematic drawing of the developed (a)laser bore tool and (b)TIG bore tool for ITER blanket hydraulic pipes [102]

Table 2 Results of comparative study using developed laser and TIG welding tools [102]

	Laser	TIG
Key parameters	Laser power 2.8kW Laser spot diameter 1.2mm Welding speed 1m/min Gas glow rate 80L/min Heat input 1.7kJ/cm	Pulse frequency 1.7Hz Peak width 35% Current (peak/base) 121-130/43-45A Voltage (peak/base) 9.8/9.2V 5.5kJ/cm
Allowable gap and linear misalignment	0.2mm 0.7mm	0.5mm 1mm
Tool lifetime and maintenance	Small power drop from 2.82kW to 2.77kW after 50 times welding	Electrode damage after 10 times welding
Necessity of rescue for tool head	no	Electrode-sticking was avoided by employing DC power, touch start with arc voltage control
Shielding gas	N_2 for inside	Ar and He for inside, N_2 for outside
Production of welding fumes and spatter	large amount of fumes, post cleaning to be considered	Almost no, no post cleaning is needed
Cable handling and transmission	Relative cables/fibres to be separated from In-vessel Transporter cabling system	Tool cables to be developed in addition to the In-vessel Transporter cabling system

Welding trials also proved that TIG welding could offer greater fit-up tolerance in practice. The allowable linear misalignment of 0.7mm for laser welding was larger than the required linear misalignment of 0.2mm that is defined in the ISO and the internal standard. To ensure weldability and avoid handling filler material during remote welding, special fitting configuration of the groove was designed to expand allowable gap [104]. Welding trials were carried out on flat plate and pipes to identify the maximum achievable gap. In butt welding trials, a partially thickened groove design on one side was adopted to obviate the filler wire (Figure 8). By adjusting the welding parameters developed for pipe welding, an allowable initial gap was increased from 0.2mm to 0.7mm when the laser beam impingement point was 1.5mm from the groove edge. The additional metal in the groove was 0.5mm in height and in 2.5mm wide. Similar concept was also adopted in later study on JT-60SA (JT-60 Super Advanced) tokamak pipes to assess the robustness of the in-bore laser tooling for groove gaps, axial and angular misalignment [105], [106].

An in-bore laser welding tool (Figure 9) has been developed for JT-60SA cooling water pipes which connect between the divertor cassette and the vacuum vessel with bellow in the outboard side [105], [106]. During the deployment, the welding head is to be inserted vertically in the SS316L cooling pipes, in 59.8mm diameter and 2.8mm wall thickness, to access the depth of 500mm from the mounting surface on the cassette frame followed by performing circumferential welding. After butt welding of the pipes, an upper plug then to be lap welded to seal the access hole. The original laser welding tool is equipped with a linear motion mechanism and a rotation mechanism. The tool head is approximately 1 meter in length. Three feeding lines of nitrogen gas, two cross jet line and one central shielding line, were designed in order to extend the life spans of mirror and lenses as well as prevent the weld from oxidation [105].

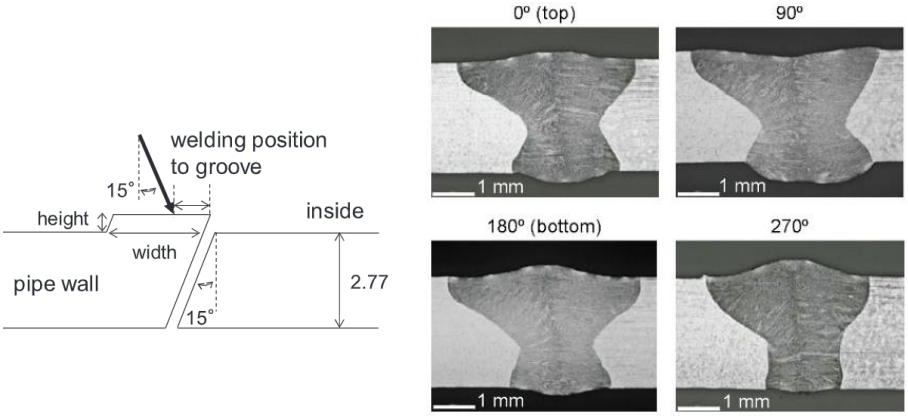

Figure 8 Partially thickened groove design for laser in bore welding with increase allowable gap, (a) plate trials and (b) validation test result on pipes [104]

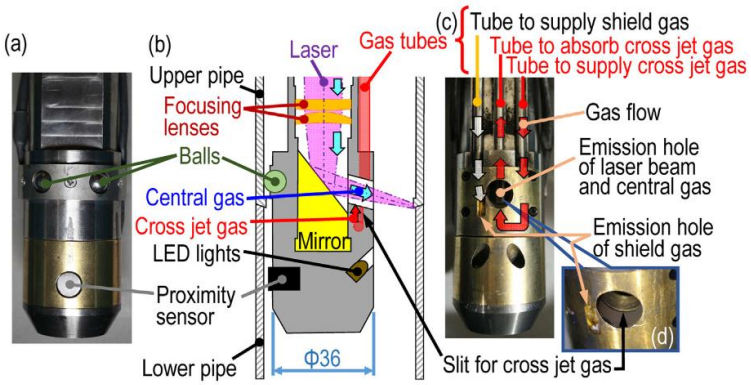

Figure 9 The original design of the laser welding bore tool head and its gas line system for JT-60 SA [106]

However, lifespan of the laser reflecting mirror was short due to the adhesion of fumes and spatters which also blocked the consistent laser energy transmission to the material. This was caused by the interference between the upward-following cross jet and the downward-flowing coaxial laser beam shielding gas. An upgraded tooling design was carried and reported in 2022 [106]. The new tool (Figure 10) is approximately the same dimensions as the original design, but with an added air-driven shutter to protect the two LEDs from the spatters generated by the laser welding process. In addition, size reduction in the laser injection port and the width of the cross-jet gas resulted in significant increase in the gas flow velocity, providing tighter protection for the mirror from spatter and fumes. Furthermore, by changing the direction the cross-jet gas downwards, it stopped colliding with the central shielding gas, leaving a smoother gas flow.

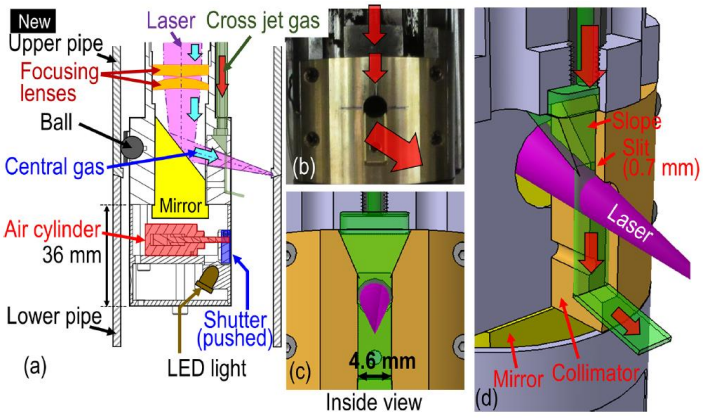

Figure 10 New design of the laser welding bore tool with added shutter and updated cross-jet gas line for JT-60 SA [106]

In DEMO there are 752 remote pipe cuts and reconnections required for the replacement of the blankets and

divertors [107]. In the DEMO Pre-Concept Design Phase, the service joining strategy was focused on the development of the remote in-bore deployment systems [8]. Two separated tool prototypes, a welding tool and a cutting tool were designed to use laser for process operation. The tool consists of two radial clamping sections at the tool ends, an articulation section that allows the tool to travel around a pipe bend of 1500mm, a pneumatic actuator to assist pipe fit-ups and a central rotating section with a miniaturised laser package for process operations [9]. Additional external pipe alignment features shown in Figure 11 will also provide the gross alignment of the pipes to within millimetres to guarantee tight fit-up for welding. In-bore welding trials have been demonstrated on successfully joining 3mm thick P91 and SS316 pipes within 25 seconds using 2.4kW laser power at 0.5m/min travel speed [8], [108].

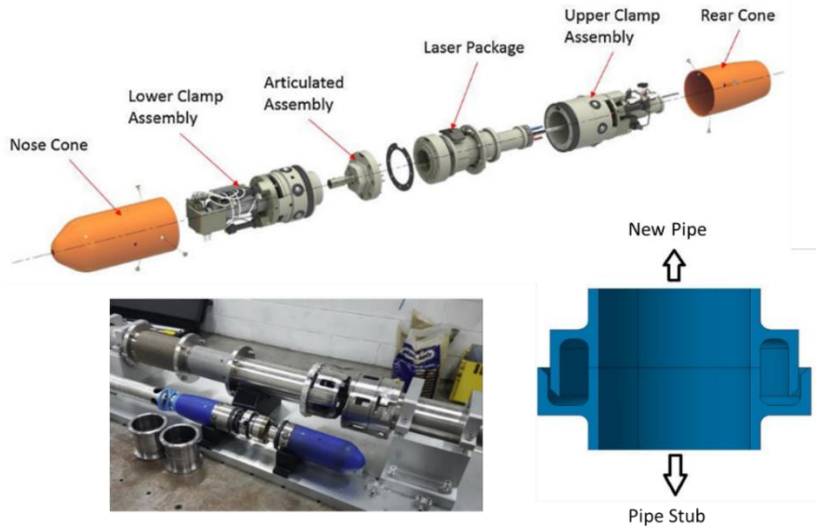

Figure 11 DEMO welding tool design concept and the pipe alignment features [8], [9]

4 Pipe cutting and tooling development

The development of remote handling tools for pipe joints cutting at Joint European Torus (JET) required the tools to be compatible with the limited access to the JET machine. More importantly, tools were also required to produce cuts ready for re-welding and effectively remove the swarf during the process. Prior to prototyping various cutting processes using thermal, erosion and mechanical techniques were reviewed (Table 3). Two mechanical cutting mechanisms, turning and sawing, were down selected for prototyping cutting tools and then validation tested on pipe butt joints and sleeve joints [14].

Table 3 Comparison of the potential cutting processes for JET pipes [14]

Processes	Technique principle	Suitability	Reasons
Thermal	Laser Plasma	no	• Oxidation if inert gas is not used • Irregular cut needs further preparation • Impracticability of laser delivery • Generation of debris from process
Erosion	EDM Water Jet cutting	no	• Involvement of using liquid • Production of fine debris particles • Power transmission limitation
Mechanical	Grinding	no	• Cutting wheel fragments • Metal particle contaminations • High power input requirement
	Turning	yes	• Narrow cut from incremental radial feed • Flat surface suits re-welding
	Milling (sawing)	yes	• Several sawing options to choose from • Suitable cut quality
	Wheel cutters	no	• High force required and poor cut finish

The first of these tools is a sleeve cutting tool, shown in Figure 12, which clamps and performs the cutting ex-bore [14]. The tool employs turning mechanism uses two interchangeable lathe type tool bits that generate the cutting action on the pipe. The hinged mechanism of the stator allows for the tool to be flexibly clamped and unclamped

on a continuous pipe run. These engage in a location groove on the sleeve and are locked by hydraulic clamps which provides a rigid frame for two semi-circular rotor elements to rotate. The rotor elements contain a radial feeding mechanism that is achieved by the leadscrews. Each leadscrew is indexed by a star wheel which is actuated by a striker pin in the stator once per revolution. Any swarf produced was extracted via a duct in the stator. In comparison, the sawing mechanism was adopted for both ex-bore and in-bore cutting. The slitting saw tool was to use a 100mm diameter saw blade to slice the 50 mm pipe, guided by a feed carriage, from ex-bore. A bore cutting tool used a 40mm diameter by 1.6mm thick saw to cut a 45mm pipe section. Both tools were driven by a 24 V D.C. motor and equipped with vacuum extraction ducts for the removal of the cutting debris. Selected cutting techniques have successfully demonstrated the feasibility of remote cutting of JET pipes. Cutting of Inconel Alloy and stainless-steel pipes was performed without using any cutting fluid; however, the feeds and the speeds must be low. For ex-bore pipe cutting designs the lathe technique was preferable over the slitting saw as it offers faster cutting rate and used cost-effective tool bits [14].

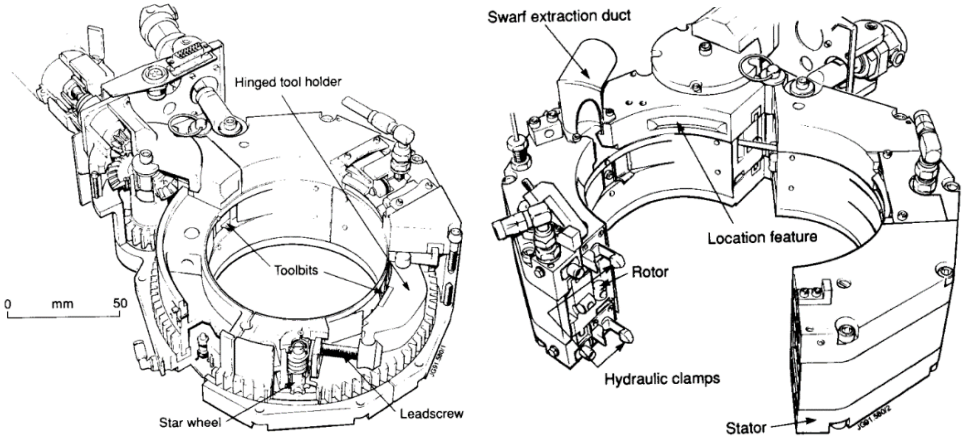

Figure 12 Sleeve cutting tool in clamped and unclamped configurations [14]

Inspired by the JET remote handling operations, a lathe-based cutting tool was developed for ITER NB pipes to prove the feasibility of using commercially available equipment [96]. A U-shaped rotor was selected considering the limited deployment volume and a spring fed cutter was used due to its simplicity and reliability (Figure 13). The rotor consists of a deployment ramp which interfaces with the swing arm pin, that allows for accurate positing of the tool but holding off the pipe surface and preventing damage to cutting tip during installation. The tool comprised a dual worm drive that driven through a series of bevel gearboxes, two recovery gears that work with a worm gear disengagement mechanism to ensure the rotor can be recovered to its home position in the event of drivetrain failure as well as safely release drivetrain components. The tool is also designed with a bellow restraint and capitation system that can restrict the motion of the tensioned bellows, so that the realises on break through towards the end of cutting can be controlled.

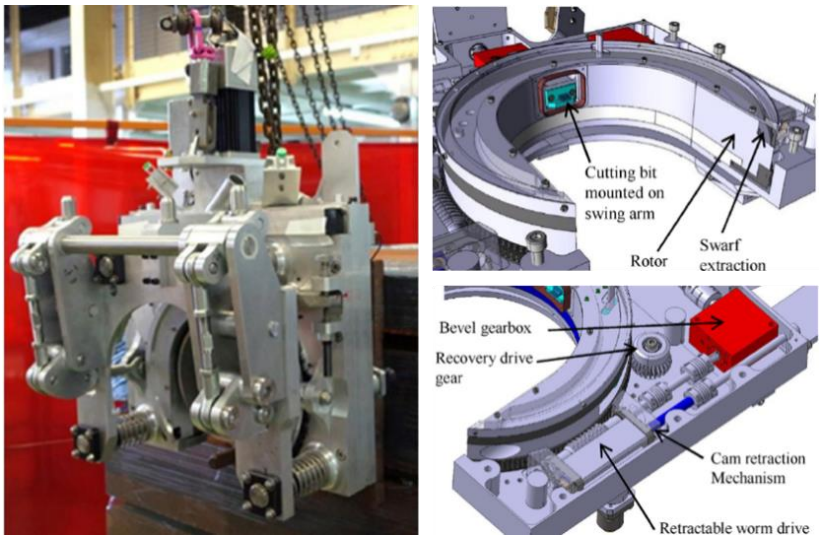

Figure 13 A lathe-based cutting tool and its drive system for ITER pipes [96]

Cutting trials demonstrated feasibility of using the tool for operation. However, the challenges of remote cutting are unique, requiring optimisation of the tool. Firstly, commercially available equipment is not necessarily suitable for adaptation for remote deployment, such as recovery and rescue, positioning and swarf management. The lathe-based spring fed mechanism was not successful, and swarf was trapped under the tip which slowed down the process. Besides, the bit geometry greatly affects the cutting reliability and swarf formation. Well balancing the two factors will in return affect the tool life. Dry cutting also must be performed extremely slow to control the heat in order to avoid tool bits failure.

Swarf management is critical in remote mechanical cutting [97], [98]. Testing of BTS on ITER 160mm straight divertor pipes, cutting was firstly performed 80% of the required work using a milling tool. Then a swage cutter was used to carried out the final cut to prevent chips from falling off the pipe and remove the debris from the cutting tool head [97]. After the reduction of the divertor pipe size, an orbital lathe-based cutting tool was developed (Figure 14). The tool is able to provide torque, speed and inertia comparable to a remote tool, along with the capability of measuring surface and feed speed, radial and tangential force, and temperature during the cutting processes. Tool bit wear was assessed using various tool materials and swarf generated from the cut trials were also characterised. Tests proved swarf of a manageable size for extraction, with average size of 10mm, could be achieved reliably and repeatably using a dry, lathe-based parting off process at low speed with a HSS cutting tip and an incremental feed mechanism. After a single cut, HSS tips showed little to no wear, compared to P30 carbide tips which was severely worn and damaged. Further work was recommended to determine the tool life with respect to the number of successful cuts possible using a single cut.

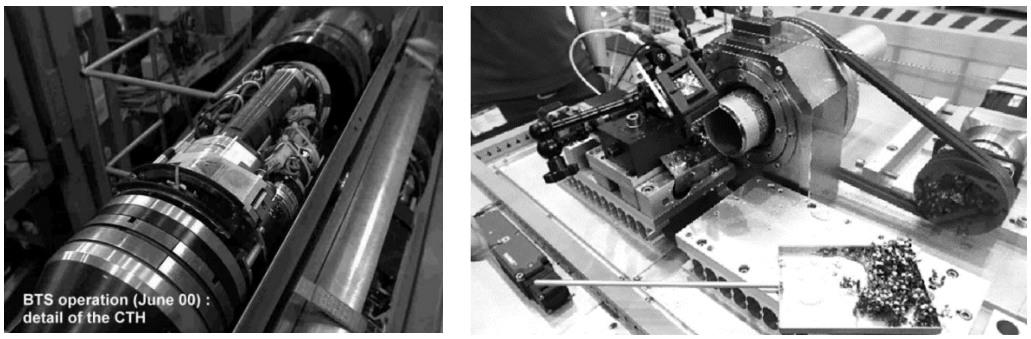

Figure 14 Cutting rig for ITER Divertor cooling pipe, (a) cutting tool head for 160mm straight pipe BTS and (b) orbital lathe-based cutting test bed [98]

Japan Domestic Agency (JADA) have developed a compact swage-cutting tool, to perform cutting from inside of the ITER blanket cooling pipe [101]. The cutting force transmission system and the cutting tool components are shown in Figure 15. A disc cutter, sat inside a φ40.4mm tool head and contacted with pipe inner surface, was pushed outward while tool head was rotating. This enabled pipe cut and left a cut surface with roughness less than 6.3μm which was the target arithmetical mean roughness for subsequent laser welding. And the whole process did not generate swarf during cutting.

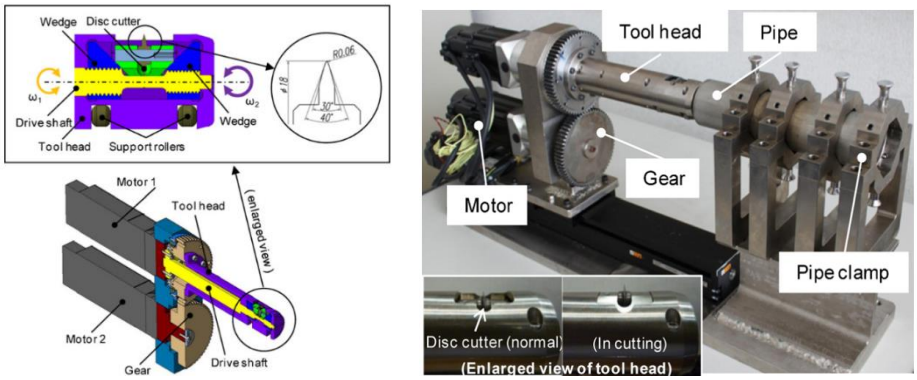

Figure 15 design of the swage cutter and experiment setups [101]

A similar disc cutting tool (Figure16) was developed for JT-60SA cooling pipes which connecting between the divestor cassettes and vacuum vessel [109]. The tool outer diameter is 44mm and is able to cut a pipe with an inner diameter up to 65mm. The length of the cutting tool head is approximately 1m so that the deepest cutting point of 480mm could be reached. The cutting system is also equipped with two cutting heads which means the target inner

plate unit that supported by two cooling pipes in the cassette frame could be cut simultaneously. Prior to cutting the cooling pipe, a plug (double-layered pipe) that located on the top must be removed. Cutting trials was carried out using the same cutting tool. Although some swarf was deposited on the bottom of the plug which would not be used for re-welding, by pulling out the plug all the swarf could be collected successfully.

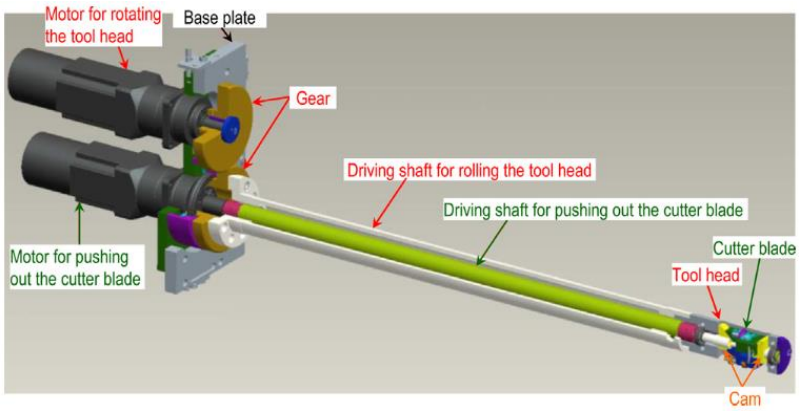

Figure 16 Overall view of the cutting tool head with the power transmission system [109]

A face mill tool with swarf collection mechanism was developed for pipe end cutting [101]. The face mill has six sintered tungsten blades. Each blade shares the function of reducing the cutting load and producing narrow swarf. The design of the blades allowed swarf flow to be controlled during cutting, where the swarf was collected from the inside the face mill along the blade surface by vacuuming (Figure 17). With the optimal cutting parameters, the tool demonstrated high stability in a lifetime test, which the swarf collection and cut quality maintained high after cutting 200 holes.

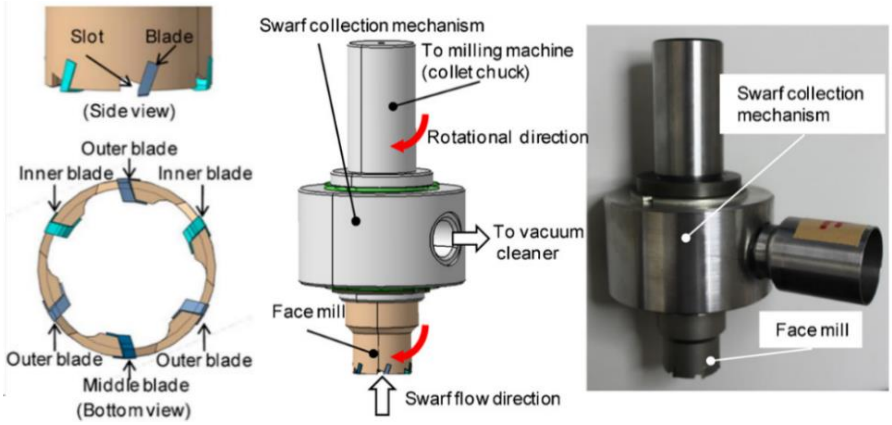

Figure 17 Design of the face mill and swarf collection mechanism [101]

Thermal cutting processes have been investigated using laser as power source because of high cutting rate and non-contact nature. An in-bore remote laser cutting tool has been developed for DEMO service pipe disconnections [8], [110]. The prototype is similar to the remote laser cutting head, except for that the processing head has a focused nozzle to create a parallel cutting gas jet at the laser spot (Figure18). In-bore cutting trials were performed on 5mm wall thickness SS316 and P91 pipes. The whole process requested laser power of 1.9kW and it took only 34 seconds, at cutting speed of 0.5m/min, to successfully cut through the pipe wall [111]. The cut samples achieved rough surface finishing and significant dross retained on the kerf. The P91 alloy steel pipe also had severe discolouration in the cut surface. However, this cut quality could be accepted under operational regimes not requiring rewelding to be conducted on the same pipe, but with a new pipework [108].

Conventionally, gas-assisted laser cutting performs with single stoke by focusing the beam on the surface of the workpiece and the molten metal is removed out of the kerf with a jet of gas close to the cut. Drawback of single pass cutting is the dispersion of the dross outside the nozzle which affects the cleanness of the component [112]. Laser ablation cutting was investigated for the hydraulic connections in the ITER diagnostic port plug [113]. In the cutting trials, a short-pulsed fibre laser was used to remove the joint between two concentrically overlapped pipes. Material in the ablation process is directly vapourised by the high peak-powered laser beam, instead of melting the metal, and blown off by the gas jet, leaving a dross free surface finish (Figure19). Since a limit amount of the

material can be removed by ablation, a multi-pass process was employed to cut through a 2.1mm-deep weld in a ϕ48.6mm inserted pipe and the process took approximately three hours. The cutting trials achieved surface roughness less than 200 μm. Higher cutting rates may be achieved by using higher laser power density per pulse, under which, however, excessive heat introduction leads to metal melting. And ejecting the metal off by gas jet leaves the kerf with burr or dross on the cutting surface which affects subsequent rewelding activity.

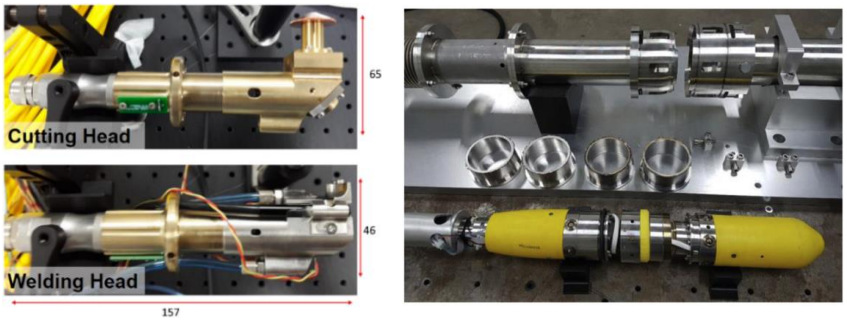

(a)

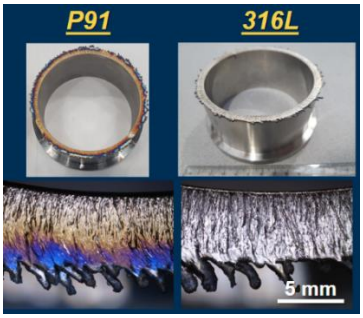

(b)

Figure 18 Remote in-bore laser cutting tool: (a) Miniaturized laser cutting head and cutting test rig [8], [110], *and cut quality of the 5mm SS316 and P91 pipes* [111]

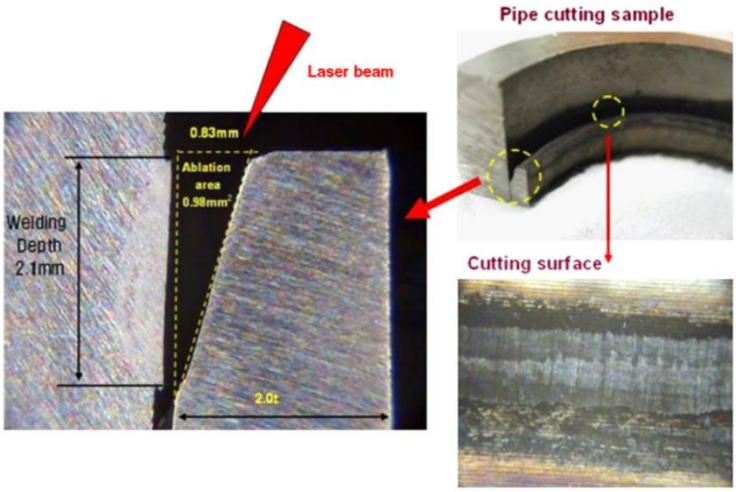

Figure 19 Ablation cutting results in the two concentrically overlapped pipes using short pulse laser at 20kW peak power, 25ns pulse duration and 60kHz frequency [113]

5 Other pipe tooling and joining methods

Removable Bellow Assembly (RBA) allows for the flexibility to join the rigid cooling water system pipe to the rigid component [94], [96]. The design was introduced to ITER neutral beam remote maintenance, with which the cut end would be made prior to installation of the RBA to determine the misalignment between the pipe studs. Then a replacement bellows is prepared to ensure an optimal fit. A datum flange located on either side of each cut location also allows for accurate position of the tools and manipulation of the bellows (Figure 20). A pipe alignment

tool is then to bring and hold the joints into alignment to satisfy the fit-up tolerance for subsequent welding, and also support and position the weld tool as well as tension the bellows. The prototype alignment tool, with the function of providing polar alignment, angular alignment, axial alignment and join close-up, was designed and tested on ND200 pipe. Since the bellows were designed very stiff to resist internal water pressure, the tool was required to have very tight tolerance and provide high forces for the alignment. As a consequence, the resulting tool had a weight of over 100kg in order to provide sufficient stiffness, which increased the complexity during the deployment demonstration [96].

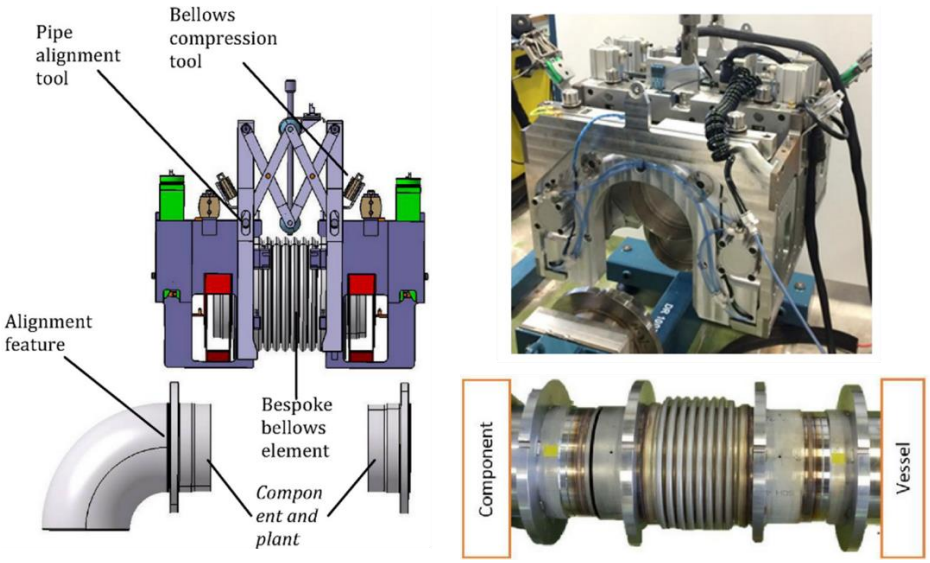

Figure 20 The concept of using a removable bellow compression assembly with the pipe alignment tool for ITER water pipe maintenance activities [94], [96]

Unlike ITER NB and divertor maintenance, blanket module cooling pipes can only be accessed from in-bore and the concept of using bellows is not applicable due to limited space. The requirement of allowable gap and step for joining of blanket module pipes are less than 0.2 and 0.3mm, respectively. It was essential to correct the misalignment to guarantee the welding activities. A prototype of the pipe alignment tool (Figure 21) was designed and fabricated based on FEA analysis followed by mock-ups testing. The tool has an outer diameter of 39mm at the head with pads closed and it can be expanded so that it pushed against the pipe inner wall. The weld grooves are then aligned by expanding pads that are driven by a rotating hexagonal bit via a wedge mechanism. This allows for a correction of maximum 1.5mm axial displacement and 0.5° angular displacement [114].

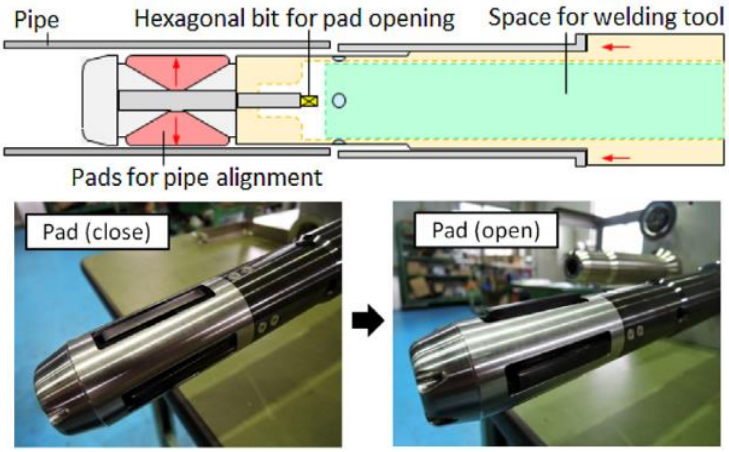

Figure 21 Alignment tool for ITER first wall cooling pipes [114]

In the scenario where permanent joints are not required, welding and cutting may be avoided and replaced by mechanical joining solutions such as bolted or mechanically clamped flange type joints. This allows for easier disassembly and higher reusability of the pipe components. In the ITER vacuum vessel pressure suppression systems, pipes are to be maintained using a remote flange bolting tool (FBT) to bolt and unbolt the flanges (Figure 22). The strategy is to engage the tool on the pipe with a permanently positioned rail system which provide a datum

position and guidance for the tooling to rotate in relation to. The lower arms actuate, closing the arms around the pipe and the nut runners to engage with the bolts and provide the bolting/unbolting torque. The prototype was developed and tested on a mock-up rig to represent the functionality of the device [115]. The mock-up environment has 18 pop-up bolts in a flange for the DN300 pipeline. Testing was only performed in a semi-automated fashion, which supervision and in-situ adjustment of the tool was made by the remote handling operators. It was also identified that cable management of the tooling during rotation was very challenging.

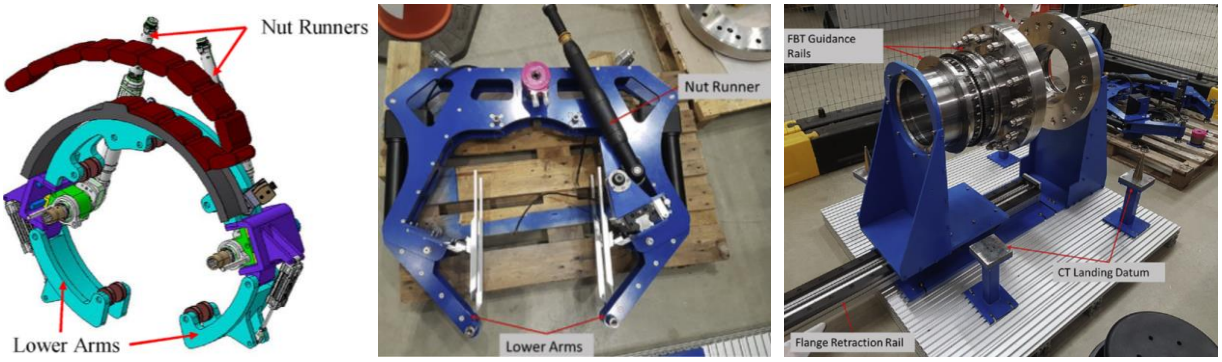

Figure 22 Prototype flange bolting tool (FBT) and mock-up test rig for DN300 pipe [103]

Mechanical Pipe Connections (MPC) are also being developed to connect and disconnect multiple cooling and purge pipes during blanket maintenance, as an alternative to the cut-and-weld concept, for DEMO [116]. Simultaneously connecting several pipes offers minimised downtime, however, the process needs to fulfil multiple requirements. For instance, large tooling is needed to be able to provide extremely high sealing loads at the same time maintaining an acceptable level of sealing between the high-pressure fluid and vacuum surroundings. Besides, no seals have been qualified for a high pressure, high temperature, and extremely low leakage rate required environment. Moreover, connecting pipes in multiple sizes and fluids will introduce additional forces and stress due to the interaction between pipe flow through the manifold flange[107], [116]. Hub and clap connection (Figure 23), one of the two MPC concepts, was further studied as it showed robust nature of design from finite element analysis. Modification of the design was made to improve stress and sealing force distribution, which included increasing the flange diameter, thickness, clamp sizes, and distance between each pipe, etc. The amount of cooling pipes per flange also has been reduced from two pairs to one pair according to the HCPB blanket design change. As in the design stage major simplifications have been made for numerical modelling, a test bench is being constructed for further validation.

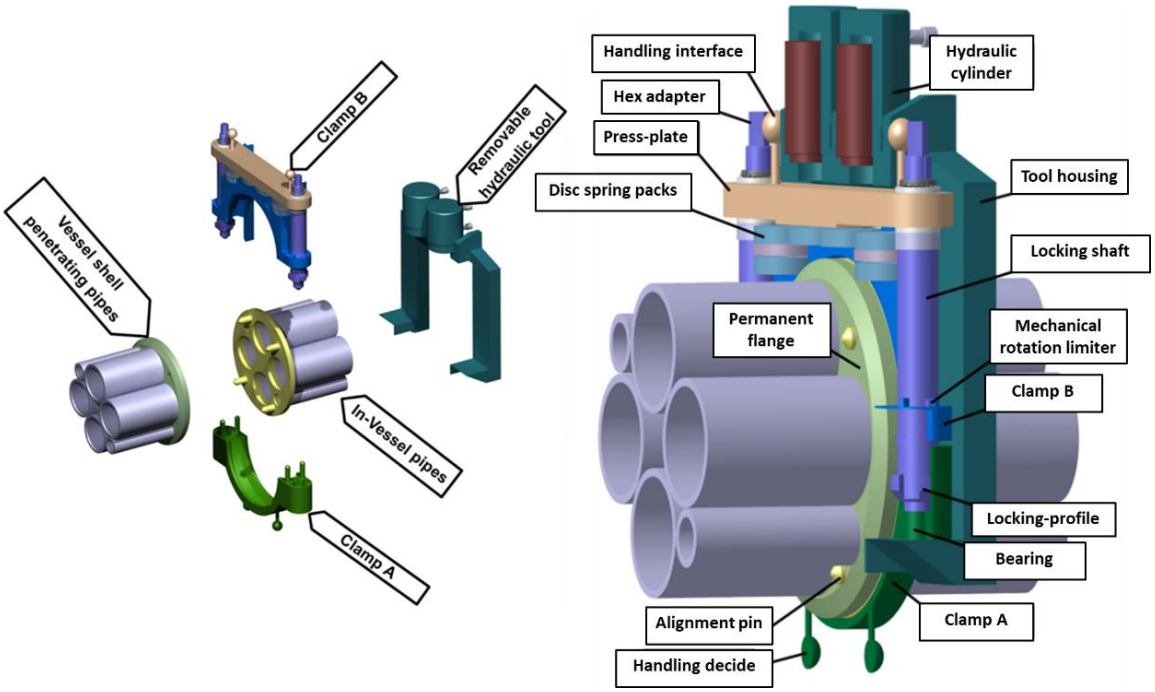

Figure 23 Hub and Clamp Connection concept for DEMO blanket cooling pipe mechanical connection [116]

A remote handling compatible pipe jointing system based on reversable brazing technique was studied, aiming to provide improved jointing with the ease of disassembly and re-use [13], [117]. The addition a layer of Nickel which prevented undesired fusing of joint cause by dissolution between parent materials and braze, this also allowed for remelting and ultimately disassembly (Figure 24). The joint was designed in a butt configuration interface with bolted flanges and structural reinforcement. The flange also incorporated a built-in inert atmosphere chamber and integral induction coil. The joint is created by melting pre-placed foils through electromagnetic induction heating under Argon mixed with 10% Hydrogen. Alignment and internal shielding were provided by a separate pipe bore tool. Disassembly could simply unbolt flange and remelt the braze under the same heating and shielding system.

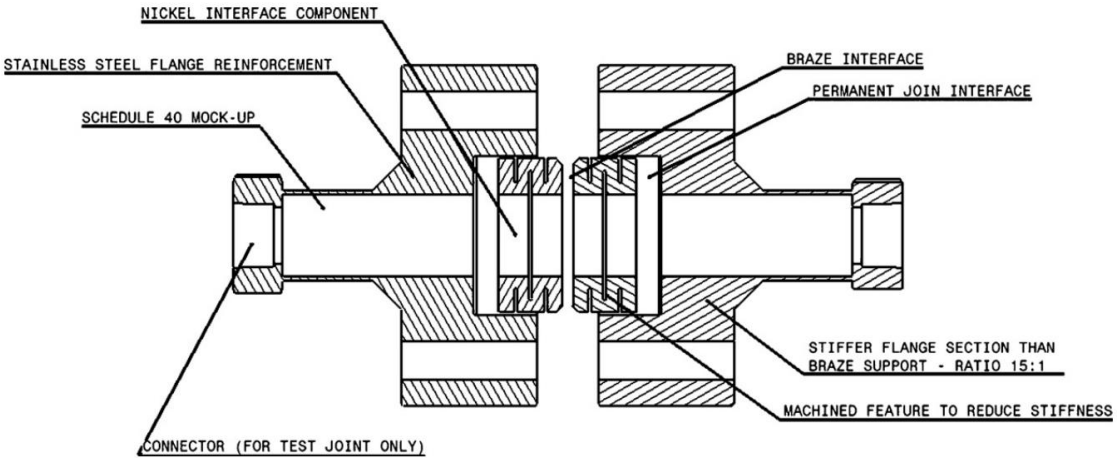

Figure 24 Concept of remote handling compatible pipe reversable brazing technique [13]

Inspired by above concept, a self-brazing/de-brazing connector was designed to be used with helium, lead-lithium and water pipes in DEMO [118], [119]. The internal body of the component is made of Ni-200 and the concentric external body is made of SS316. They are permanently joined by brazing in an external furnace with vacuum conditions. When bringing in situ, the Ni-200 bodies are brazed and de-brazed cyclically under helium and hydrogen atmosphere using induction heating. The design of the external mechanical connections, for strengthening the stiffness of the brazed connector assembly, came with two concepts (Figure 25). One was to use Hanford Purex clamp with separated remote handling equipment, which the tightening mechanism was simplified by using a central ring with gear profile, three jaws placed at 120◦, and a spring that provides the force to ensure the strength of the assembly. The spring could also guarantee the hooks synchronized and closed at rest position. Considering spring might be degraded under high temperature and neutron irradiation, an alternative spring-free concept was proposed, where the relative movement between the mechanical part of the connector and the pipe was achieved through a geared component in the pipe and gears in the head of the hooks that transfer the movement Although such complex design could avoid the risk of mechanical degradation, jamming issue might be increased from the large number of geared components.

Figure 25 Brazed pipe connector and design of the clamping systems [119]

6 Candidate NDE technologies

6.1 Welding leak testing

Leak testing is a non-destructive test method. It is an essential procedure to be conducted for inspecting the tightness of the pipe welds. The principle of leak testing is to examine the pressure difference between the inner and outer side of the object using liquid or gas as search medium. Helium is an ideal search gas to detect defect cracks in the weld as it is a safe inert gas. Helium atoms and small and low viscosity so that they can travel quickly in the materials. Helium mass spectrometer is often used to detect the leaks. Diluted hydrogen, a mixture of 5% hydrogen in nitrogen, can also be used as search gas. Such mixture is neither inflammable nor explosive. Mass spectrometer leak detectors can be calibrated for hydrogen, but a simpler solution is to use the semiconductor sensor that no vacuum is required for hydrogen detection.

There are mainly two methods used for leak localisation and detection: vacuum method and sniffer method. In the vacuum method, the object is evacuated and sprayed from the outside with small amount search gas around the weld [120]. The gas enters through any leak present in the object is detected by a sensor connected to the leak test instrument. In the sniffer method, by contrast, the object is filled with search gas and under slight overpressure. The search gas escapes though the leaks present to the outside and is then detected by a sniffer probe that connected to the mass spectrometer leak detector. Both methods were tested on ITER cooling branch pipe welds [121]. In both methods, the ionization gauge and sniffer tube were moved inside the pipe along the cooling manifold to access to the branch pipe connection to detect a standard leak. The preliminary experiment showed better detectability when the probe head was inserted into the branch pipe compared to the sniffer method.

6.2 Remote visual inspection

Visual inspection is a procedure to examine the surface flaws or defects of the weld after welding process using naked eyes, with or without optical aids. Optical aids such as low-power magnifier, microscopes, telescopes and specialised devices such as borescope, endoscopes and other fibre-optic devices are often employed to enhance operators' capability. These devices can also be integrated with cameras, computer systems, digital image analysers, robotic crawlers or other specialised tools to form advanced Remote Visual Inspection (RVI) system. RVI can reduce the risks associated with confine space entry and to be deployed to the locations not accessible in-situ to the naked eyes.

Optical profilometer employs a laser emitter and a conical mirror to generate a conical light that projected onto the pipe inner surface. Camera-based inspections allow for visual images of the pipeline to be stored for further analysis. This method is often used for examining weld dimensions as well as mismatch between the two parts. In theory if everything is well aligned after the tool deployment and the pipe section is circular, the resulting image viewed by the camera would be a circle. Endeavours have been made to reduce the errors related to localisation inside the pipe from autonomous motion, for the generation of a 3D reconstruction of the pipe interior [122]–[125]. Vision sensors such as fisheye cameras and omni-directional cameras that with a wide field of views showed great potential in mobile robot navigation (Figure 26) and environmental measurement and recognition [125]–[128]. In addition, utilising a combination of visual odometry, encoders and inertial measurement unit obtains higher accuracy of locational information compared to measuring the insertion distance with encoders as the errors build up from slippage.

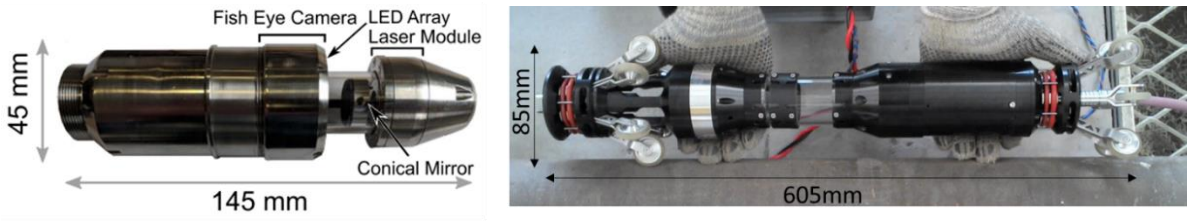

(a) (b)

Figure 26 Prototype examples of laser profiler RVI tool used for inspecting (a)2-6 inch pipes [125] *and (b) 3.5-5.2 inch pipes* [123]

In the real world, the relationship between the radius in pixel of the laser line images and the actual radius of the pipe in real work coordinates is nonlinear due to wide lens distortion plus the refraction of the supporting glass or plastic window built in the tool. Besides, the misalignment and imperfection of the components results in an uneven behaviour of different angles [123]. Therefore, optical calibration of laser alignment as well as correction of angular misalignment during assembly is crucial for the subsequent defect sizing [125]. In the case of limitation of

mechanical centralisation, post-inspection centralisation method which comprising active pose estimation and an unwrapping algorithm was also introduced undistorted view of the pipe interior [129].

Fiberscopes, or fibre optical scopes, use coherent fibre-optic bundles to transfer images from the object site that difficult-to-reach to the display panel. Fibre-optical cables are made of optically pure glass and are as thin as human's hair. They are fragile but flexible. Fiberscope tubes can be threaded and snaked into tight and small spaces making it well suited for RVI of narrow assays in industrial equipment and system. In a fiberscope, there are often two types of fibre-optic bundles. The illumination bundle is designed to carry light to the area in front of the lens which located at one end of the device to capture image. The imaging bundle is designed to transfer the image to the eyepiece for live viewing of the object.

An advanced prototype probing system was developed by JAEA for nuclear powerplant maintenance [130]–[134]. The system was designed to inspect the inner wall of a 1-inch diameter tube of the heat exchanger units as well as perform microcrack repair. The tool comprised a multi-coil ETC section for crack inspection, a laser processing head to perform repair and a composite-type optical fiberscope (Figure 27). The total length of the composite-type optical fibre was 10m. the fibre was made of synthetic quartz with three cylindrical structures: a centre optical fibre with 0.2 diameter transmits high energy laser beam, surrounded by 20,000 image fibres to deliver high resolution image to the CCD camera, and light guide fibres to supply illumination which located on the outer side of the image fibres. This fiberscope was further developed with an advanced optical fibre coupling device which allowed for transmission of pulsed laser for material cleaning process, albeit the fiberscope was originally developed for inspecting and repairing the robot system for tritium breeding blanket in ITER project [135]. In nuclear environments, radiation at the major inspection areas can impact the illumination system and imaging device. Radiation resistance of fused silica core optical fibres has been studied and especially fluorine doped and heat-treated optical fibres showed substantial potential in radiation environments in fission reactor [136], [137].Visible observation could be realized up to a fast neutron fluence of $1x10^{23}$ n/m^2, indicating that it had potential to be used as in-vessel plasma diagnostics and remote sensing in nuclear fusion devices.

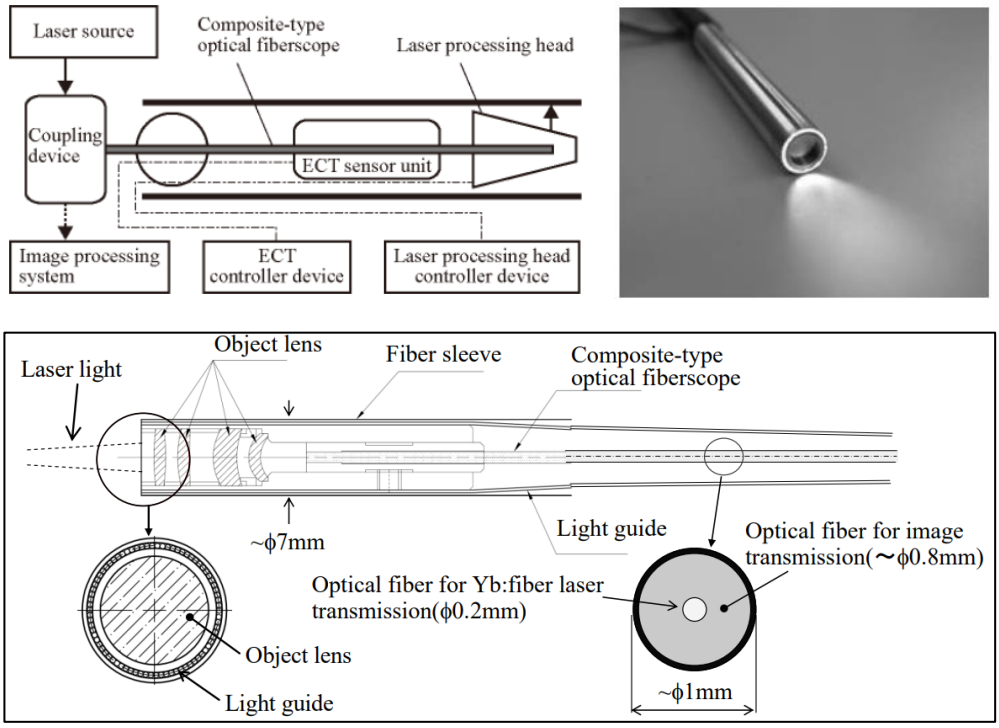

Figure 27 Composite-type fiberscope probing system [130], [133]

Images taken using a fiberscope are indirect, in that they are projection of light transferred by the fibre optical cable. Captured image quality may not be as good as by borescopes with high-definition camera captured in detail. Besides, fiberscope devices are prone to broken pixels and black dots due to damages fibre optical cables which the issues are not present in borescope devices. Borescope can be flexible or rigid. A video borescope or inspection camera is similar to fiberscope but uses a miniature video camera at the end of the flex tube. Usually, a light at the end of the insertion tube makes it possible to capture video or still images deep within equipment, engines and other dark spaces. Instead of using fibre waveguide as that in fiberscope, video borescope uses inexpensive

electrical cable, which is much less costly and better resolution. Rigid borescope, in contrast, though have the limitation that access to what is to be viewed must be in a straight line, it generally provides superior image with even less cost.

6.3 Ultrasonic testing

In the field of non-destructive testing, ultrasonic probes or ultrasonic transducers are most used to excite and detect ultrasonic waves, for volumetric flaw examination and material characterisation. When short electric pulses are applied to a piezoelectric crystal, it vibrates at very high frequency, thus ultrasonic waves are generated as a response to the applied alternating current and transmitted into the test material mostly via a suitable couplant. There are two fundamental methods receiving ultrasound waveform, reflection and attenuation. In reflection (or pulse-echo) mode, a single transducer acts as both the signal generator and receiver. In attenuation (or through-transmission) mode, a transmitter sends ultrasound through one surface, and a separate receiver detects the amount that has reached it on another surface after traveling through the medium.

Angled beam transducers are typically single element transducers used with a wedge to introduce a refracted shear wave and longitudinal wave, in a pulse-echo scenario, into the test sample. It is the plastic wedge that serves to transmit longitudinal waves to the test part surface where mode conversion occurs. Angled beam testing is most commonly used in weld defects inspection using refracted shear wave where discontinuities are typically not oriented parallel to the surface of the part, which in comparison straight beam techniques are highly effective to reflect enough sound back to the transducer at finding laminar flaws. Materials having a large grain structure, such as stainless steel may require refracted longitudinal waves for successful inspection.

Phased array ultrasonic testing (PAUT) is more advanced form of conventional pulse-echo ultrasonic testing. It improves on simple, or monolithic ultrasonic scanning with the use of a series of piezoelectric elements, from 16 to as many as 256, within a single probe which allows for beam angling (linear scan), sweeping (steering), and focusing through constructive and destructive wave interference, without physically scanning the beam through the area of interest [138]. The piezoelectric elements are arranged in patterns, such as linear array, ring, and circular matrix, and can be pulsed individually at a computer-calculated delay so that to achieve particular wavefront or beam focusing on a specific depth and angle (dynamic depth focusing). Full Matrix Capture (FMC) enables the collection of all the possible transmit/receive combinations. This has greatly improved efficiency to characterise defects and reduce the number of false alarms. Combining FMC data with advanced imaging algorithms like Total Focusing Method (TFM) allows for areas to be inspected with ideal wave focus at all points on the image.

A high-temperature, autonomous deployable, liquid filled, PAUT roller probe (Figure 28) was developed to perform in-process inspection of multiphases welds [139]. This 5MHz, 64 element linear phased array roller probe was configured to perform sectorial scans introducing transverse waves into the material. The soft conformable silicone rubber tyre in thickness of 6mm, made of HT-Silicone S20A was able to withstand surface temperature up to 350°C, which allowed for inspection performed alongside the weld with angled beam using 55° transverse wave immediately after process. The probe successfully detected artificial defects embedded into a real weld at approximate 230°C. Tailored designed was also made to inspect Wire Arc Additive Manufacturing (WAAM) components in-process, which the roller probe is configured to perform both linear and sectorial scans creating longitudinal waves into the material [140]. The performance of the roller probe was tested on Ti-6Al-4V WAAM sample with artificial defects, 1mm diameter flat bottom holes, at various depths. The poorest signal associated with the shallowest defects which was 6mm from the surface was only 6 dB lower than the calibration signal.

An in-bore PAUT tool has been developed for JT-60SA to inspect pipe welds in the inboard target in the first actively cooled divertor cassette without fully filling the pipe with water, [141]. The UT probe is commercially available and particularly used for thin-wall inspection. The probe and the wedge were bolted on the L-shape holder and then mounted on the welding tool with elevation, rotation and tilt mechanisms (Figure 29). Localized couplant supply pipes were integrated to the tool, supplying the couplant from just above the wedge on the probe, to avoid conventional submerged method where the pipe would be required completely filled with water. The tool was tested on a known internal defect in the weld, which the peak intensity of 80% indicated the axial length of the defect. The circumferential length of the detect in 2.5mm was measure by moving the probe at 1mm/s travel speed. It was suggested the tool was efficient in the revealing and in the measurement of internal defects of 0.5mm or larger, nevertheless, the tool detected an unknown circumferential defect shorter than 0.5mm in a lap welded pipe joint.

Although PAUT is fast and effective, cracks and defects may be still difficult to fully image due to their orientation compared to the path of the ultrasonic pulse. One possible solution is to scan the surface from multiple points such

as from above and from below the weld which, however, may have limited access to the other side of the weld in practice. Time-of-Flight Diffraction (ToFD) technique uses two transducers - transmitter and receiver positioned in a pitch-catch arrangement on the opposite side of a weld where the transducer produces pulsed ultrasonic waves that diffracted to various degrees by irregularities in the scanned material, then collected by the receiver.

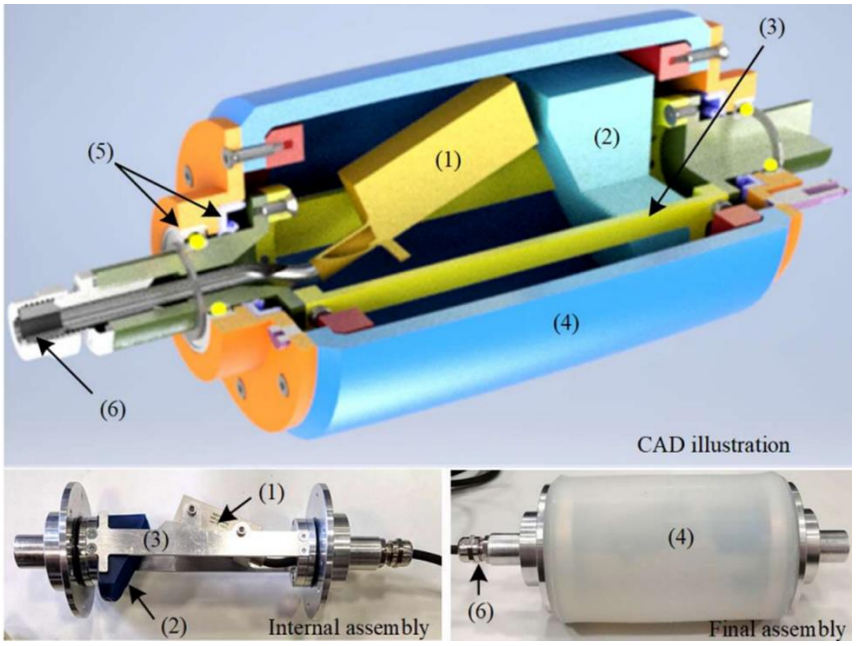

Figure 28 computer-aided design and physical assembly of the PAUT roller probe: (1)A 5MHz-64 element PAUT transducer, (2) absorber (3) holding structure, (4) high temperature tire, (5) being and shaft seal and (6) cable gland [139]

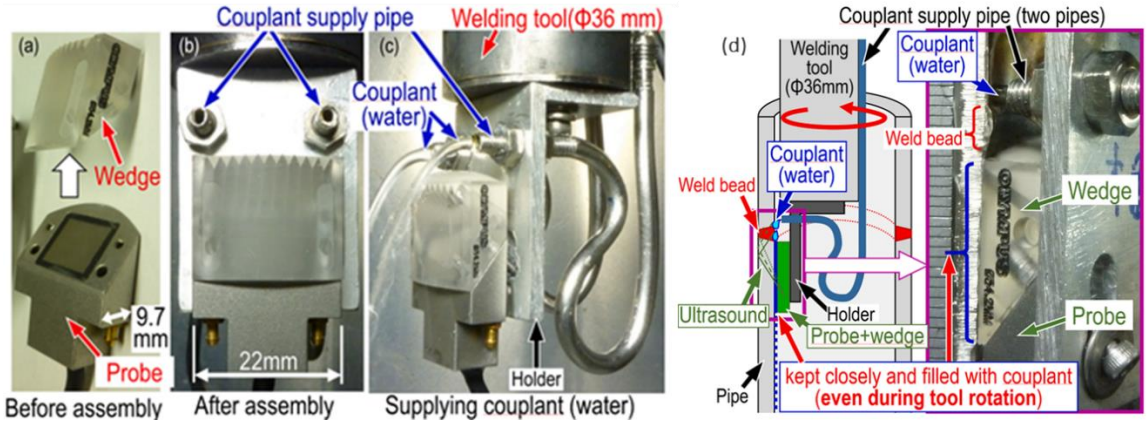

Figure 29 UT probe assembly with the local couplant supply [141]

Most of the ToFD inspection is conducted using high energy longitudinal waves which also travel two times faster than shear wave. Signals received during ToFD inspection include lateral wave, back wall echo, mode converted shear wave and defect signals as the result of longitudinal wave propagation. In a flawless sample, the signals picked up by the receiver are the lateral wave that travels along the surface and back wall echo that corresponds to the time of flight equal to material thickness. The location and the size of a discontinuity can be determined from the time of the flight of the diffracted waves and the depth of the discontinuity can be calculated by trigonometry [142].

Longitudinal wave ToFD has the limitations for near surface defects detection due to signal superposition, and thin sections where spacing between back wall longitudinal reflected signal and lateral signal is small. Therefore, diffracted shear wave ToFD has the advantages of having slower velocity that allowing discontinuities signals to be repeated at longer times allowing near-surface responses to be recognized easily [143]. However, ToFD has certain imaging weaknesses just as that with PAUT. If a single scan is made, technicians may encounter a lateral flaw wave dead zone, off-axis errors, timing errors and resolution errors. It is recommended to combine both techniques in order to achieve rapid, accurate scans of welds, pipes and other critical metallic components where

the use of couplant is allowed.

Electromagnetic acoustic transducer (EMAT) is a transducer for non-contact acoustic wave generation and reception in conducting materials. The electromagnetic acoustic excitation of ultrasound is based on two mechanisms: the Lorentz forces and the magnetostriction in ferromagnetic materials. The main components of a EMAT transducer consist of an electric coil and a magnet which is to produce a bias magnetic field. When the coil is placed near the surface of an electrically inducting object and is driven by a an alternative current (AC) at the desired ultrasonic frequency, eddy currents is generated in a near surface region of the object. With the presence of a bias magnetic field, the eddy currents will experience Lorentz force which triggers the motion of charged particles in the object. These charged particles, which are in motion, collide with the crystal lattice and result in ultrasound propagation [144]. For ferromagnetic material the AC current in the coil induced an AC magnetic field and thus produces magnetostriction, which the material is under dimensional change when this magnetic field is applied, at ultrasonic frequency. The disturbances caused by magnetostriction then propagate in the material as an ultrasound wave.

Compared to piezoelectric based transducers, EMATs owe the advantages of being couplant free, suitable for high temperature and moving components. They have shown to function up to 450°C for nuclear industry and used at speeds of 15km/h^3 in railway industry [145]. Deployment of the sensors is easier as the angle of the sensors does not affect the direction of propagation. The coil and magnet configuration can be designed to excite a variety of wave types such as longitudinal and shear bulk waves that excited normal to a sample surface, angled shear waves and guided mode, including a shear wave with polarization parallel to the boundary without mode conversion and amplitude change [145]–[149]. This makes EMATs well suited for surface-breaking defect inspection for pipelines even through coatings. Applying horizontal shear wave that fills up the full volume of the material also allows for inspecting the full cross section of the weld [149]. In addition, EMATs do not require surface preparation [150] and are suitable for examining austenitic welds and/or materials with dendritic grain structures. [149]

EMAT was investigated for nuclear components inspection owing to its advantage of being radiation hardened [121], [151], [152]. ITER project have tested EMAT under irradiation does rate about 10kGy/h and no significant degradation was observed up to 10MGy. Therefore, an inspection bored tool accommodating with an EMAT was designed and fabricated for ITER branch pipe welds. Test proved the tool was able to travel at 1m/min in bore and detect the surface defect with 20% depth of the branch pipe thickness. EMAT also has been developed in a 12-element phased array format just as PAUT but adapted to hot and opaque environment for in-service inspection of Sodium Fast Reactors [153]. The sensors were able to steer and focus the ultrasonic beam to the desired focal sport using electronic delay laws. Lab based test showed sufficient sensitivity to image side drilled holes 6mm in diameter located at 180mm depth in an 250m-mm-thickn aluminium blocks.

EMATs have low transduction efficiency because of electromagnetic transduction process where the input energy is lost in the form of heat. As a result, the signal-to-noise ratio (SNR) is low. Therefore, high power input and specific electronics are required to improve the SNR. For example, a compact ‘coil only EMATs’ with effective areas of 1-5cm^2 were driven to excessive power level at MHz frequencies, using pulsed power technologies. Even at considerable lift-off distance the ultrasound can be readily detected in aluminium, ferromagnetic steel and stainless steel [154].

Laser ultrasonic testing (LUT) is using material itself to transduce optical energy first to thermal and then ultimately to elastic energy which propagate as ultrasound in the material. The generation of elastic ultrasonic waves within a structure is achieved by high-energy laser pulse with pulse duration up to 100 nanoseconds. The laser light is partially absorbed by the material within a small volume near the surface. Depending on the power density of the laser pulse, two possible mechanisms, thermoelasticity and material ablation, may contribute to the transduction of the ultrasonic energy.

In thermoelastic regime, low power-density pulse, typically $<10^7 W\ cm^{-2}$, results in a rapid local transient heating giving rise to sharp thermal gradient within the material [155]. The heated region then expands producing a thermal elastic strain and a corresponding stress that is the source of waves that propagating in the material and at its surface [156]. Thermoelastic transduction mechanism is entirely non-destructive. The penetration depth of the laser light and the amount of energy absorbed depend on the absorption characteristics of the material at the wavelength of the laser. Pulse duration is also important in order to operate in a nondamaging regime. In metals where absorption of visible or near infrared light takes place at or very near the surface of the material, the laser source gives rise in the far-field to directivity patterns for both the longitudinal and the shear bulk wave trace out a hollow cone radiating from the source point [156], [157]. In ablation regime, higher laser power density leads to the melting

and vaporization of a small amount of surface material. Material is ejected from the surface and results in recoil effect produces principal stresses normal to the surface and strong longitudinal waves travelling perpendicular to the surface. In this regime, a crater mark is left on the surface which although is not entirely non-destructive, the usual surface damage of a few microns is often accepted or insignificant for course materials.

When a point of laser light focused on the surface the direction of sound propagation from that surface is independent of the angle of incident for the laser beam. This allows for the flexibility of testing on material with irregular surface geometry, small footprint on the material surface, and significantly relaxes the constraints on a robotic scanning system which might be used to perform conventional UT. The transduction of the ultrasound does not require mechanical coupling between the transducer and external material. The optical access which the material absorbs light from the laser source is fully non-contact and remote. Therefore, laser ultrasonic inspection can be performed for harsh environment at elevated temperature or hazardous conditions.

For detection of the ultrasound, material surface is illuminated by a second laser beam, continuous or of pulse duration sufficiently long to capture all the ultrasonic signal of interest. The detection laser beam is scattered from the specimen's surface and directly detects the small fluctuation in surface produced by the ultrasonic displacements, which the light is collected by an optical receiver such as interferometer, or a non-interferometric device applying the schemes based on detection of the change of reflectivity produced by the ultrasound strain or the knife-edge technique [158], [159]. Laboratory design of the optical interferometric detectors are based on various sensing mechanisms [160]. The most basic principle is homodyne detection which uses two interfering beams that act as the reference beam and the sample beam, respectively. When ultrasound wave introduces displacement to the sample surface, modifies parameters of the sample beam, the evolution of the intensity of the interference allows for calculation of the temporal dependence of vibrational surface displacement [159]. Laser Doppler Vibrometers (LDV) are heterodyne interferometers, which measure the surface vibration using the principle of light beam modulation due to the Doppler effect. The displacement signal is reconstructed from optical phase modulation, and the surface velocity is obtained from the optical frequency shift.

To interpret the results, signals are processed to obtain high quality images using Synthetic Aperture Focusing Technique (SAFT) [161], [162] or Full Matrix Capture combined (FMC) with the Total Focusing Method (TFM) algorithm [163], [164] which have been initially developed for conventional PAUT. Two imaging algorithms were compared using same data collected from Laser Induced Phase Array (LIPA) technique and both showed good detectability outside the array aperture however the TFM had lower quality image which indicated lower defect sizing and characterization capability [164], [165]. LIPAs also have the advantages of using one-dimensional (1D) data to produce two-dimensional (2D) cross sectional image and 2D data to generate three-dimensional (3D) volumetric images [166].

Implementing laser-ultrasonics in industry is complex compared to conventional piezoelectric-based ultrasonics. So far, the applications have been explored, either lab-based or field-applicable, based on the distinguishing features of laser-ultrasonics such as non-contact, complex shapes, vert broadband, efficiency for surface wave generation and detection [156]. Laser ultrasonic technique has been successfully applied to image artificial defects in additive manufactured components [167], even for highly scattering titanium alloy [168], to detect multiple delamination defects in carbon fibre reinforced plastic (CFRP) composites [169], to monitor the process and indicate the position of solidification crack and the lack of penetration in the joint during welding process (Figure 30) without considering the temperature influence [170].

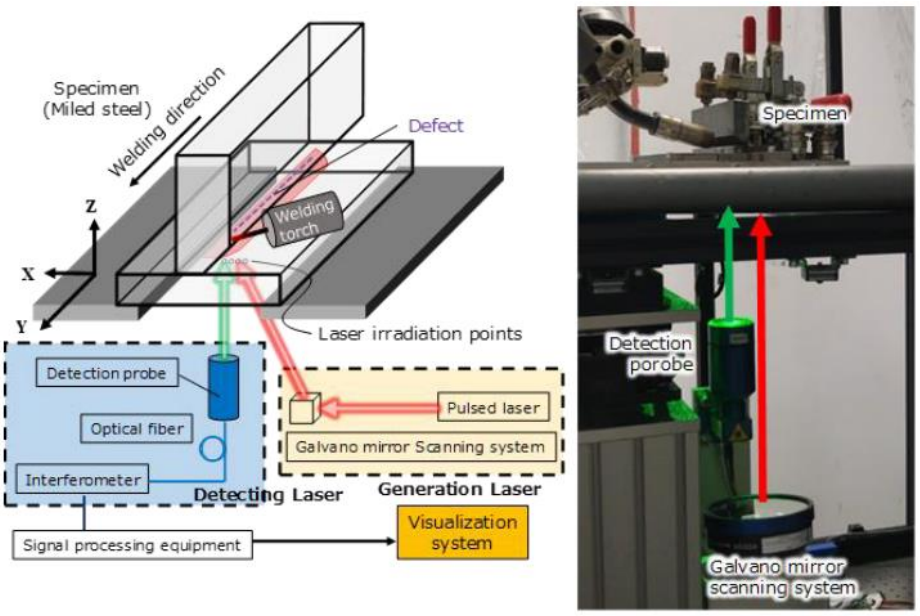

Figure 30 Schematic and experimental setup using laser ultrasonic technique for corner joints [170]

6.4 Electromagnetic testing

Eddy current testing (ECT) is an electromagnetic testing method used to inspect electrically conductive material. When an alternating current is passed through the coil, an alternating primary magnetic field is developed. This field expands and contracts as the alternating current rises and falls. When the coil is brought close to another electrically conductive material, the fluctuating magnetic field surrounding the coil permeates the material and induces an eddy current to flow in the material. These eddy currents induce a secondary magnetic field, which is opposed to the primary field, thus weakening it. As the strength and form of the secondary field is highly dependent on the magnetic properties and shape of the tested part, the resulting magnetic field can give insights about the geometrical and material imperfections and the discontinuities in the tested part.

ECs are affected by magnetic permeability of the materials. The greater the permeability the smaller the depth of penetration. For non-ferromagnetic materials, such as SS, Al and Cu with low permeability, ECT is used for surface and subsurface inspection. For ferro magnetic materials, such as ferritic steels, ETC can detect surface defects. The depth of penetration is varied by changing the frequency of the alternation current – the lower the frequency, the greater depth of penetration. However, the intensity of eddy current decrease exponentially with depth. Then the defect detection sensitivity is reduced, albeit the frequency is decreased to give greater penetration. As flow of EC is always parallel to the surface, thus EC will not detect a planar defect does not cross or interfere with the current. For all the reasons above, ETC is often used to inspect a relatively small area for surface and near surface defects such as corrosion damage and other damage that causes a thinning in tubing walls.

Advanced eddy current inspection techniques include Pulsed Eddy Current (PEC) and Eddy Current Array (ECA). PEC uses a stepped or pulsed input signal that consist of a spectrum of frequencies, which means each pulse signal contains information from a range of depths within a given test specimen. ECA shares the same basic principle as that of conventional ECT but reduces the additional movement such as surface probes or coaxial probes [171]. The difference is it uses multiple coils, e.g., pan cake coils, to cover large area thus scaling up the coverage of the probes while get effective reading of small defects in a single pass. Though rotating pancake probes have high inspection sensitivity, by scanning the inner surface of the tube following a spiral path in order to obtain both axial and circumferential information of the defect at the same time, the method has significant disadvantages of very slow testing speed and short probe service life [172]. Bobbin probe, in comparison, has the advantage of high testing speed but has limited detectability to outer defects especially circumferential cracks. To overcome the shortcomings, X Probe (Figure 31), for example, was developed for small-diameter tube inspection using ECA and bobbin coil in one tool for both axial and circumferential flaw detection without mechanical rotation or motors [173].

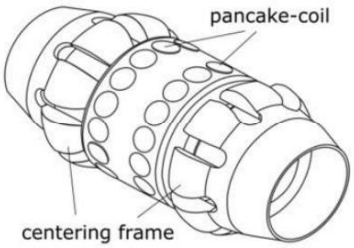

Figure 31: X-Probe: bobbin coil and high density, high speed ECA [173]

A novel array of ECT probes was proposed for small-diameter steam generator tubes for future Tokamak service [174]. The excitation of unit of the probe contains several large spiral shaped coils and the pick-up unit consists of four small pancake coils with rectangular arrangement (Figure 32). The detection signal is taken as the specific difference of the outputs of the four pickup coils. The unique coil arrangement and signal mode significantly reduces the wobbling noise due to both the probe lift-off change and inclination. Both numerical simulation and simplified experiments suggested the proposed configuration of the array ECT has outstanding performance for the inspection of both axial and circumferential crack in both inside and outside surface of the stainless-steel tubes.

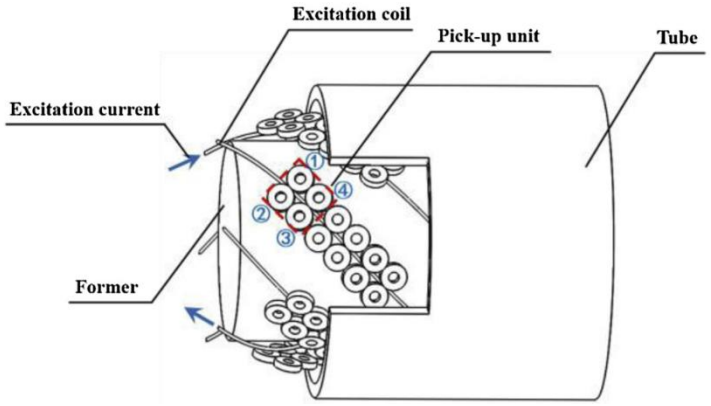

Figure 32 overall structure and arrangement of the array probe [174]

Multi-elements EC flexible probe was developed for inspecting of complex shaped surface [175], [176]. The probe is made of a thin Kapton film with etched micro-coils on it. The Kapton film is then adapted on a silicone roll in order to comply the specimen geometry, which could change according to the chose application (Figure 33). This technology has been evaluated on 316L stainless steel pipe section, with inner diameter of 160mm, to replicate the reactor residual heat removal pipes which have been subjected to heating cycles to create cracking and crazing induced thermal fatigue [175]. The examination picked up all major cracks on the inner surface of the component, even cracks as narrow as 20µm showed excellent signal to noise ratio. It is known EC performances are limited by the fact that the coil sensitivity decreases with frequency and size, an EC probe based Giant Magneto Resistance (GMR) sensor at low frequency was developed and successfully detected deeply embedded flaw located under a ligament of 7mm from the pipe outer surface without disturbance from the inner surface cracking [177].

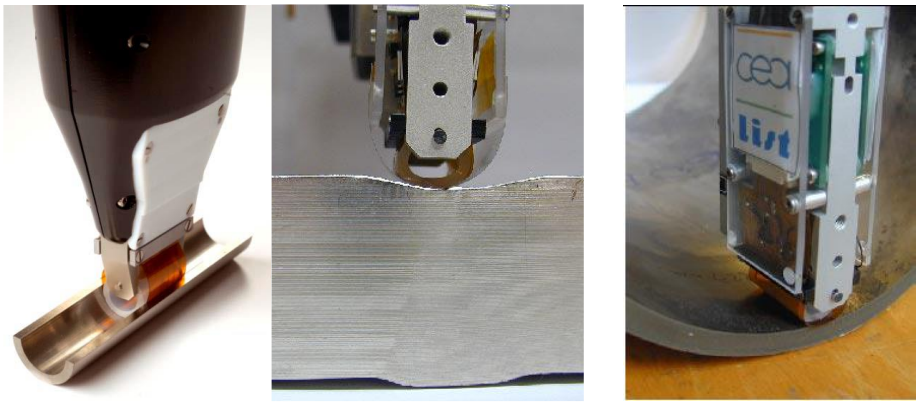

Figure 33 Flexible EC probe prototypes for complex shape inspection [175], [176]

EC probes with linear arrays of planar trapezoidal coils produced using Print Circuit Board (PCB) in a flexible

substrate, used alone or together with different winded drive coils, were developed for the inspection of the inner surface of the round-in-square profile jacket, made of JK2LB stainless steel, for ITER central solenoid conductor [178]. Five probes were proposed with different configuration in order to enhance the output signals and decrease the detectability threshold, for any orientation on the inner surface of the tubular components and provide information on the defect's axial and tangential position. Schematic representation of Probe with absolute planar trapezoidal spiral coils on a flexible substrate around a 3D printed cylindrical chassis as shown in Figure 34.

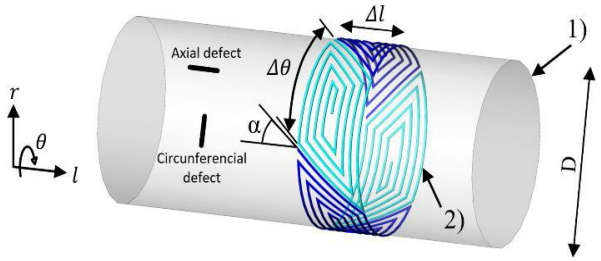

Δl – width of the trapezoidal coils
α - angle between 2 consecutive coils, approx.45°
D [m] - pipe perimeter
Δθ [m] - length of each trapezoidal coil

Figure 34 Schematic representation of the probe with absolute planar trapezoidal spiral coils. Legend: 1) Cylindrical chassis; 2) Trapezoidal spiral coils. [178]

Compared to the conventional EC probes that composed of planar circular spiral coils, a trapezoidal spiral coil configuration can avoid the blind zone and cover the whole pipe perimeter. In addition, the spatial resolution of the probe is superior with same number of coils in the array when circular or rectangular spiral coils are used. Additional probes were also designed to operate on a reflection mode, where the array of trapezoidal coils was the pickup coil, and the excitation windings were designed in circumferential, axial, helical, and twisted configuration, respectively [178]. Tests were performed both numerically and experimentally. Reflection type probes presented enhanced signals compared to the absolute type. Artificial defects were produced on a round-in-square jacket with a pipe inner diameter of 35.5mm. Probe with twisted excitation windings and trapezoidal sensing coils (Figure 35), evidenced a superior reliability to be able to detect all defects, with a depth of 0.5 mm, in any scanning position.

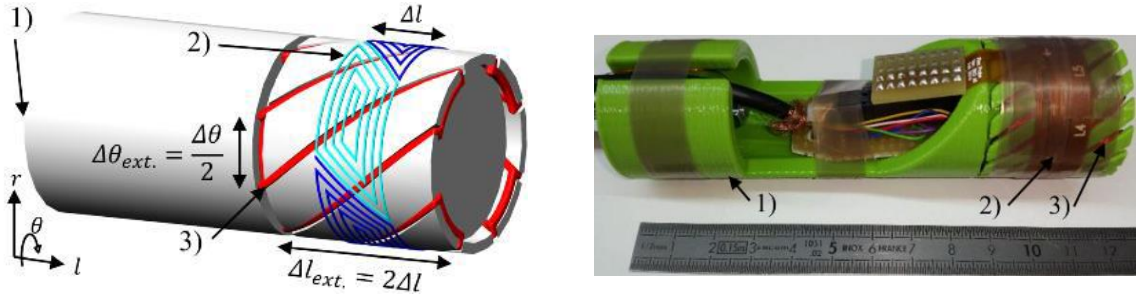

Δl – width of the trapezoidal coils, Δθ [m] – length of each trapezoidal coil,
Δl_{ext} – width of the excitation coils, $\Delta\theta_{ext}$ [m] – length of the excitation coil.

Figure 35 Schematic representation and functional prototype of the probe with twisted excitation windings and trapezoidal sensing coils. Legend: 1) Cylindrical chassis; 2) Trapezoidal spiral coils; 3) Twisted winding [178]

Applicability of ECT for ITER blanket module hydraulic pipes material was investigated numerically and experimentally [179]. Laser welded 3mm-thick SS316 plates were artificially introduced with surface holes and slits to represent weld detects. A 'plus point' probe from Zetec. Inc. was used to sweep along the weld line on the same and opposite sides of the defects, applying frequencies at 50and 70 kHz. In addition, Frequencies below 30 kHz were investigated by numerical analysis. Results suggested ETC has great potential for surface defects inspection for ITER pipe welds, which the slit-like detects on the opposite side of the test part can even be detected using optimised measurement conditions. However, it was more challenging to detect the hole-like defects from the back wall.

Though the term 'electromagnetic testing' is often to imply just ECT, with an expanding number of electromagnetic and magnetic testing methods and this term now is more frequently used to define the whole class of electromagnetic testing techniques. Magnetic flux leakage (MFL) is a magnetic testing technique which is often involved in detecting corrosion and pitting in steel structures such as oil and gas pipelines and storage tanks. It is also widely used to detect cracks in both the axial and circumferential directions in the pipes with a PIG (Pipeline inspection gauge) tool [180], [181]. An example of a circumferential MFL PIG system is shown in Figure 36. The tool consists of a magnetizer (back yoke) with circumferentially distributed hall sensors and permanent magnets.

Brushes are typically act as a transmitter of magnetic flux from the tool into the material [182].

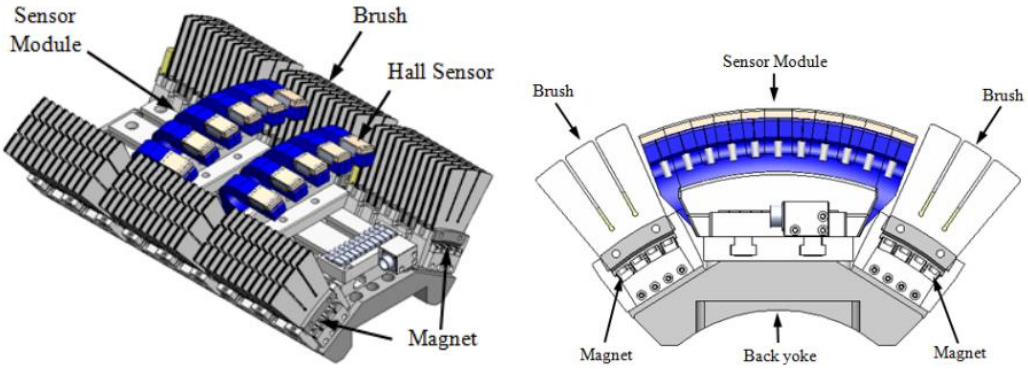

Figure 36 Design of circumferential MFL PIG system [182]

When a steel pipe wall is magnetised, a magnetic circuit is created. Most of the magnetic flux is constrained in the materials when no defects are presented until the high field MFL tools saturate the pipe wall then it no longer holds any more flux at the defects site. Magnetic permeability at the defect site is much smaller and magnetic resistance will increase so the magnetic field in the region is distorted and even leaking out of the pipe wall [180], [183]. The magnetic sensors, such as induction coils, Hall components, magnetic flux gates, magnetic sensitive diodes and transistors, and magnetic resistances, giant magnetoresistance (GMR) based sensors, etc. then transform the magnetic signals into electrical signa [180], [184].

Magnetic particle inspection (MPI) is often used to defect near and sub surface defects in ferrimagnetic materials and is primarily used for crack defection. Similar to the MFL, components to be inspected are magnetized and a magnetic field is generated with field flux sustain within the workpiece and parallel to the surface. To identify a leak, fine ferromagnetic particles, either dry or in a wet suspension, are applied to the surface which will be attracted to the flux leakage and form what is known as an indication. MPI is a quick, portable, and fairly inexpensive technique. It allows the results visible and indicates the defects immediately on the surface of the material. It also can inspect parts with irregular shapes. However, this technique is only effective on ferromagnetic materials and in most conditions the maximum depth sensitivity is approximate 0.1 inch. It is also not viable for remote application in nuclear environment as demagnetization is required after inspection and potentially post cleaning to be perform if the paint is thicker than 0.005 inch.

Alternating current field measurement (ACFM) is a non-contact electromagnetic inspection technique which introduces a uniform alternating current into the surface of a component and measures the associated electromagnetic fields close to the surface to defect and size the cracks [185]–[187]. The magnitude of any disturbance in the magnetic field can then be relayed back to the size of defect causing them using mathematical models. ACFM is a technique that performs immediate defect sizing and recording and often used for in-service inspection as an alternative to MPI and penetrant testing (PT). It works on all metals, ferrous or non-ferrous at elevated temperature in excess of 500°C. This technique has been widely used for weld and thread inspection and for subsea inspection of offshore platforms. In addition, due to the non-contact nature, this technique can be used to inspect through paint and coatings.

Remote field testing (RFT) is also referred as remote field eddy current testing, which uses low frequency alternating current to introduce an electromagnetic field in the material to be inspected. It is often used to inspect ferromagnetic tubular product which in comparison difficult to achieve using conventical ETC due to the strong skin effect. This technique can be used to detect flaws on both inner and outer surfaces of the tube, but not distinguished, and it is also used to discover all loss and changes in wall thickness.

6.5 Electromagnetic waves

X-rays and gamma rays, sitting at the end of the electromagnetic waves spectrum, span the range from low energy (keV) to high energy (MeV) photons, respectively but not always. Radiographic Testing (RT) involves using of either X-rays or gamma rays to view the internal structure of a component. It is often used in industry to locate and quantify defect and degradation of weldments and cast parts, that would lead to structure failure. After crossing the specimen, photons are captured by a detector, such as a silver halide film used in conventional radiography.

X-ray is generated by applying high voltage between the cathode and anode of the X-ray tube and in heating the

tube filament to start the electron emission. The electrons are then accelerated and then directed this stream of high-speed electrons at a target material. When the electron slowed or stopped by the interaction with the atomic particles of the target material, X-ray is produced. X-ray generators have been designed as stationary units for lab use or portable systems suitable for onsite jobs. Most new systems use constant potential generators to produce a constant stream of relatively consistent radiation. Flash X-ray generators are useful when examining objects in rapid motion or when studying transient events as they produce microsecond, intense burst of radiation.

Digital radiography is the generic term for radiographic techniques that detect x-rays with digital sensors instead of photoplates or photographic films. Compared to conventional film radiography, digitalization significantly reduced the effort of generating and administrating X-ray images. Digital pictures archiving and distribution are far easier than before, and subsequent image processing is made possible. Typical representatives of this technology (Table 4) are Computed Radiography (CR), Direct Radiography (DR), real-time radiography (RTR) and computed tomography (CT).

Table 4 Comparison of the digital radiography technologies and their image detectors

Digital radiography	Image readout	Examples of the digital sensors	Output image	Advantages
CR	Indirect	phosphor plate	2D	Imaging plate is reusable. Information to be erased by exposing it to the room-intensity white light.
DR	Direct	digital detector or a linear diode array	2D	shorter exposure time and instantaneous image interpretation
RTR	Simultaneously while the radiation passing through the object	special phosphor screen or flat panel detector that containing micro-electronic sensors	2D	Real time image viewing and analysing, industrial application ready
CT	3D virtual reconstruction and sectional images by superimposing a set of 2D projections	digital flat panel detector or charge-coupled device camera	3D	detailed morphologic virtual reproductions of parts of a body or other specimens

Compared to other NDT techniques, RT has the advantages of being highly reproducible. It can be used on a variety of materials and data gathered can be stored for later analysis. It required little preparation of the material surface. Moreover, many radiographic systems are portable and can be purchased off-the-shelf, plus robotic technology services, allows for their use in the field and at elevated positions. Portable X-ray generators from Golden Engineering, Inc. have been widely used in industrial inspections. They are battery-powered, light-weighted, pulsed X-ray technology that compatible with most digital imaging system such as inspection acquisition and control software developed by OR Technology. OR systems are designed either in a compact suitcase or backpack size with all components fit in, providing direct digital X-ray solutions (Figure 37).

Figure 37 Leonado DR systems developed by OR Technology, connecting to X-ray generator from Golden Engineering, Inc. (Image courtesy of OR Technology website)

Test of the efficiency of digital radiography was conducted both in the lab and in the field [188]. Lab trials (Figure 38) were carried out on carbon steel 5355 pipe structure with a few internal known defects, such as slag, undercut, corrosion, porosity, and cracks, in various joint configurations. A Vidisco Ltd. foXRayzor portable X-ray inspection system which contains the flat amorphous Silicon panel with Golden XRS-3, a 270kV pulsed X-ray source was used. The results captured all the defects successfully and the digital images were of higher quality than conventional film method. In addition, data archiving in a digital data base improved analysis and

documentation.

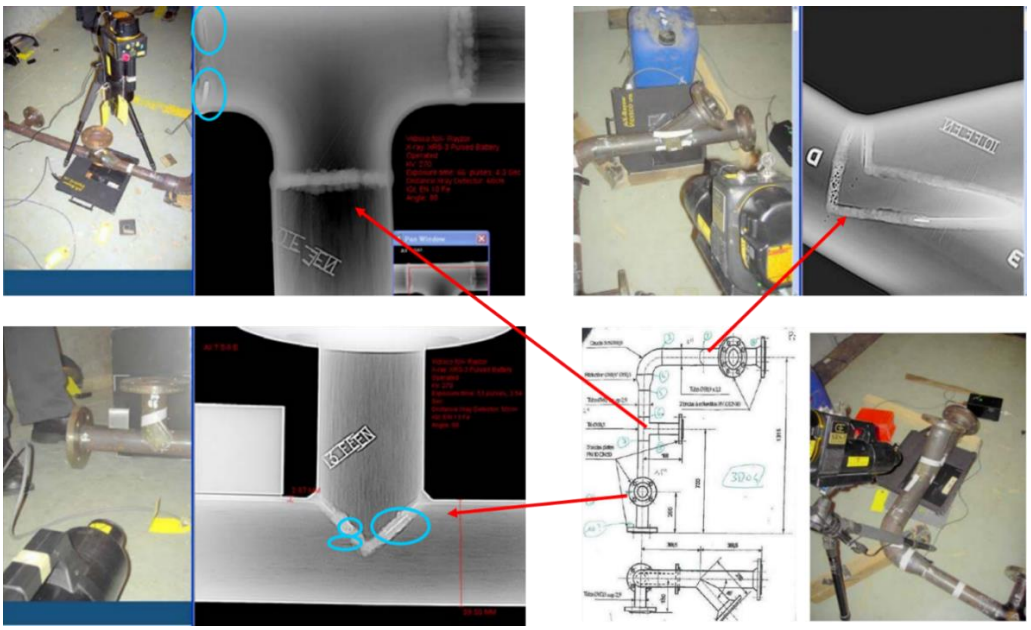

Figure 38 Setups and digital images from portable X-ray equipment in the pipe structure [188]

Gamma-rays are generated from the radioactive decay of atomic nuclei. They consist of the shortest wavelength electromagnetic waves, typically shorter than those of the X-rays. Two common industrial gamma-ray sources for industrial radiography are Iridium-192 and Cobalt-60. They produce higher energy compared to X-ray which make it possible to penetrate thick materials with a relatively short exposure time. Therefore, these manmade sources are made to be portable and used for field radiography. The disadvantage of a radioactive sources is that it can never be turned off and safely managing the source is a constant responsibility.

In field test was carried out in one of the TOTAL refineries in France, using an Ir192, 16Ci gamma ray source and amorphous silicon flat panel [188]. The images appeared on the screen in real time with good quality, without the need for development or scanning. The setup of the digital portable inspection system Vidisco foX-Rayzor in the refinery site is shown in Figure 39. Advanced software tools were used for image process which makes the onsite analysis quicker and accurate. Further study was made in the lab, using the same system, for a comparison between Golden XRS-3 pulsed X-ray source and the gamma ray source, which suggested in laboratories and in field NDT portable X-ray system made analysis easier due to sophisticated enhancement software. Results were immediate and images were of the highest quality.

Figure 39 Setups of the portable digital radiography system in TOTAL refinery [188]

A recent publication reported an automatic inspection system (Figure 40) for multi-layered flexible riser for subsea applications [189]. The prototype demonstrated the capability to deploy an in-situ radiography-based inspection robot that could provide precise scanning motion of a gamma ray source and digital detector moving in alignment. Test was carried out on a flexible riser during shallow water sea trials with the system placed around a riser by a remote operated vehicle.

Inspecting the pipe from outside requires the source passing through double pipe wall before reaching the detector. Defects showing on the images may be from either wall. An in-bore solution has been proposed that allows for

single wall to be inspected [190]. The concept is explained in Figure 41 in which an irradiation rod, with a low energy isotope Ir192 gamma source guide tube, is adapted to the robotic system. The low energy isotope is propelled, by a hand crank, from the source projector though the source guide tube to the exposure position. Films are placed outside the pipe wall to collect photons.

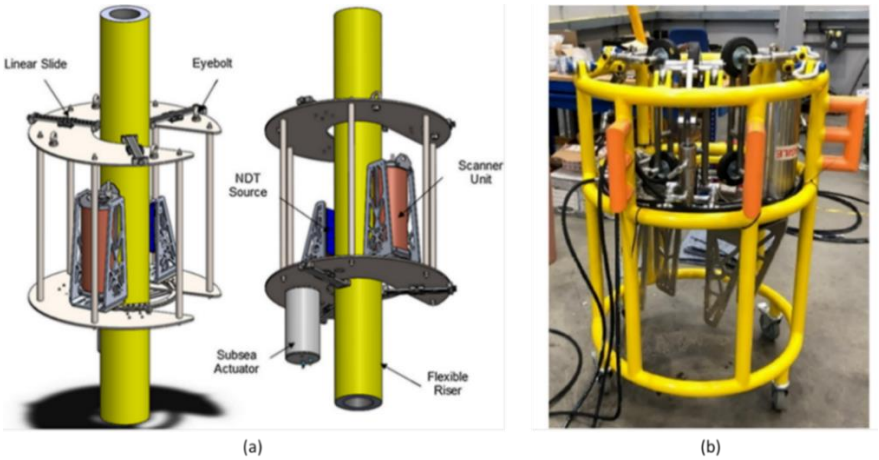

Figure 40 Robotic scanner system prototype with gamma ray source for subsea riser inspection (a) 3-D model and (b) actual mechanical assembly [189]

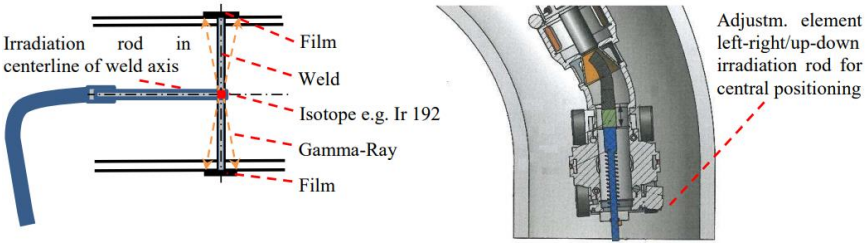

Figure 41 Schematic radiographic exposure- single wall technique on girth well and the RT-module with irradiation rod position at pip bend [190]

Infrared thermography (IRT), also known as thermal video or thermal imaging, is a process where a thermal camera captures and creates an image of an object by using infrared radiation emitted from the object. The amount of radiation emitted by an object increased with temperature, therefore, thermography allows one to see variation in temperature. IRT is a non-destructive testing method which distinguishes between active and passive applications. Passive thermography observes the heat emission of an object without influencing its temperature, while in active thermography, an energy source is introduced to the specimen to produce a thermal contact between the feature of interest and the background. Using either method, the presence of a defect causes an anomaly in the response of the inspected specimen. Active IRT have been used as a non-contact NDT technique for metallic weld inspection [191]–[194]. Once the material is excited and the heat distribution during heating and cooling is recorded. If the material is uniform and no presence of surface breaking or subsurface defects the thermal wave will dissipate rapidly through the material, whereas a defect will retain the heat for longer in response to the surface temperature distribution [195]. The thermal camera will monitor the evolution of infrared radiation from the surface of the object.

There are three main excitation mechanisms for crack detection in metal: electromagnetic, optical or mechanical, of which the first two are non-contact [196]–[200]. Induction thermography has demonstrated crack detectability using induction coil, which the crack disturbs the distribution of the locally induced eddy currents around it thus causes a local inhomogeneous heating around the crack [199], [200]. The optical methods employ light excitation using laser, high energy lamp or UV lamp, illuminate the test piece[197], [198]. Normally metals reflect a large amount of the light due to low emissivity and absorptivity. The absorbed light heats the surface slightly. If the light enters a crack, it will reflect multiple times before it can leave therefore deposit a large amount of energy in the crack. Therefore, the crack will be heated up more than the surrounding that illuminated with high intensity light [197]. Scanning laser source has also demonstrated suitability to detect surface breaking defects. Any lateral flow of heat is disturbed by such a defect with a change in thermal spot shape or by an apparent increase in temperature and then was detected by an infrared camera [201]. However, the major disadvantage of using thermography on

metal structure is reflections of infrared radiation from hot objects from surroundings, such as the excitation site and metal surface, which will decrease the signal to noise ratio[198].

Heat excitation in optical techniques can be either pulsed or lock-in. Pulsed thermography testing has been well-developed and widely used in high-speed inspection, coverage of large area and online inspection convenience. However, it is limited by structural geometry, object thickness and high requirement for the uniformity of the pulsed heat source. In term of excitation source, pulse laser has shown better crack detectability and easier control of heated area and pulse length, compared to flash lamp, on both artificial notches and real cracks in metallic welds [197]. Infrared lock-in thermography uses periodic modulated heat waves to heat the specimen and the data is recorded in stationary domain [194], [195]. The presence of a defect leaves a periodical effect on the surface distribution, also showing up as a phase difference between the defective and non-defective area. This technique is not affected by uneven heating compared to pulsed method; however, multiple trials may be needed to confirm the optimal modulation frequencies. In addition, when it comes to automation, it is more time consuming than pulsed thermography [192].

In addition to the heat sources excitation parameters, other factors affecting the detection accuracy include thermal imaging system, heat flow injection direction, environmental factors, and material and defect parameters [195]. Once performed the inspection, collected IR data by the camera may be processed with noise reduction, image enhancement and reconstruction, special processing and patterns recognition and temporal analysis of the selected area [193]. Because the original image may gain high noise from the interference of various aforementioned factors such as material surface optical conditions, which influence the emissivity, could directly cause results misinterpretation and noise, image processing is an indispensable step to eliminate the interference of adverse factors, increase the signal-to noise ratio and enhance the displace of defects.

Microwave and millimetre waves occupy the frequency spectrum ranging from approximate 300 MHz to 30 GHz and 30 to 300 GHz, corresponding to wavelengths of 1000 to 1 mm, respectively [202], [203]. Figure 42 shows where these considered methods lie on the electromagnetic spectrum with respect to other common NDT&E methods. Materials interact with these waves in ways that make them extremely useful for certain NDT applications. Waves at these frequencies generally do not penetrate highly conductive materials such as metals or carbon-based composites due to the limited skin depth which describes the extent to which waves penetrate and decay in conductors or lossy dielectrics [204]. Despite this, microwaves still interact with the surface of the conductive materials and these techniques have been studied for detecting tight surface-breaking cracks in metals [205]–[207]. Terahertz radiation, also known as submillimetre radiation, sits between the infrared and microwave region with frequency between 300GHz and 3000GHz (3THz) and corresponding wavelength from 1mm to 0.1mm. Similar to microwaves, Terahertz radiation can penetrate a wide variety of non-conducting materials but not metals. Ground Penetrating Radar (GPR) transmit electromagnetic waves (in the range of 10-1000MHz) in to probed material and receive the reflected pulses as they encounter discontinuities. This method is often used to locate cracks, objects and other hazards in concrete structures such as bridges, walls and dams, etc. Although Radar is the only remote sensing technology that can detect both conductive and non-conductive material, it cannot penetrate metal for detailed inspection.

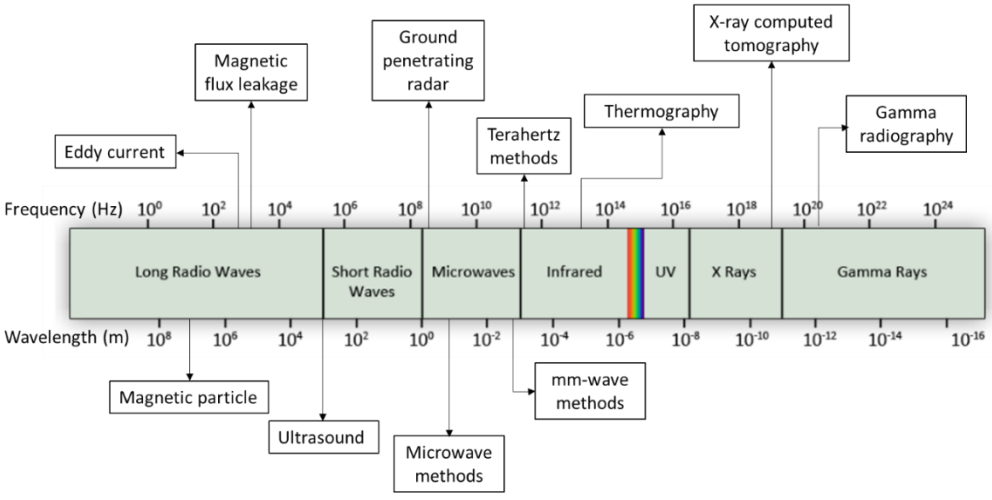

Figure 42 Inspection frequency ranges of varies NDT&E techniques against electromagnetic spectrum [203]

6.6 *In-pipe robotic NDE*

In-pipe inspection robot that move inside pipelines are widely used to perform inspection operations. In-pipe robots can be categorised, according to moving patterns, as PIG type robot, wheel type robots, caterpillar type robots, wall-press type robots, walking type robots, inchworm type robots and screw type robots [208]–[212]. PIG type robots, for example, are most well-known commercially available for oil and gas industry. The movement of the PIG is passively driven by the fluid pressure. It is widely used for leak detection, corrosion-erosion inspection and thickness measurement [213]–[216].

Wheel-driven inspection robots are most researched types [211], [217]–[223]. Wheels that powered by actuator are in contact with the surface while moving. Simple structured wheel drive robots are mostly used for horizontal pipe inspection. The screw type robots are also a type of wheeled robot but with better steering characteristics. Forward movement of the robot in a pipeline is achieved by the helical motion of the wheels, such locomotion is unlikely to damage pipe inner wall as the robot does not drag its body [224]–[228].

Instead of using wheels, caterpillar type robots move inside the pipes on tracks, which increase the surface contact area therefore, traction and stability [229]–[233]. Wall-press type robots, using either wheel or caterpillar to realise locomotion, have the advantage of climbing vertical or inclined pipelines with appropriate adhesion such as spring tension to establish contact within the robot and the surface [232]–[237].

The waking robots and inchworm robots are non-wheeled types. The walking robots process articulated legs to produce sophisticated motions inside the complicated pipe geometries and internal environments[238]–[241]. Inchworm type robot is one of the bio-inspired robots. Their movement is achieved by repetitive contraction and expansion actions to propel the robot forward, which have slower driving speeds and generate a lot of friction while moving[242]–[246]. They are well suited for pipeline with small diameters.

Continuum robots, characterized by infinite degrees of freedom and number of joints, have been studied increasingly in recent years. Inspired by snakes or trunks, continuum robots are jointless, compared to the conventional robots, and with backbone structures that capable of continuous and actuatable bending [247]–[249]. A continuum robot can be made of many compliant elements or a single flexible body and actuated by transmitting the motion along the backbone through tendons, concentric tubes, and rods, or local control over the backbone shape through pneumatic, shape memory alloys, and magnetic methods (Figure 43).

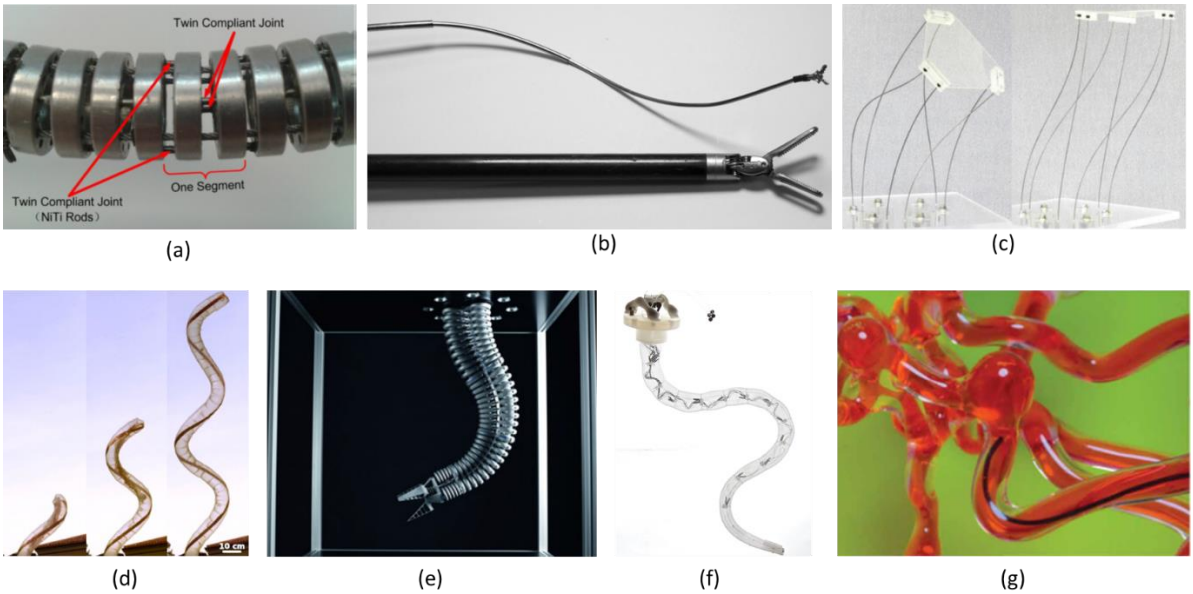

Figure 43 Continuum robots actuation principles: (a) tendon-driven [250], *(b) Concentric tube* [251], *(c) Parallel continuum Stewart-Gough platform* [252], *(d) Soft inflatable* [253], *(e) Festo's Bionic Handling Assistant with pneumatically actuated bellows* [254], *(f) Shape Memory Alloy* [255], *(g) Magnetically actuated by magnetic composite polymers* [256]

Owing to the low diameter to length ratio and flexibility, continuum robots are suitable to deploy tools though tortuous paths and work in the in the hard-to-reach area, confined space, and highly unstructured environment for non-destructive inspection, repair, and operation[249], [257]–[263]. Continuum robots have shown great potential being used or developed for use in aerospace and nuclear industrials.

Pipe inline inspection robotics may require the tool to be able to traverse the entire length of the pipe and reach a specific location without getting stuck. Both tethered and un-tethered robots share similar challenges including:

- Ensuring the energy source efficiently feed all electrical and electromechanical components such as electronic circuit, motors, etc., especially in tether-free operation, robot must totally rely on on-board resources.
- Carrying out inspection with expected accuracy and safely storing and transmitting the data to the outside world. Robot may be programmed to handle all situations that arise during its traversal of the pipe.
- Miniaturizing the parts and components due to small pipe diameters and complicated pipe configurations. Robots may also have to traverse sharp angle such as bends and elbows, imposed constrains on the shape and dimensions of the mechanical parts as well as on the packaging of the electronics, and selection of locomotion mechanism.
- Designing NDE sensors for pipe material and pipe defects [264]. For example, MFL and UT are popular for ferromagnetic pipes. and EC and remote field Eddy Current are utilized for non-ferromagnetic metallic pipes. Butt welds inside the pipe act as mechanical obstacles that would disturb the bond between the detector ad reflector of a UT sensor. They would also damage the MFL sensor components that must operate very closed to the pipe wall.

7 Discussion and needs for further research

The challenges and opportunities identified in this review suggest that the development of remote in-situ maintenance technologies for fusion reactor pipework must focus on customizing and upgrading existing technologies as well as testing out the emerging technologies under researching, taken into account other relevant technological limitations. The design requirements of the fusion device, such as pipework structures and material characteristics, primarily influence on the selection of the joining, cutting and inspection methods as well as tooling development.

7.1 Discussion

In terms of welding solutions, both laser and TIG welding techniques, demonstrated in previous work have showed their own advantages and disadvantages under different environmental constraints. TIG welding is very versatile and can be used on various materials. The process does not produce fumes or smokes during welding and is a safe process overall. It has great reliability in terms of power delivery, process control and in general achieving consistent good weld quality if applying appropriate process procedures. In the case of welding thicker sections, laser welding has the advantage of producing a weld with high precision, deep penetration, and potentially achieving with single-pass process where the joint has narrower heat-affected zone therefore less distortion. The process is much faster so that the downtime for the maintenance of the power plant can be significantly reduced. In contract, TIG welding has to adopt multi-pass process with filler material. Although the gap tolerance between the parts is higher than that of required in laser welding, mastering the stability of the arc while feeding the filler to the molten pool requires special equipment and sophisticated mechanisms when welding remotely. Besides, defects such as tungsten inclusions can be generated during the process which is not an issue in laser welding. However, it has not been fully proved the viability of using laser as the power source for pipe welding and cutting processes on nuclear fusion components. The generation of large amount of heat during welding and/or cutting requires efficient heat dissipation to allow the equipment stay cool thus functioning. For most industrial or bench top setups water is used for cooling which is not compatible to the stringent environment in fusion devices. Plus, the requirements of size reduction of the laser equipment and robust optics for energy transmission makes it extremely challenging using high-power laser in confined space.

The approval of the compliance of the welds by NDE procedures are critical to ensure the structural integrity of the joint in the subsequence service life. In practice, in other industrial piping systems, NDEs are conducted for leak tight proof as well as flaw quantification and qualification, which, however, standardised procedures cannot be directly applied to assess the welds in fusion operating environment. Factors such as high temperature, high radioactivity, mechanical vibration, coolant corrosion, etc. that contribute to defect coalescence and growth can lead to the acceleration of structural failure. Although some of the off-the-shelf probes and sensors have showed potential in previous feasibility studies, under complex environmental impact, one technique is limited to the material type and material thickness, allowable defect detectability, sizing capability, and inspection sensitivity. Development should be focused on exploring novel techniques published in the research domain and assessing their viability for fusion applications. Customizing existing probes and sensors those already applied in similar industries and develop tools using combines techniques that complement each other.

The ultimate goal of maintaining the pipes in the fusion device is to carry out the activities vie RH tools and robotic

deployment strategies. Although pipes are in simple geometries, the entire cooling system is complicated, and the material conditions are unknown after a period of operation. Autonomous robots need to be deployed with essential sensors and tools, that can provide accurate localization, map internal environment, and conduct inspections and maintenance tasks, at the locations of interest. Bench top equipment used for process development is often designed to achieve maximum working envelope and with the flexibility to attach auxiliary tools or sub systems. Transferring process developed in a lab-based environment is facing the challenge of tooling miniaturisation for the activities performed in a confined space, which requires size reduction of the end effectors and robotic hardware without compromising the performance. In fusion reactor especially in-vessel environment, deploying robotics with added functionalities and high payload manipulation capability will also lead to the increase of size and weight of the hardware, therefore more power consumption and complex actuation and control. Robot with extra-long but rigid body that deployed inside the pipe has the risk of getting stuck at the pipe bends and unknown constrains, which requires retrieve, recovery and rescue strategies. Depending on the location and necessary mission, deployed systems may be subjected to high level of radiation, which vulnerable materials and components degrade quickly, leaving the tasks uncompleted, affecting the quality and transmission of collected data, and overall maintenance efficiency. Consequently radiation-hardened systems and components are also indispensable in nuclear fusion.

7.2 Areas requiring further attention

Future fusion devices may have their unique characters, the development of RH strategies and remote in-situ pipe maintenance are driven by the design requirements. Areas to further research in the future are recommended in the following aspects:

- Developing in-bore welding tools and process procedures for joining of thick materials using laser and TIG techniques. Delivering high power laser beam through optical fibre and miniaturized equipment with improved cooling and advanced optic design, aiming to achieving the joint in a single-pass process. Investigating the feasibility of multi-pass TIG welding using filler material, though challenging in terms of process control and complex setups, less stringent fit-up requirement brings benefit for remote process.
- Cutting strategies are dependent on the needs of the processes during maintenance. Laser beam cutting is recommended for disassembling the pipe and plasma-facing interfaces owing to its fast process speed. In the case of higher cut quality is required for subsequent re-welding, mechanical cutting and/or post machining must be applied, with compromised operation efficiency.
- In existing industrial approved NDE technologies, ECT is the most promising solution for inspection of thin-walled the structures and better detectability on stainless steels, such as ITER cooling pipes. For thicker pipe walls, non-contact, couplant-free, laser ultrasonic inspection has great potential to fit for fusion environment and must be further researched. Area worth of exploring include size reduction of instrumentation, improvement of scan speed and data transmission, and investigation of fusion environment compatibility such as high-temperate performance and radiation resistance, etc. Similarly, efforts are to be made to improve the radiation resistance of RVI components such as cameras and optical fibres.
- In addition to employing welding as the primary joining solution that considered in the current fusion device design, mechanical connections in conjunction with fusion or non-fusion welding (sealing) can provide high flexibility and reversibility for pipe structures at critical locations in the future fusion reactors, assuming the engineering design comes with extremely thick-walled pipe to cope with even higher temperature, radiation doses or if the material is non-weldable.
- With clearly addressed engineering and design and maintenance requirements, other tools may be required for pipe alignment, pre- and post- weld heat treatment, inner wall coating, defective part repair, contamination cleaning, etc. Among all the untacked challenges and emerging issues in fusion pipe maintenance, research in the future should focus on exploring of the unknown and developing in-pipe robotics and tools with RH compatibility and high tolerance to environmental constraints.

8 Acknowledgements

This work has been funded by the EPSRC Energy Programme [grant number EP/W006839/1]. To obtain further information on the data and models underlying this paper please contact PublicationsManager@ukaea.uk.

Reference

[1] I. T. Chapman and A. W. Morris, "UKAEA capabilities to address the challenges on the path to delivering fusion power," in *Philosophical Transactions of the Royal Society A: Mathematical, Physical and Engineering Sciences*, Royal Society Publishing, Mar. 2019. doi: 10.1098/rsta.2017.0436.

[2] "Nuclear Fusion Power," https://world-nuclear.org/information-library/current-and-future-generation/nuclear-fusion-power.aspx.

[3] X. Litaudon *et al.*, "Overview of the JET results in support to ITER," *Nuclear Fusion*, vol. 57, no. 10. IOP Publishing Ltd, Jun. 15, 2017. doi: 10.1088/1741-4326/aa5e28.

[4] M. Shimada *et al.*, "Chapter 1: Overview and summary," *Nuclear Fusion*, vol. 47, no. 6, Jun. 2007, doi: 10.1088/0029-5515/47/6/S01.

[5] G. Federici, W. Biel, M. R. Gilbert, R. Kemp, N. Taylor, and R. Wenninger, "European DEMO design strategy and consequences for materials," *Nuclear Fusion*, vol. 57, no. 9, Jun. 2017, doi: 10.1088/1741-4326/57/9/092002.

[6] G. Federici *et al.*, "Overview of EU DEMO design and R&D activities," in *Fusion Engineering and Design*, Elsevier Ltd, 2014, pp. 882–889. doi: 10.1016/j.fusengdes.2014.01.070.

[7] C. Damiani *et al.*, "Overview of the ITER remote maintenance design and of the development activities in Europe," *Fusion Engineering and Design*, vol. 136, pp. 1117–1124, Nov. 2018, doi: 10.1016/j.fusengdes.2018.04.085.

[8] T. Tremethick, S. Kirk, K. Keogh, A. O'Hare, E. Harford, and B. Quirk, "Service Joining Strategy for the EU DEMO," *Fusion Engineering and Design*, vol. 158, Sep. 2020, doi: 10.1016/j.fusengdes.2020.111724.

[9] K. Keogh, S. Kirk, W. Suder, I. Farquhar, T. Tremethick, and A. Loving, "Laser cutting and welding tools for use in-bore on EU-DEMO service pipes," *Fusion Engineering and Design*, vol. 136, pp. 461–466, Nov. 2018, doi: 10.1016/j.fusengdes.2018.02.098.

[10] O. Crofts and J. Harman, "Maintenance duration estimate for a DEMO fusion power plant, based on the EFDA WP12 pre-conceptual studies," *Fusion Engineering and Design*, vol. 89, no. 9–10, pp. 2383–2387, 2014, doi: 10.1016/j.fusengdes.2014.01.038.

[11] JET Team (prepared by M.A. Pick), "Development of key fusion technologies at JET," *Nuclear Fusion*, vol. 40, no. 3Y, pp. 611–618, 2000.

[12] A. C. Rolfe, "A perspective on fusion relevant remote handling techniques," *Fusion Engineering and Design*, vol. 82, no. 15–24, pp. 1917–1923, Oct. 2007, doi: 10.1016/j.fusengdes.2007.04.049.

[13] R. Shuff and S. Mills, "A Study of Pipe Jointing Technology with Reference to ITER Requirements," *Fusion Engineering and Design*, vol. 84, no. 7–11, pp. 1767–1769, Jun. 2009, doi: 10.1016/j.fusengdes.2008.11.007.

[14] S. F. Mills, A. Loving, and M. Irving, "The design, development and use of pipe cutting tools for remote handling in JET," in *Proceedings - Symposium on Fusion Engineering*, Institute of Electrical and Electronics Engineers Inc., 1991, pp. 559–562. doi: 10.1109/FUSION.1991.218859.

[15] T. L. Martin *et al.*, "INSIGHTS INTO PROSPECTIVE FUSION REACTOR COOLING SYSTEMS FROM FISSION REACTOR COOLING CIRCUITS," in *Conference19th International Conference on Environmental Degradation of Materials in Nuclear Power Systems - Water Reactors, EnvDeg 2019*, Boston, Aug. 2019, p. 10.

[16] N. Baluc *et al.*, "Status of R&D activities on materials for fusion power reactors," *Nuclear Fusion*, vol. 47, no. 10, Oct. 2007, doi: 10.1088/0029-5515/47/10/S18.

[17] H. Tanigawa *et al.*, "Development of benchmark reduced activation ferritic/martensitic steels for fusion energy applications," *Nuclear Fusion*, vol. 57, no. 9, Jun. 2017, doi: 10.1088/1741-4326/57/9/092004.

[18] K. Li, M. A. Klecka, S. Chen, and W. Xiong, "Wire-arc additive manufacturing and post-heat treatment optimization on microstructure and mechanical properties of Grade 91 steel," *Addit Manuf*, vol. 37, Jan. 2021, doi: 10.1016/j.addma.2020.101734.

[19] v. K. Sikka, C. T. W. a, and C. T. W. a, "Modified 9Cr1Mo Steel – An Improved Alloy for Steam Generator Application," in *Ferritic Steels for High-Temperature Applications*, A. K. Khare, Ed., OH: American Society for Metals, Metals Park, , 1983, pp. 65–84.

[20] F. V. Ellis, J. F. Henry, and B. W. Roberts, "Welding, Fabrication, and Service Experience with Modified 9Cr-1Mo Steel," in *New Alloys for Pressure Vessels and Piping, PVP*, NY: American Society of Mechanical Engineers, 1990, pp. 55–63.

[21] V. K. Sikka, "DEVELOPMENT OF MODIFIED 9 Cr-1 Mo STEEL FOR ELEVATED-TEMPERATURE SERVICE*," in *TMS/AIME topical conference on ferritic alloys for use in nuclear energy technologies*, Snowbird, UT, USA, Jun. 1983.

[22] R. D. Hottenstine, N. A. Phillips, and R. L. Dail, "Development plan for advanced fossil fuel power plants," Palo Alto, California, USA: Electric Power Research Institute, Jan. 1985.

[23] R. W. Swindeman, M. L. Santella, P. J. Maziasz, B. W. Roberts, and K. Coleman, "Issues in replacing Cr-Mo steels and stainless steels with 9Cr-1Mo-V steel," *International Journal of Pressure Vessels and Piping*, vol. 81, no. 6, pp. 507–512, Jun. 2004, doi: 10.1016/j.ijpvp.2003.12.009.

[24] C. Cabet, F. Dalle, E. Gaganidze, J. Henry, and H. Tanigawa, “Ferritic-martensitic steels for fission and fusion applications,” *Journal of Nuclear Materials*, vol. 523, pp. 510–537, 2019, doi: 10.1016/j.jnucmat.2019.05.058ï.
[25] T. Takagi, Y. Yoshida, P. Ruatto, and L. v Boccaccini, “Progress of electromagnetic analysis for fusion reactors,” 1998.
[26] T. Nakayama, M. Abe, T. Tadokoro, and M. Otsuka, “Evaluation of magnetic ®elds due to the ferromagnetic vacuum vessel and their in¯uence on plasma discharge in tokamak devices.”
[27] R. L. Klueh and A. T. Nelson, “Ferritic/martensitic steels for next-generation reactors,” *Journal of Nuclear Materials*, vol. 371, no. 1–3, pp. 37–52, Sep. 2007, doi: 10.1016/j.jnucmat.2007.05.005.
[28] A. Kohyama, A. Hishinuma, D. S. Gelles ’, R. L. Klueh, W. Dietz ’, and K. Ehrlich, “Low-activation ferritic and martensitic steels for fusion application,” 1996.
[29] S. J. Zinkle *et al.*, “Development of next generation tempered and ODS reduced activation ferritic/martensitic steels for fusion energy applications,” *Nuclear Fusion*, vol. 57, no. 9, Jun. 2017, doi: 10.1088/1741-4326/57/9/092005.
[30] N. Baluc *et al.*, “Review on the EFDA work programme on nano-structured ODS RAF steels,” in *Journal of Nuclear Materials*, Elsevier B.V., Oct. 2011, pp. 149–153. doi: 10.1016/j.jnucmat.2010.12.065.
[31] M. J. Alinger, G. R. Odette, and D. T. Hoelzer, “On the role of alloy composition and processing parameters in nanocluster formation and dispersion strengthening in nanostuctured ferritic alloys,” *Acta Mater*, vol. 57, no. 2, pp. 392–406, Jan. 2009, doi: 10.1016/j.actamat.2008.09.025.
[32] T. Muroga *et al.*, “Fabrication and characterization of reference 9Cr and 12Cr-ODS low activation ferritic/martensitic steels,” in *Fusion Engineering and Design*, Elsevier Ltd, 2014, pp. 1717–1722. doi: 10.1016/j.fusengdes.2014.01.010.
[33] L. Tan, L. L. Snead, and Y. Katoh, “Development of new generation reduced activation ferritic-martensitic steels for advanced fusion reactors,” *Journal of Nuclear Materials*, vol. 478, pp. 42–49, Sep. 2016, doi: 10.1016/j.jnucmat.2016.05.037.
[34] B. W. Baker and L. N. Brewer, “Joining of Oxide Dispersion Strengthened Steels for Advanced Reactors,” *JOM*, vol. 66, no. 12. Minerals, Metals and Materials Society, pp. 2442–2457, Nov. 25, 2014. doi: 10.1007/s11837-014-1206-6.
[35] G. Federici, L. Boccaccini, F. Cismondi, M. Gasparotto, Y. Poitevin, and I. Ricapito, “An overview of the EU breeding blanket design strategy as an integral part of the DEMO design effort,” *Fusion Engineering and Design*, vol. 141, pp. 30–42, Apr. 2019, doi: 10.1016/j.fusengdes.2019.01.141.
[36] J. H. You *et al.*, “European DEMO divertor target: Operational requirements and material-design interface,” *Nuclear Materials and Energy*, vol. 9, pp. 171–176, Dec. 2016, doi: 10.1016/j.nme.2016.02.005.
[37] L. M. Giancarli *et al.*, “Overview of the ITER TBM Program,” in *Fusion Engineering and Design*, Aug. 2012, pp. 395–402. doi: 10.1016/j.fusengdes.2011.11.005.
[38] M. Gorley *et al.*, “The EUROfusion materials property handbook for DEMO in-vessel components—Status and the challenge to improve confidence level for engineering data,” *Fusion Engineering and Design*, vol. 158, Sep. 2020, doi: 10.1016/j.fusengdes.2020.111668.
[39] E. Gaganidze, F. Gillemot, I. Szenthe, M. Gorley, M. Rieth, and E. Diegele, “Development of EUROFER97 database and material property handbook,” *Fusion Engineering and Design*, vol. 135, pp. 9–14, Oct. 2018, doi: 10.1016/j.fusengdes.2018.06.027.
[40] G. Aiello, J. Aktaa, F. Cismondi, G. Rampal, J. F. Salavy, and F. Tavassoli, “Assessment of design limits and criteria requirements for Eurofer structures in TBM components,” *Journal of Nuclear Materials*, vol. 414, no. 1, pp. 53–68, Jul. 2011, doi: 10.1016/j.jnucmat.2011.05.005.
[41] A.-A. F. Tavassoli, J.-W. Rensman, M. Schirra, and K. Shiba, “Materials design data for reduced activation martensitic steel type F82H.” [Online]. Available: www.elsevier.com/locate/fusengdes
[42] G. Yu, N. Nita, and N. Baluc, “Thermal creep behaviour of the EUROFER 97 RAFM steel and two European ODS EUROFER 97 steels,” *Fusion Engineering and Design*, vol. 75–79, no. SUPPL., pp. 1037–1041, Nov. 2005, doi: 10.1016/j.fusengdes.2005.06.311.
[43] A. Bhattacharya *et al.*, “Irradiation damage concurrent challenges with RAFM and ODS steels for fusion reactor first-wall/blanket: A review,” *JPhys Energy*, vol. 4, no. 3, Jul. 2022, doi: 10.1088/2515-7655/ac6f7f.
[44] S. J. Zinkle and J. T. Busby, “Structural materials for fission & fusion energy,” *Materials Today*, vol. 12, no. 11. pp. 12–19, Nov. 2009. doi: 10.1016/S1369-7021(09)70294-9.
[45] E. Gaganidze *et al.*, “Mechanical properties and TEM examination of RAFM steels irradiated up to 70 dpa in BOR-60,” in *Journal of Nuclear Materials*, Oct. 2011, pp. 93–98. doi: 10.1016/j.jnucmat.2010.12.047.
[46] S. J. Zinkle and N. M. Ghoniem, “Operating temperature windows for fusion reactor structural materials,” 2000. [Online]. Available: www.elsevier.com/locate/fusengdes
[47] M. Gorley *et al.*, “DEMO structural materials qualification and development,” *Fusion Engineering and Design*, vol. 170, Sep. 2021, doi: 10.1016/j.fusengdes.2021.112513.
[48] S. J. Zinkle and A. Möslang, “Evaluation of irradiation facility options for fusion materials research and development,” in *Fusion Engineering and Design*, 2013, pp. 472–482. doi: 10.1016/j.fusengdes.2013.02.081.

[49] L. Peng and Y. Dai, “Helium-induced hardening effect in ferritic/martensitic steels F82H and Optimax-A irradiated in a mixed spectrum of high energy protons and spallation neutrons,” in *Journal of Nuclear Materials*, Oct. 2011, pp. 996–1000. doi: 10.1016/j.jnucmat.2010.12.208.

[50] L. Pilloni, C. Cristalli, O. Tassa, L. Bozzetto, E. Zanin, and N. Bettocchi, “Development of innovative materials and thermal treatments for DEMO water cooled blanket,” *Nuclear Materials and Energy*, vol. 19, pp. 79–86, May 2019, doi: 10.1016/j.nme.2019.01.026.

[51] K. Shiba, H. Tanigawa, T. Hirose, and T. Nakata, “Development of the toughness-improved reduced-activation F82H steel for demo reactor,” in *Fusion Science and Technology*, American Nuclear Society, 2012, pp. 145–149. doi: 10.13182/FST12-A14127.

[52] Q. Huang *et al.*, “Recent progress of R&D activities on reduced activation ferritic/martensitic steels,” *Journal of Nuclear Materials*, vol. 442, no. 1-3 SUPPL.1, 2013, doi: 10.1016/j.jnucmat.2012.12.039.

[53] J. Konys, W. Krauss, J. Novotny, H. Steiner, Z. Voss, and O. Wedemeyer, “Compatibility behavior of EUROFER steel in flowing Pb-17Li,” *Journal of Nuclear Materials*, vol. 386–388, no. C, pp. 678–681, Apr. 2009, doi: 10.1016/j.jnucmat.2008.12.271.

[54] A. Santucci *et al.*, “The issue of Tritium in DEMO coolant and mitigation strategies,” *Fusion Engineering and Design*, vol. 158, Sep. 2020, doi: 10.1016/j.fusengdes.2020.111759.

[55] Y. J. Huang, K. Kawakita, and A. Kimura, “Stress corrosion cracking susceptibility of 310S stainless steel in hydrogenated hot water,” *Nuclear Materials and Energy*, vol. 15, pp. 103–109, May 2018, doi: 10.1016/j.nme.2018.03.004.

[56] Y. J. Huang and A. Kimura, “Stress corrosion cracking behavior of type 316L and type 310S stainless steels in fusion relevant environments,” in *Materials Transactions*, Japan Institute of Metals (JIM), 2018, pp. 1267–1274. doi: 10.2320/matertrans.M2018064.

[57] Y. Ueki, T. Kunugi, N. B. Morley, and M. A. Abdou, “Electrical insulation test of alumina coating fabricated by sol-gel method in molten PbLi pool,” *Fusion Engineering and Design*, vol. 85, no. 10–12, pp. 1824–1828, Dec. 2010, doi: 10.1016/j.fusengdes.2010.06.004.

[58] A. Aiello, A. Ciampichetti, and G. Benamati, “An overview on tritium permeation barrier development for WCLL blanket concept,” in *Journal of Nuclear Materials*, Aug. 2004, pp. 1398–1402. doi: 10.1016/j.jnucmat.2004.04.205.

[59] J. Konys, W. Krauss, Z. Voss, and O. Wedemeyer, “Comparison of corrosion behavior of bare and hot-dip coated EUROFER steel in flowing Pb-17Li,” *Journal of Nuclear Materials*, vol. 367-370 B, no. SPEC. ISS., pp. 1144–1149, Aug. 2007, doi: 10.1016/j.jnucmat.2007.03.205.

[60] J. Konys, W. Krauss, and N. Holstein, “Development of advanced Al coating processes for future application as anti-corrosion and T-permeation barriers,” *Fusion Engineering and Design*, vol. 85, no. 10–12, pp. 2141–2145, Dec. 2010, doi: 10.1016/j.fusengdes.2010.08.018.

[61] H. G. Yang, Q. Zhan, W. W. Zhao, X. M. Yuan, Y. Hu, and Z. B. Han, “Study of an iron-aluminide and alumina tritium barrier coating,” in *Journal of Nuclear Materials*, Oct. 2011, pp. 1237–1240. doi: 10.1016/j.jnucmat.2011.03.040.

[62] T. Shikama *et al.*, “Status of development of functional materials with perspective on beyond-ITER,” *Fusion Engineering and Design*, vol. 83, no. 7–9. pp. 976–982, Dec. 2008. doi: 10.1016/j.fusengdes.2008.07.034.

[63] B. A. Pint *et al.*, “Recent progress in the development of electrically insulating coatings for a liquid lithium blanket,” in *Journal of Nuclear Materials*, Aug. 2004, pp. 119–124. doi: 10.1016/j.jnucmat.2004.04.010.

[64] F. Koch *et al.*, “Crystallization behavior of arc-deposited ceramic barrier coatings,” in *Journal of Nuclear Materials*, Aug. 2004, pp. 1403–1406. doi: 10.1016/j.jnucmat.2004.04.206.

[65] D. Levchuk, S. Levchuk, H. Maier, H. Bolt, and A. Suzuki, “Erbium oxide as a new promising tritium permeation barrier,” *Journal of Nuclear Materials*, vol. 367-370 B, no. SPEC. ISS., pp. 1033–1037, Aug. 2007, doi: 10.1016/j.jnucmat.2007.03.183.

[66] A. Sawada, A. Suzuki, H. Maier, F. Koch, T. Terai, and T. Muroga, “Fabrication of yttrium oxide and erbium oxide coatings by PVD methods,” *Fusion Engineering and Design*, vol. 75–79, no. SUPPL., pp. 737–740, Nov. 2005, doi: 10.1016/j.fusengdes.2005.06.050.

[67] P. Arena *et al.*, “The demo water-cooled lead–lithium breeding blanket: Design status at the end of the pre-conceptual design phase,” *Applied Sciences (Switzerland)*, vol. 11, no. 24, Dec. 2021, doi: 10.3390/app112411592.

[68] D. Rapisarda *et al.*, “The European Dual Coolant Lithium Lead breeding blanket for DEMO: Status and perspectives,” *Nuclear Fusion*, vol. 61, no. 11, Nov. 2021, doi: 10.1088/1741-4326/ac26a1.

[69] J. Aubert, G. Aiello, R. Boullon, F. A. Hernández, and J. C. Jaboulay, “DEMO Breeding Blanket Helium Cooled First Wall design investigation to cope high heat loads,” *Fusion Engineering and Design*, vol. 146, pp. 514–517, Sep. 2019, doi: 10.1016/j.fusengdes.2019.01.009.

[70] P. Aubert, F. Tavassoli, M. Rieth, E. Diegele, and Y. Poitevin, “Review of candidate welding processes of RAFM steels for ITER test blanket modules and DEMO,” in *Journal of Nuclear Materials*, Oct. 2011, pp. 43–50. doi: 10.1016/j.jnucmat.2010.12.248.

[71] L. v. Boccaccini *et al.*, “Objectives and status of EUROfusion DEMO blanket studies,” *Fusion Engineering and Design*, vol. 109–111, pp. 1199–1206, 2016, doi: 10.1016/j.fusengdes.2015.12.054.
[72] Y. Poitevin *et al.*, “Development of welding technologies for the manufacturing of European Tritium Breeder blanket modules,” in *Journal of Nuclear Materials*, Oct. 2011, pp. 36–42. doi: 10.1016/j.jnucmat.2010.12.259.
[73] Z. Yu, Z. Feng, D. Hoelzer, L. Tan, and M. A. Sokolov, “Friction Stir Welding of ODS and RAFM Steels,” *Metallurgical and Materials Transactions E*, vol. 2, no. 3, pp. 164–172, Sep. 2015, doi: 10.1007/s40553-015-0054-9.
[74] B. Zhu *et al.*, “Revealing the residual stress distribution in laser welded Eurofer97 steel by neutron diffraction and Bragg edge imaging,” *J Mater Sci Technol*, vol. 114, pp. 249–260, Jul. 2022, doi: 10.1016/j.jmst.2021.12.004.
[75] T. Hirose, H. Sakasegawa, M. Nakajima, and H. Tanigawa, “Mechanical properties of TIG and EB weld joints of F82H,” *Fusion Engineering and Design*, vol. 98–99, pp. 1982–1985, Oct. 2015, doi: 10.1016/j.fusengdes.2015.06.133.
[76] T. Sawai, K. Shiba, and A. Hishinuma, “Microstructure of welded and thermal-aged low activation steel F82H IEA heat,” *Journal of Nuclear Materials*, vol. 283–287, pp. 657–661, 2000, [Online]. Available: www.elsevier.nl/locate/jnucmat
[77] X. Li *et al.*, “Effect of post weld heat treatment on the microstructure and properties of Laser-TIG hybrid welded joints for CLAM steel,” *Fusion Engineering and Design*, vol. 128, pp. 175–181, Mar. 2018, doi: 10.1016/j.fusengdes.2018.02.034.
[78] S. Kirk, W. Suder, K. Keogh, T. Tremethick, and A. Loving, “Laser welding of fusion relevant steels for the European DEMO,” *Fusion Engineering and Design*, vol. 136, pp. 612–616, Nov. 2018, doi: 10.1016/j.fusengdes.2018.03.039.
[79] W. Suder, S. Ganguly, S. Williams, K. Keogh, and S. Kirk, “Fabrication of advanced structural steels for fusion reactors by laser-laser hybrid processing Fabrication of advanced structural steels for fusion reactors by laser-laser hybrid joining,” 2017. [Online]. Available: http://www.euro-fusionscipub.org.
[80] S. Wu, J. Zhang, J. Yang, J. Lu, H. Liao, and X. Wang, “Investigation on microstructure and properties of narrow-gap laser welding on reduced activation ferritic/martensitic steel CLF-1 with a thickness of 35 mm,” *Journal of Nuclear Materials*, vol. 503, pp. 66–74, May 2018, doi: 10.1016/j.jnucmat.2018.02.038.
[81] G. Srinivasan, B. Arivazhagan, S. K. Albert, and A. K. Bhaduri, “Development of filler wires for welding of reduced activation ferritic martenstic steel for India’s test blanket module of ITER,” *Fusion Engineering and Design*, vol. 86, no. 4–5, pp. 446–451, Jun. 2011, doi: 10.1016/j.fusengdes.2011.04.003.
[82] S. Noh, A. Kimura, and T. K. Kim, “Diffusion bonding of 9Cr ODS ferritic/martensitic steel with a phase transformation,” in *Fusion Engineering and Design*, Elsevier Ltd, 2014, pp. 1746–1750. doi: 10.1016/j.fusengdes.2013.12.023.
[83] D. T. Hoelzer, K. A. Unocic, M. A. Sokolov, and Z. Feng, “Joining of 14YWT and F82H by friction stir welding,” *Journal of Nuclear Materials*, vol. 442, no. 1-3 SUPPL.1, 2013, doi: 10.1016/j.jnucmat.2013.04.027.
[84] S. Noh, R. Kasada, and A. Kimura, “Solid-state diffusion bonding of high-Cr ODS ferritic steel,” *Acta Mater*, vol. 59, no. 8, pp. 3196–3204, May 2011, doi: 10.1016/j.actamat.2011.01.059.
[85] S. Noh, R. Kasada, A. Kimura, S. H. C. Park, and S. Hirano, “Microstructure and mechanical properties of friction stir processed ODS ferritic steels,” in *Journal of Nuclear Materials*, Oct. 2011, pp. 245–248. doi: 10.1016/j.jnucmat.2011.01.059.
[86] S. Hoon Kang, S. Noh, J. Hwan Kim, and T. Kyu Kim, “Dissimilar Joining of ODS and F/M Steel Tube by Friction Stir Welding.”
[87] J. Fu, I. Richardson, and M. Hermans, “Microstructure study of pulsed laser beam welded oxide dispersion-strengthened (Ods) eurofer steel,” *Micromachines (Basel)*, vol. 12, no. 6, Jun. 2021, doi: 10.3390/mi12060629.
[88] F. Naimi *et al.*, “Joining of oxide dispersion-strengthened steel using spark plasma sintering,” *Metals (Basel)*, vol. 10, no. 8, pp. 1–10, Aug. 2020, doi: 10.3390/met10081040.
[89] J. Fu, J. van Slingerland, H. Brouwer, V. Bliznuk, I. Richardson, and M. Hermans, “Applicability study of pulsed laser beam welding on ferritic–martensitic ODS eurofer steel,” *Metals (Basel)*, vol. 10, no. 6, Jun. 2020, doi: 10.3390/met10060736.
[90] Y. Yano, T. Kaito, T. Tanno, and S. Ohtsuka, “Weldability of dissimilar joint between PNC-FMS and Type 316 steel under electron beam welding,” *J Nucl Sci Technol*, vol. 52, no. 4, pp. 568–579, Apr. 2015, doi: 10.1080/00223131.2014.964789.
[91] L. Commin *et al.*, “Characterization of ODS (Oxide Dispersion Strengthened) Eurofer/Eurofer dissimilar electron beam welds,” *Journal of Nuclear Materials*, vol. 442, no. 1-3 SUPPL.1, 2013, doi: 10.1016/j.jnucmat.2012.11.019.
[92] R. Lindau, M. Klimenkov, U. Jäntsch, A. Möslang, and L. Commin, “Mechanical and microstructural characterization of electron beam welded reduced activation oxide dispersion strengthened - Eurofer steel,” *Journal of Nuclear Materials*, vol. 416, no. 1–2, pp. 22–29, Sep. 2011, doi: 10.1016/j.jnucmat.2011.01.025.
[93] C. H. Choi *et al.*, “Remote handling concept for the neutral beam system,” *Fusion Engineering and Design*, vol.

86, no. 9–11, pp. 2025–2028, Oct. 2011, doi: 10.1016/j.fusengdes.2011.01.122.
[94] R. Shuff, M. Van Uffelen, C. Damiani, A. Tesini, C. H. Choi, and R. Meek, "Progress in the design of the ITER Neutral Beam cell Remote Handling System," *Fusion Engineering and Design*, vol. 89, no. 9–10, pp. 2378–2382, 2014, doi: 10.1016/j.fusengdes.2014.01.043.
[95] N. Sykes *et al.*, "Status of ITER neutral beam cell remote handling system," in *Fusion Engineering and Design*, Oct. 2013, pp. 2043–2047. doi: 10.1016/j.fusengdes.2013.02.087.
[96] L. Thomson *et al.*, "Neutral beam remote cutting & welding development," *Fusion Engineering and Design*, vol. 124, pp. 487–491, Nov. 2017, doi: 10.1016/j.fusengdes.2017.04.078.
[97] J.-P. Friconneau *et al.*, "Overview of Bore Tools Systems for divertor remote maintenance of ITER," 2001. [Online]. Available: www.elsevier.com/locate/fusengdes
[98] C. Lamb *et al.*, "Pipe Maintenance Tooling development for the ITER Divertor Remote Handling System," *Fusion Engineering and Design*, vol. 136, pp. 983–987, Nov. 2018, doi: 10.1016/j.fusengdes.2018.04.051.
[99] O. David *et al.*, "Carrier and bore tools for 4 in. bent pipes," *Fusion Engineering and Design*, vol. 69, no. 1-4 SPEC, pp. 123–128, Sep. 2003, doi: 10.1016/S0920-3796(03)00277-1.
[100] "Annual Report of the Association EURATOM/CEA 2003." [Online]. Available: http://www-fusion-magnetique.cea.fr
[101] S. Shigematsu *et al.*, "Verification test results of a cutting technique for the ITER blanket cooling pipes," *Fusion Engineering and Design*, vol. 87, no. 7–8, pp. 1218–1223, Aug. 2012, doi: 10.1016/j.fusengdes.2012.02.108.
[102] H. Tanigawa *et al.*, "Comparative study of laser and TIG welding for application to ITER blanket hydraulic connection," *Fusion Engineering and Design*, vol. 87, no. 7–8, pp. 999–1003, Aug. 2012, doi: 10.1016/j.fusengdes.2012.02.055.
[103] S. Kawano, R. Sumiya, and K. Fukuya, "Simulation of helium bubble behavior in neutron-irradiated stainless steel during welding."
[104] H. Tanigawa, T. Maruyama, Y. Noguchi, N. Takeda, and S. Kakudate, "Laser welding to expand the allowable gap in bore welding for ITER blanket hydraulic connection," *Fusion Engineering and Design*, vol. 98–99, pp. 1634–1637, Oct. 2015, doi: 10.1016/j.fusengdes.2015.06.155.
[105] T. Hayashi *et al.*, "Development of remote pipe welding tool for divertor cassettes in JT-60SA," *Fusion Engineering and Design*, vol. 101, pp. 180–185, Dec. 2015, doi: 10.1016/j.fusengdes.2015.06.195.
[106] T. Hayashi, M. Takechi, G. Matsunaga, and A. Isayama, "In-bore laser welding tool for actively cooled divertor cassettes in JT-60SA," *Fusion Engineering and Design*, vol. 177, Apr. 2022, doi: 10.1016/j.fusengdes.2022.113040.
[107] O. Crofts *et al.*, "EU DEMO Remote Maintenance System development during the Pre-Concept Design Phase," *Fusion Engineering and Design*, vol. 179, Jun. 2022, doi: 10.1016/j.fusengdes.2022.113121.
[108] S. Kirk, K. Keogh, L. Naidu, and T. Tremethick, "In-bore Robotic Laser Cutting and Welding Tools for Nuclear Fusion Reactors," *Lasers in Eng*, vol. 46, pp. 295–304, 2020.
[109] T. Hayashi, S. Sakurai, K. Shibanuma, and A. Sakasai, "Development of remote pipe cutting tool for divertor cassettes in JT-60SA," *Fusion Engineering and Design*, vol. 89, no. 9–10, pp. 2299–2303, 2014, doi: 10.1016/j.fusengdes.2014.04.026.
[110] S. Kirk, K. Keogh, W. Suder, T. Tremethick, C. Allen, and I. Farquhar, "Remote in-bore laser cutting and welding tools for use in future nuclear fusion reactors," 2018.
[111] S. Kirk, K. Keogh, S. Kirk, K. Keogh, L. Naidu, and T. Tremethick, "Remote in-bore laser cutting & welding tools for the EU-DEMO," in *Symposium on Fusion Engineering*, Jun. 2019. doi: 10.13140/RG.2.2.16610.79042.
[112] L. P. Jones *et al.*, "Assembly of ITER blanket module to vacuum vessel experimental investigations," 2001. [Online]. Available: www.elsevier.com/locate/fusengdes
[113] S. Pak, Y. Kim, K. Y. Park, K. D. Lee, M. S. Cheon, and H. G. Lee, "Laser welding and ablation cutting process for hydraulic connections by remote handling in the ITER diagnostic port plug," *Fusion Engineering and Design*, vol. 85, no. 2, pp. 190–196, Apr. 2010, doi: 10.1016/j.fusengdes.2009.11.003.
[114] Y. Noguchi, T. Maruyama, and N. Takeda, "Development of in-vessel pipe alignment tool for ITER blanket remote maintenance," *Fusion Engineering and Design*, vol. 124, pp. 623–627, Nov. 2017, doi: 10.1016/j.fusengdes.2017.02.070.
[115] K. Keogh *et al.*, "Remote handling strategy and prototype tooling of the ITER vacuum vessel pressure suppression system bleed line valve assembly and rupture disk assembly," *Fusion Engineering and Design*, vol. 153, Apr. 2020, doi: 10.1016/j.fusengdes.2020.111485.
[116] V. Milushev, A. Azka, and M. Mittwollen, "Development of Mechanical Pipe-Connection Design for DEMO," *Journal of Nuclear Engineering*, vol. 4, no. 1, pp. 111–126, Jan. 2023, doi: 10.3390/jne4010008.
[117] J. D. Pierce, J. J. Stephens, C. A. Walker, F. M. Hosking, and R. M. Curlee, "Development of a re-brazeable containment system for special nuclear material storage and transport," in *International conference on packaging and transportation of radioactive materials*, Las Vegas: Sandia National Labs., Albuquerque, NM (United States), Dec. 1995.
[118] I. Fernández, E. V. Rosa, and I. Palermo, "Design of a brazing connector for DEMO in-vessel components,"

Fusion Engineering and Design, vol. 89, no. 9–10, pp. 2363–2367, 2014, doi: 10.1016/j.fusengdes.2014.02.002.
[119] I. Fernández, E. Rosa, and Á. Ibarra, "Progress on the design of a brazing connector for DEMO in-vessel components," *Fusion Engineering and Design*, vol. 98–99, pp. 1483–1487, Oct. 2015, doi: 10.1016/j.fusengdes.2015.06.145.
[120] R. Hansen and L. Jeppesen, "Industrial Application of Helium Leak Test," in *7th European Conference on NDT* , Copenhagen, 1998. [Online]. Available: https://www.ndt.net/article/ecndt98/offshore/268/268.htm
[121] A. Itoh *et al.*, "Development of Bore Tools for Blanket Cooling Pipe Connection in ITER," *Proc. of 17th IEEE/NPSS Symposium Fusion Engineering (SOFE'97)*, vol. 2, pp. 921–924, 1997.
[122] P. Hansen, H. Alismail, P. Rander, and B. Browning, "Visual mapping for natural gas pipe inspection," *International Journal of Robotics Research*, vol. 34, no. 4–5, pp. 532–538, Apr. 2015, doi: 10.1177/0278364914550133.
[123] P. Buschinelli, T. Pinto, F. Silva, J. Santos, and A. Albertazzi, "Laser Triangulation Profilometer for Inner Surface Inspection of 100 millimeters (4″) Nominal Diameter," in *Journal of Physics: Conference Series*, Institute of Physics Publishing, Oct. 2015. doi: 10.1088/1742-6596/648/1/012010.
[124] T. Vidal-Calleja, J. V. Miro, F. Martin, D. C. Lingnau, and D. E. Russell, "Automatic Detection and Verification of Pipeline Construction Features with Multi-modal data," in *2014 IEEE/RSJ International Conference on Intelligent Robots and Systems (IROS 2014)*, Chicago, IL, USA: IEEE, Sep. 2014, pp. 3116–3122.
[125] W. Jackson, G. Dobie, C. MacLeod, G. West, C. Mineo, and L. McDonald, "Error Analysis and Calibration for a Novel Pipe Profiling Tool," *IEEE Sens J*, vol. 20, no. 7, pp. 3545–3555, Apr. 2020, doi: 10.1109/JSEN.2019.2960939.
[126] K. Matsui, A. Yamashita, and T. Kaneko, "3-D Shape Measurement of Pipe by Range Finder Constructed with Omni-Directional Laser and Omni-Directional Camera," in *2010 IEEE International Conference on Robotics and Automation*, Anchorage, AK, USA: IEEE, May 2010, pp. 2537–2542.
[127] J. Gaspar, N. Winters, and J. Santos-Victor, "Vision-based navigation and environmental representations with an omnidirectional camera," *IEEE Transactions on Robotics and Automation*, vol. 16, no. 6, pp. 890–898, 2000, doi: 10.1109/70.897802.
[128] J. Gluckman and S. K. Nayar, "Ego-Mot ion and Omnidirectional Cameras*," in *Sixth International Conference on Computer Vision*, Bombay, India, Jan. 1998, pp. 999–1005.
[129] S. Hosseinzadeh *et al.*, "A novel centralization method for pipe image stitching," *IEEE Sens J*, vol. 21, no. 10, pp. 11889–11898, May 2021, doi: 10.1109/JSEN.2020.3031637.
[130] A. Nishimura *et al.*, "Development of inspection repair technology for tube inner wall of aging nuclear power plants," *Japan Society of Maintenology*, vol. 17, no. 4, pp. 207–212, Oct. 2010.
[131] A. Nishimura and Y. Shimada, "DEVELOPING MAINTENANCE TECHNOLOGIES FOR FBR's HEAT EXCHANGER UNITS by ADVANCED LASER PROCESSING," in *Proceedings of the ICONE-19, The 19th international conference on nuclear engineering*, Osaka, Japan, 2011.
[132] K. Oka and T. Seki, "A composite-type optical fiberscope system with hybrid functions of diagnosis and medical treatment," in *JSAP-OSA Joint Symposia 2014*, Optica Publishing Group, Sep. 2014.
[133] K. Oka, A. Nishimura, T. Seki, T. Akatsu, and T. Yamashita, "Development of a Laser Processing Head Using a Composite-type Optical Fiberscope to Inspect and Repair 1-inch Heat Exchanger Pipes," *Maintenology*, vol. 8, no. 4, pp. 37–43, 2010.
[134] A. Nishimura, A. Furusawa, and Y. Takenaka, "Development of laser instrumentation devices for inner wall of high temperature piping system," in *AIP Conference Proceedings*, American Institute of Physics Inc., Nov. 2018. doi: 10.1063/1.5067091.
[135] Y. Yonemoto, A. Nishimura, K. Oka, and Y. Shimada, "Optical Fiber Device For Coupling A Composite-Type Optical Fiber Scope And Pulse Laser Processing For Plant Maintenance," *International Journal of Research in Engineering and Science (IJRES)*, vol. 1, no. 6, pp. 1–08, 2013, [Online]. Available: www.ijres.org
[136] C. Ito *et al.*, "Development of radiation-resistant optical fiber for application to observation and laser spectroscopy under high radiation dose," *J Nucl Sci Technol*, vol. 51, no. 7–8, pp. 944–950, Aug. 2014, doi: 10.1080/00223131.2014.924883.
[137] T. Shikama, T. Kakuta, N. Shamoto, M. Narui, and T. Sagawa, "Behavior of developed radiation-resistant silica-core optical fibers under fission reactor irradiation," *Fusion Engineering and Design*, vol. 51–52, pp. 179–183, Nov. 2000, [Online]. Available: www.elsevier.com/locate/fusengdes
[138] Noël Dubé. (coordinator) and Dr. Michael D. C. Moles (technical reviewers and advisers), *Advances in Phased Array Ultrasonic Technology Applications*. Olympus NDT, 2007.
[139] R. K. W. Vithanage *et al.*, "A Phased Array Ultrasound Roller Probe for Automated in-Process/Interpass Inspection of Multipass Welds," *IEEE Transactions on Industrial Electronics*, vol. 68, no. 12, pp. 12781–12790, Dec. 2021, doi: 10.1109/TIE.2020.3042112.
[140] R. K. W. Vithanage *et al.*, "Development of a phased array ultrasound roller probe for inspection of wire + arc additive manufactured components," *J Manuf Process*, vol. 80, pp. 765–774, Aug. 2022, doi: 10.1016/j.jmapro.2022.06.045.

[141] T. Hayashi, G. Matsunaga, M. Takechi, and A. Isayama, “In-bore ultrasonic testing of cooling pipes in lower divertor cassette of JT-60SA,” *Fusion Engineering and Design*, vol. 194, Sep. 2023, doi: 10.1016/j.fusengdes.2023.113666.
[142] R. C. Mayworm, A. V. Alvarenga, and R. P. B. Costa-Felix, “A metrological approach to the time of flight diffraction method (ToFD),” *Measurement (Lond)*, vol. 167, Jan. 2021, doi: 10.1016/j.measurement.2020.108298.
[143] K. Manjula, K. Vijayarekha, B. Venkatraman, and D. Karthik, “Ultrasonic Time of Flight Diffraction Technique for Weld Defects: A Review,” *Research Journal of Applied Sciences, Engineering and Technology*, vol. 4, no. 24, pp. 5525–5533, 2012.
[144] F. Huang, Z. Zhou, and J. Lin, “A New Testing Method Combining EMAT with Eddy Current,” in *17th World Conference on Nondestructive Testing*, Shanghai, China, 2008, pp. 25–28. [Online]. Available: https://www.ndt.net/?id=6457
[145] C. Thring, W. E. Somerset, and R. S. Edwards, “Enhanced surface defect detection using focused electromagnetic acoustic transducers (EMATs),” in *Proceedings of Meetings on Acoustics*, Acoustical Society of America, 2017. doi: 10.1121/2.0000683.
[146] H. Salzburger and W. Mohr, “Electromagnetic-Acoustic Generation of Ultrasound,” *2nd Seminar on Characterization of ultrasonic Equipment. October 9-12, 1979. I.Z.S.P, Saarbrücken, Germany*.
[147] S. Aliouane, M. Hassam, A. Badidi Bouda, and A. Benchaala, “Electromagnetic Acoustic Transducers (EMATs) Design Evaluation of their Performances,” in *Proceedings of the 15th World Conference on NDT*, Oct. 2000. [Online]. Available: https://www.ndt.net/article/wcndt00/papers/idn591/idn591.htm
[148] P. A. Petcher, S. E. Burrows, and S. Dixon, “Shear horizontal (SH) ultrasound wave propagation around smooth corners,” *Ultrasonics*, vol. 54, no. 4, pp. 997–1004, Apr. 2014, doi: 10.1016/j.ultras.2013.11.011.
[149] B. Lopez, “Weld Inspection with EMAT Using Guided Waves,” *eJNDT Articles & News*, Jun. 2008, [Online]. Available: https://www.ndt.net/?id=5947
[150] S. H. Cho *et al.*, “Feasibility study on the utilization of EMAT technology for in-line inspection of gas pipeline,” *Journal of Magnetics*, vol. 16, no. 1, pp. 36–41, Mar. 2011, doi: 10.4283/JMAG.2011.16.1.036.
[151] K. Oka, A. Ito, K. Taguchi, Y. Takiguchi, H. Takahashi, and E. Tada, “DEVELOPMENT OF PIPE WELDING, CUTTING & INSPECTION TOOLS FOR THE ITER BLANKET,” 1999.
[152] K. Oka, M. Nakahira, K. Taguchi, and A. Ito, “Development of Bore Tools for Pipe Inspection,” *Journal of Robotics and Mechatronics*, vol. 10, no. 2, pp. 110–115, Apr. 1998, doi: 10.20965/jrm.1998.p0110.
[153] L. Pucci, R. Raillon, L. Taupin, and F. Baqué, “Design of a phased array EMAT for inspection applications in liquid sodium,” *Sensors (Switzerland)*, vol. 19, no. 20, Oct. 2019, doi: 10.3390/s19204460.
[154] D. Rueter and T. Morgenstern, “Ultrasound generation with high power and coil only EMAT concepts,” *Ultrasonics*, vol. 54, no. 8, pp. 2141–2150, 2014, doi: 10.1016/j.ultras.2014.06.012.
[155] S. J. Davies, C. Edwards, G. S. Taylor, and S. B. Palmer, “Laser-generated ultrasound: Its properties, mechanisms and multifarious applications,” *J Phys D Appl Phys*, vol. 26, no. 3, pp. 329–348, Jan. 1993, doi: 10.1088/0022-3727/26/3/001.
[156] J.-P. Monchalin, “LASER-ULTRASONICS: PRINCIPLES AND INDUSTRIAL APPLICATIONS,” *e-Journal of Nondestructive Testing*, vol. 25, no. 3, 2020, [Online]. Available: http://www.ndt.net/?id=25250
[157] J. Wagner and J. Spicer, “A Technology Assessment of LASER ULTRASONICS,” Jun. 1998.
[158] J. Monchalin, “Optical detection of ultrasound,” *IEEE Transactions on Ultra- sonics, Ferroelectrics and Frequency Control*, vol. 33, no. 5, pp. 485–499, Sep. 1986.
[159] J. Spytek, L. Ambrozinski, and I. Pelivanov, “Non-contact detection of ultrasound with light – Review of recent progress,” *Photoacoustics*, vol. 29. Elsevier GmbH, Feb. 01, 2023. doi: 10.1016/j.pacs.2022.100440.
[160] G. Wissmeyer, M. A. Pleitez, A. Rosenthal, and V. Ntziachristos, “Looking at sound: optoacoustics with all-optical ultrasound detection,” *Light: Science and Applications*, vol. 7, no. 1. Nature Publishing Group, Dec. 01, 2018. doi: 10.1038/s41377-018-0036-7.
[161] A. Blouin, D. Lévesque, C. Néron, D. Drolet, and J.-P. Monchalin, “Improved resolution and signal-to-noise ratio in laser-ultrasonics by SAFT processing,” *Opt Express*, vol. 2, no. 13, pp. 531–539, Jun. 1998.
[162] C. Y. Ni *et al.*, “Non-destructive laser-ultrasonic Synthetic Aperture Focusing Technique (SAFT) for 3D visualization of defects,” *Photoacoustics*, vol. 22, Jun. 2021, doi: 10.1016/j.pacs.2021.100248.
[163] T. Stratoudaki, M. Clark, and P. D. Wilcox, “Full matrix capture and the total focusing imaging algorithm using laser induced ultrasonic phased arrays,” in *AIP Conference Proceedings*, American Institute of Physics Inc., Feb. 2017. doi: 10.1063/1.4974563.
[164] T. Stratoudaki, M. Clark, and P. Wilcox, “Laser induced ultrasonic phased array using Full Matrix Capture data acquisition and Total Focusing Method,” in *54th Annual British Conference of Non-Destructive Testing, NDT 2015*, British Institute of Non-Destructive Testing, 2015. doi: 10.1364/oe.24.021921.
[165] F. Qian, G. Xing, P. Yang, P. Hu, L. Zou, and T. Koukoulas, “Laser-induced ultrasonic measurements for the detection and reconstruction of surface defects,” *Acta Acustica*, vol. 5, 2021, doi: 10.1051/aacus/2021031.
[166] P. Lukacs, G. Davis, T. Stratoudaki, Y. Javadi, G. Pierce, and A. Gachagan, “REMOTE, VOLUMETRIC

ULTRASONIC IMAGING OF DEFECTS USING TWO-DIMENSIONAL LASER INDUCED PHASED ARRAYS," in *Proceedings of the ASME 2021 48th Annual Review of Progress in Quantitative Nondestructive Evaluation*, Virtual, Jul. 2021. [Online]. Available: http://asmedigitalcollection.asme.org/qnde/proceedings-pdf/QNDE2021/85529/V001T18A001/6820584/v001t18a001-qnde2021-74694.pdf

[167] D. Pieris *et al.*, "Laser Induced Phased Arrays (LIPA) to detect nested features in additively manufactured components," *Mater Des*, vol. 187, Feb. 2020, doi: 10.1016/j.matdes.2019.108412.

[168] P. Lukacs, G. Davis, T. Stratoudaki, S. Williams, C. N. MacLeod, and A. Gachagan, "Remote Ultrasonic Imaging of a Wire Arc Additive Manufactured Ti-6AI-4V Component using Laser Induced Phased Array," in *Conference Record - IEEE Instrumentation and Measurement Technology Conference*, Institute of Electrical and Electronics Engineers Inc., May 2021. doi: 10.1109/I2MTC50364.2021.9459823.

[169] T. Gao, Y. Wang, and X. Qing, "A new laser ultrasonic inspection method for the detection of multiple delamination defects," *Materials*, vol. 14, no. 9, May 2021, doi: 10.3390/ma14092424.

[170] K. Nomura, S. Otaki, R. Kita, and S. Asai, "In-situ detection of weld defect during the welding process by laser ultrasonic technique," in *Proceedings of Meetings on Acoustics*, Acoustical Society of America, 2019. doi: 10.1121/2.0001171.

[171] B. Heutling, H.-J. Uebrig, M. Awerbuch, W. Sievert, E. Köllner, and S. Köllner, "Application of Eddy Current Array Technology from the Point of View of a Service Provider," 2016.

[172] Q. Yang *et al.*, "A novel circumferential eccentric eddy current probe and its application for defect detection of small-diameter tubes," *Sens Actuators A Phys*, vol. 331, Nov. 2021, doi: 10.1016/j.sna.2021.113023.

[173] G. Lafontaine, F. Hardy, and J. Renaud, "X-Probe ECT array: A high-Speed Replacement for Rotating Probes," in *3nd International Conference on NDE in Relation to Structural Integrity for Nuclear and Pressurized Components*, Seville, 2001. [Online]. Available: https://www.ndt.net/article/v07n08/lafontai/lafontai.htm

[174] Y. Zhao *et al.*, "A new array eddy current testing probe for inspection of small-diameter tubes in Tokamak fusion devices," *Fusion Engineering and Design*, vol. 157, Aug. 2020, doi: 10.1016/j.fusengdes.2020.111627.

[175] C. Gilles-Pascaud, J. M. Decitre, F. Vacher, C. Fermon, M. Pannetier, and G. Cattiaux, "Eddy current flexible probes for complex geometries," in *AIP Conference Proceedings*, Mar. 2006, pp. 399–406. doi: 10.1063/1.2184556.

[176] J. , Decitre, D. , Prémel, G. , Mangenet, E. , Juliac, and W. Feist, "Flexible EC Array Probe for the Inspection of Complex Parts Developed Within the European VERDICT Project," in *9th European Conference on NDT - September 2006 - Berlin (Germany)*, 2006. [Online]. Available: https://www.ndt.net/?id=3546

[177] F. Vacher, C. Gilles-Pascaud, J. M. Decitre, C. Fermon, and M. Pannetier, "Non Destructive Testing with GMR Magnetic Sensor Arrays," in *9th European Conference on NDT - September - Berlin (Germany)*, 2006. [Online]. Available: https://www.ndt.net/?id=3545

[178] M. A. Machado *et al.*, "Novel eddy current probes for pipes: Application in austenitic round-in-square profiles of ITER," *NDT and E International*, vol. 87, pp. 111–118, Apr. 2017, doi: 10.1016/j.ndteint.2017.02.001.

[179] Y. Noguchi, M. Tsunokai, K. Nakata, and N. Takeda, "Applicability of eddy current technique in in-bore NDT tool for ITER hydraulic pipe welds," *Fusion Engineering and Design*, vol. 146, pp. 2571–2576, Sep. 2019, doi: 10.1016/j.fusengdes.2019.04.044.

[180] Y. Shi, C. Zhang, R. Li, M. Cai, and G. Jia, "Theory and application of magnetic flux leakage pipeline detection," *Sensors (Switzerland)*, vol. 15, no. 12. MDPI AG, pp. 31036–31055, Dec. 10, 2015. doi: 10.3390/s151229845.

[181] H. M. Kim, H. R. Yoo, and G. S. Park, "A New Design of MFL Sensors for Self-Driving NDT Robot to Avoid Getting Stuck in Curved Underground Pipelines," *IEEE Trans Magn*, vol. 54, no. 11, Nov. 2018, doi: 10.1109/TMAG.2018.2846283.

[182] H. M. Kim, H. R. Yoo, Y. W. Rho, and G. S. Park, "Detection Method of Cracks by Using Magnetic Fields in Underground Pipeline," in *10th International Conference on Ubiquitous Robots and Ambient Intelligence (URAI)*, Jeju, Nov. 2013, pp. 734–737.

[183] J. D. Bernal-morales, "A Method for Defect Detection and Characterisation through Magnetic Flux Leakage Signals Using 3D Magnetoresistive Sensors," A Thesis presented for the degree of Master in Science by Research, Durham University, Durham, 2020. [Online]. Available: http://etheses.dur.ac.uk

[184] B. Feng, J. Wu, H. Tu, J. Tang, and Y. Kang, "A Review of Magnetic Flux Leakage Nondestructive Testing," *Materials*, vol. 15, no. 20. MDPI, Oct. 01, 2022. doi: 10.3390/ma15207362.

[185] D. A. Topp, "Quantitative In-Service Inspection using the Alternating Current Field Measurement (ACFM) Method," in *NDTISS '99 - International Symposium on NDT Contribution to the Infrastructure Safety Systems*, Torres: Center of Tecnology, Federal University of Santa Maria (UFSM), Nov. 1999. [Online]. Available: https://www.ndt.net/article/v05n03/topp/topp.htm

[186] S. P. Farrell, M. Lugg, and K. Avery, "Application of Alternating Current Field Measurement for Determination of Surface Cracks and Welds in Steel Structures at Lift-off," Defence R & D Canada External Literature DRDC-RDDC-2015-N093, Mar. 2015.

[187] A. M. Lewis, D. H. Michael, M. C. Lugg, and R. Collins, "THIN-SKIN ELECTROMAGNETIC FIELDS AROUND SURFACE-BREAKING CRACKS IN METALS," *J. Appl.Phys*, vol. 64, no. 8, pp. 3777–3784, 1988.

[188] R. Pincu and O. Kleinberger-Riedrich, “Advanced Digital Radiography for Field NDT,” in *International Symposium on Digital Industrial Radiology and Computed Tomography (DIR)*, Berlin, Germany, Jun. 2011. [Online]. Available: https://www.ndt.net/?id=11144

[189] A. P. Kaur, T. Sattar, R. Anvo, and M. O. Tokhi, “Development of a Robot for In-service Radiography Inspection of Subsea Flexible Risers,” *Journal of Artificial Intelligence and Technology*, vol. 1, no. 3, pp. 180–187, Jul. 2021, doi: 10.37965/jait.2021.0015.

[190] A. Reiss, “Pipe Robots for Internal Inspection, Non-Destructive Testing and Machining of Pipelines, 19th World Conference on Non-Destructive Testing (WCNDT 2016), 13-17 June 2016 in Munich, Germany,” *e-Journal of Nondestructive Testing*, vol. 21, no. 7, [Online]. Available: http://creativecommons.org/licenses/by-nd/3.0/

[191] L. Forejtová, T. Zavadil, L. Kolarík, M. Kolaríková, J. Sova, and P. Vávra, “Non-destructive inspection by infrared thermography of resistance spot welds used in automotive industry,” *Acta Polytechnica*, vol. 59, no. 3, pp. 238–247, 2019, doi: 10.14311/AP.2019.59.0238.

[192] A. Runnemalm, J. Ahlberg, A. Appelgren, and S. Sjökvist, “Automatic inspection of spot welds by thermography,” *J Nondestr Eval*, vol. 33, no. 3, pp. 398–406, 2014, doi: 10.1007/s10921-014-0233-0.

[193] A. DE Garcia La Yedra, A. Echeverria, A. Beizama, R. Fuente, and E. Fernández, “Infrared Thermography as an Alternative to Traditional Weld Inspection Methods thanks to Signal Processing Techniques,” in *11th European Conference on Non-Destructive Testing*, Prague, Czech Republic, Oct. 2014.

[194] B. B. Lahiri *et al.*, “Defect Detection in Weld Joints by Infrared Thermography,” in *International Conference on Non Destructive Evaluation in Steel and Allied Industries*, Jamshedpur, India, 2011.

[195] Z. Qu, P. Jiang, and W. Zhang, “Development and application of infrared thermography non-destructive testing techniques,” *Sensors* , vol. 20, no. 14, p. 3851, Jul. 2020, doi: 10.3390/s20143851.

[196] A. Mendioroz, E. Apiñaniz, A. Salazar, P. Venegas, and I. Sáez-Ocáriz, “Quantitative study of buried heat sources by lock-in vibrothermography: an approach to crack characterization,” *J Phys D Appl Phys*, vol. 42, no. 5, p. 055502, Mar. 2009, doi: 10.1088/0022-3727/42/5/055502.

[197] P. Broberg and A. Runnemalm, “Detection of Surface Cracks in Welds using Active Thermography,” in *18th World Conference on Nondestructive Testing*, Durban, South Africa, Apr. 2012.

[198] A. Runnemalm and P. Broberg, “Surface crack detection using infrared thermography and ultraviolet excitation,” in *12th International Conference on Quantitative InfraRed Thermography*, Bordeaux, France, Jul. 2014. doi: 10.21611/qirt.2014.016.

[199] A. García De La Yedra *et al.*, “Defect detection strategies in Nickel Superalloys welds using active thermography,” in *12th International Conference on Quantitative Infrared Thermography*, Bordeaux, France, Jul. 2014. [Online]. Available: www.ndt.net/?id=17659

[200] U. Netzelmann and G. Walle, “Induction Thermography as a Tool for Reliable Detection of Surface Defects in Forged Components,” in *17th World Conference on Nondestructive Testing*, Shanghai, China: e-Journal of Nondestructive Testing Vol. 13(11), Oct. 2008. [Online]. Available: https://www.ndt.net/?id=6558

[201] S. E. (Susan E.) Burrows, S. Dixon, S. G. Pickering, T. (Teng) Li, and D. Almond, “Thermographic detection of surface breaking defects using a scanning laser source,” *NDT & E International*, vol. 44, no. 7, pp. 589–596, 2011.

[202] R. Zoughi, *Microwave Non-Destructive Testing and Evaluation Principles*, vol. NDEV, volume 4. Springer Science & Business Media, 2000.

[203] K. Brinker, M. Dvorsky, M. T. Al Qaseer, and R. Zoughi, “Review of advances in microwave and millimetre-wave NDT&E: Principles and applications: Microwave and Millimeter-Wave NDT&E,” *Philosophical Transactions of the Royal Society A: Mathematical, Physical and Engineering Sciences*, vol. 378, no. 2182. Royal Society Publishing, Oct. 16, 2020. doi: 10.1098/rsta.2019.0585.

[204] C. A. Balanis, *Advanced Engineering Electromagnetics*, 1st ed. New York: ohn Wiley & Sons, 1989.

[205] M. A. Abou-Khousa, M. S. U. Rahman, K. M. Donnell, and M. T. Al Qaseer, “Detection of Surface Cracks in Metals Using Microwave and Millimeter-Wave Nondestructive Testing Techniques-A Review,” *IEEE Trans Instrum Meas*, vol. 72, 2023, doi: 10.1109/TIM.2023.3238036.

[206] C. Y. Yeh and R. Zoughi, “A Novel Microwave Method for Detection of Long Surface Cracks in Metals,” *IEEE Trans Instrum Meas*, vol. 43, no. 5, pp. 719–725, 1994, doi: 10.1109/19.328896.

[207] H. Ma, C. Li, W. Wang, al -, W. Jin, and G. Zhang, “Ferromagnetic resonance flaw detection You may also like Thickness-dependent resonance frequency of non-uniform procession mode in CoZr stripe-domain magnetic films Development of Intrinsic Room-Temperature 2D Ferromagnetic Crystals for 2D Spintronics,” 1981.

[208] H. Ryeol and S. Roh, “In-pipe Robot with Active Steering Capability for Moving Inside of Pipelines,” in *Bioinspiration and Robotics Walking and Climbing Robots*, Maki K. Habib, Ed., Vienna, Austria: I-Tech Education and Publishing, 2007, pp. 375–402.

[209] B. John and M. Shafeek, “Pipe inspection robots: a review,” *IOP Conf Ser Mater Sci Eng*, vol. 1272, no. 1, p. 012016, Dec. 2022, doi: 10.1088/1757-899x/1272/1/012016.

[210] R. S. Elankavi, “DEVELOPMENTS IN INPIPE INSPECTIONROBOT: A REVIEW,” *JOURNAL OF MECHANICS OF CONTINUA AND MATHEMATICAL SCIENCES*, vol. 15, no. 5, May 2020, doi:

10.26782/jmcms.2020.05.00022.
[211] R. S. Elankavi, D. Dinakaran, R. M. K. Chetty, M. M. Ramya, and D. G. H. Samuel, “A Review on Wheeled Type In-Pipe Inspection Robot,” *International Journal of Mechanical Engineering and Robotics Research*, vol. 11, no. 10, pp. 745–754, Oct. 2022, doi: 10.18178/ijmerr.11.10.745-754.
[212] Iszmir Nazmi Ismail *et al.*, “Development of In-pipe Inspection Robot: a Review,” in *2012 IEEE Conference on Sustainable Utilization and Development in Engineering and Technology (STUDENT)*, Kuala Lumpur, Malaysia, Oct. 2012.
[213] H. Zhang, S. Zhang, S. Liu, X. Zhu, and B. Tang, “Chatter vibration phenomenon of pipeline inspection gauges (PIGs) in natural gas pipeline,” *J Nat Gas Sci Eng*, vol. 7, no. 2, pp. 1129–1140, Nov. 2015, doi: 10.1016/j.jngse.2015.09.054.
[214] A. A. Mazraeh, F. B. Ismail, W. Khaksar, and K. Sahari, “Development of Ultrasonic Crack Detection System on Multi-diameter PIG Robots,” in *Procedia Computer Science*, Elsevier B.V., 2017, pp. 282–288. doi: 10.1016/j.procs.2017.01.223.
[215] C. Liu, Y. Wei, Y. Cao, S. Zhang, and Y. Sun, “Traveling ability of pipeline inspection gauge (PIG) in elbow under different friction coefficients by 3D FEM,” *J Nat Gas Sci Eng*, vol. 75, Mar. 2020, doi: 10.1016/j.jngse.2019.103134.
[216] D. Mishra, K. K. Agrawal, A. Abbas, R. Srivastava, and R. S. Yadav, “Pig [pipe inspection gauge]: An artificial dustman for cross country pipelines,” in *Procedia Computer Science*, Elsevier B.V., 2019, pp. 333–340. doi: 10.1016/j.procs.2019.05.009.
[217] K. Suzumori, T. Miyagawa, M. Kimura, and Y. Hasegawa, “Micro Inspection Robot for 1-in Pipes,” 1999.
[218] S. A. Fjerdingen, P. Liljeb¨ack, and A. A. Transeth, “A snake-like robot for internal inspection of complex pipe structure (PIKo),” in *The 2009 IEEE/RSJ International Conference on Intelligent Robots and Systems*, St. Louis, USA: IEEE, Oct. 2009, pp. 5665–5671.
[219] H. Li, R. Li, J. Zhang, and P. Zhang, “Development of a pipeline inspection robot for the standard oil pipeline of china national petroleum corporation,” *Applied Sciences (Switzerland)*, vol. 10, no. 8, Apr. 2020, doi: 10.3390/APP10082853.
[220] A. Gunatilake, L. Piyathilaka, A. Tran, V. K. Vishwanathan, K. Thiyagarajan, and S. Kodagoda, “Stereo vision combined with laser profiling for mapping of pipeline internal defects,” *IEEE Sens J*, vol. 21, no. 10, pp. 11926–11934, May 2021, doi: 10.1109/JSEN.2020.3040396.
[221] F. Yan, H. Gao, L. Zhang, and Y. Han, “Design and motion analysis of multi-motion mode pipeline robot,” in *Journal of Physics: Conference Series*, IOP Publishing Ltd, Apr. 2022. doi: 10.1088/1742-6596/2246/1/012029.
[222] A. Kakogawa and S. Ma, “Design of a multilink-articulated wheeled inspection robot for winding pipelines: AIRo-II,” in *2016 IEEE/RSJ International Conference on Intelligent Robots and Systems (IROS)*, Daejeon, Korea (South), 2016, pp. 2115–2121. doi: 10.1109/IROS.2016.7759332.
[223] P. Debenest, M. Guarnieri, and S. Hirose, “PipeTron series - Robots for pipe inspection,” in *roceedings of the 2014 3rd International Conference on Applied Robotics for the Power Industry*, Foz do Iguacu, Brazil, 2014, pp. 1–6.
[224] P. Li, M. Tang, C. Lyu, M. Fang, X. Duan, and Y. Liu, “Design and analysis of a novel active screw-drive pipe robot,” *Advances in Mechanical Engineering*, vol. 10, no. 10, Oct. 2018, doi: 10.1177/1687814018801384.
[225] T. Ren, Y. Zhang, Y. Li, Y. Chen, and Q. Liu, “Driving mechanisms, motion, and mechanics of screw drive in-pipe robots: A review,” *Applied Sciences (Switzerland)*, vol. 9, no. 12. MDPI AG, Jun. 01, 2019. doi: 10.3390/app9122514.
[226] T. Nishihara, K. Osuka, and I. Tamura, “Development of a simulation model for inner-gas-pipe inspection robot: SPRING,” in *Proceedings of SICE Annual Conference 2010*, Taipei, Taiwan, 2010, pp. 902–904.
[227] A. Kakogawa and S. Ma, “Mobility of an in-pipe robot with screw drive mechanism inside curved pipes,” in *2010 IEEE International Conference on Robotics and Biomimetics*, Tianjin, China, 2010, pp. 1530–1535.
[228] M. Kurata, T. Takayama, and T. Omata, “Helical Rotation In-Pipe Mobile Robot,” in *Proceedings of the 2010 3rd IEEE RAS & EMBS International Conference on Biomedical Robotics and Biomechatronics*, Tokyo, Japan, 2010, pp. 313–318.
[229] W. Zhao, L. Zhang, and J. Kim, “Design and analysis of independently adjustable large in-pipe robot for long-distance pipeline,” *Applied Sciences (Switzerland)*, vol. 10, no. 10, May 2020, doi: 10.3390/app10103637.
[230] Z. Wu, Y. Wu, S. He, and X. Xiao, “Hierarchical Fuzzy Control Based on Spatial Posture for a Support-tracked Type In-pipe Robot,” *Transactions of the Canadian Society for Mechanical Engineering*, vol. 44, no. 1, pp. 133–147, Mar. 2020, [Online]. Available: https://mc06.manuscriptcentral.com/tcsme-pubs
[231] Y. S. Kwon and B. J. Yi, “Design and motion planning of a two-module collaborative indoor pipeline inspection robot,” *IEEE Transactions on Robotics*, vol. 28, no. 3, pp. 681–696, 2012, doi: 10.1109/TRO.2012.2183049.
[232] A. Sakura *et al.*, “Development of In-Pipe Robot D300: Cornering Mechanism,” in *MATEC Web of Conferences , 87, 02029. The 9th International Unimas Stem Engineering Conference (ENCON 2016) “Innovative Solutions for Engineering and Technology Challenges,”* EDP Sciences, 2017. doi: 10.1051/matecconf/20178702029.
[233] D.-W. Kim, C.-H. Park, H.-K. Kim, and S.-B. Kim, “Force Adjustment of an Active Pipe Inspection Robot,”

2009, p. 3792.
[234] L. Brown, J. Carrasco, S. Watson, and B. Lennox, “Elbow Detection in Pipes for Autonomous Navigation of Inspection Robots,” *Journal of Intelligent and Robotic Systems: Theory and Applications*, vol. 95, no. 2, pp. 527–541, Aug. 2019, doi: 10.1007/s10846-018-0904-7.
[235] H. Jang, T. Y. Kim, Y. C. Lee, Y. H. Song, and H. R. Choi, “Autonomous Navigation of In-Pipe Inspection Robot Using Contact Sensor Modules,” *IEEE/ASME Transactions on Mechatronics*, vol. 27, no. 6, pp. 4665–4674, Dec. 2022, doi: 10.1109/TMECH.2022.3162192.
[236] H. M. Kim, Y. S. Choi, Y. G. Lee, and H. R. Choi, “Novel mechanism for in-pipe robot based on a multiaxial differential gear mechanism,” in *IEEE/ASME Transactions on Mechatronics*, Institute of Electrical and Electronics Engineers Inc., Feb. 2017, pp. 227–235. doi: 10.1109/TMECH.2016.2621978.
[237] G. Feng, W. Li, Z. Li, and Z. He, “Development of a wheeled and wall-pressing type in-pipe robot for water pipelines cleaning and its traveling capability,” *Mechanika*, vol. 26, no. 2, pp. 134–145, Apr. 2020, doi: 10.5755/j01.mech.26.2.18783.
[238] G. H. Jackson-Mills *et al.*, “Non-assembly Walking Mechanism for Robotic In-Pipe Inspection,” in *Lecture Notes in Networks and Systems*, Springer Science and Business Media Deutschland GmbH, 2022, pp. 117–128. doi: 10.1007/978-3-030-86294-7_11.
[239] F. Pfeiffer, T. Rossmann, and K. Loffler, “Control of a tube crawling machine,” in *2000 2nd International Conference. Control of Oscillations and Chaos. Proceedings (Cat. No.00TH8521)*, St.Petersburg, Russia: [Institute of Electrical and Electronics Engineers], 2000, pp. 586–591.
[240] A. Zagler and F. Pfeiffer, “‘MORITZ’ a Pipe Crawler for Tube Junctions,” in *2003 IEEE International Conference on Robotics and Automation (Cat. No.03CH37422)*, Taipei, Taiwan, 2003, pp. 2954–2959.
[241] X. Yu, Y. Chen, M. Z. Q. Chen, and J. Lam, “Development of a novel in-pipe walking robot,” in *2015 IEEE International Conference on Information and Automation*, Lijiang, China, 2015, pp. 364–368.
[242] M. G. Selvamuthu *et al.*, “Development of soft inchworm robot with friction control of feet using double-network gel,” *Advanced Robotics*, vol. 37, no. 6, pp. 407–422, 2023, doi: 10.1080/01691864.2022.2152291.
[243] D. Fang, J. Shang, Z. Luo, P. Lv, and G. Wu, “Development of a novel self-locking mechanism for continuous propulsion inchworm in-pipe robot,” *Advances in Mechanical Engineering*, vol. 10, no. 1, Jan. 2018, doi: 10.1177/1687814017749402.
[244] K. Hayashi *et al.*, “Improvement of pipe holding mechanism and inchworm type flexible pipe inspection robot,” *International Journal of Mechanical Engineering and Robotics Research*, vol. 9, no. 6, pp. 894–899, Jun. 2020, doi: 10.18178/ijmerr.9.6.894-899.
[245] T. Yamamoto, S. Sakama, and A. Kamimura, “Pneumatic Duplex-Chambered Inchworm Mechanism for Narrow Pipes Driven by only Two Air Supply Lines,” *IEEE Robot Autom Lett*, vol. 5, no. 4, pp. 5034–5042, Oct. 2020, doi: 10.1109/LRA.2020.3003859.
[246] J. Qiao, J. Shang, and A. Goldenberg, “Development of inchworm in-pipe robot based on self-locking mechanism,” *IEEE/ASME Transactions on Mechatronics*, vol. 18, no. 2, pp. 799–806, 2013, doi: 10.1109/TMECH.2012.2184294.
[247] M. Russo, E. Gautreau, X. Bonnet, and M. A. Laribi, “Continuum Robots: From Conventional to Customized Performance Indicators,” *Biomimetics*, vol. 8, no. 2:147, 2023, doi: 10.3390/biomimetics.
[248] I. D. Walker, H. Choset, and G. S. Chirikjian, “Snake-like and continuum robots,” in *Springer Handbook of Robotics*, Cham, Switzerland,: Springer, 2016, pp. 481–498.
[249] M. Russo *et al.*, “Continuum Robots: An Overview,” *Advanced Intelligent Systems*, vol. 5, no. 5, May 2023, doi: 10.1002/aisy.202200367.
[250] X. Dong, M. Raffles, S. Cobos-Guzman, D. Axinte, and J. Kell, “A novel continuum robot using twin-Pivot compliant joints: Design, modeling, and validation,” *J Mech Robot*, vol. 8, no. 2, May 2016, doi: 10.1115/1.4031340.
[251] H. B. Gilbert, D. C. Rucker, and R. J. W. Iii, “Concentric Tube Robots: The State of the Art and Future Directions,” in *Robotics Research: The 16th International Symposium ISRR*, Dec. 2013, pp. 253–269.
[252] C. E. Bryson and D. C. Rucker, “Toward Parallel Continuum Manipulators,” in *2014 IEEE International Conference on Robotics & Automation (ICRA)*, Hong Kong, China, May 2014, pp. 778–785.
[253] L. H. Blumenschein, N. S. Usevitch, B. H. Do, E. W. Hawkes, and A. M. Okamura, “Helical actuation on a soft inflated robot body,” in *2018 IEEE International Conference on Soft Robotics (RoboSoft)*, Livorno, Italy, Apr. 2018, pp. 245–252.
[254] V. Falkenhahn, A. Hildebrandt, R. Neumann, and O. Sawodny, “Dynamic Control of the Bionic Handling Assistant,” *IEEE/ASME Transactions on Mechatronics*, vol. 22, no. 1, pp. 6–17, Feb. 2017, doi: 10.1109/TMECH.2016.2605820.
[255] C. Laschi and M. Cianchetti, “Soft robotics: New perspectives for robot bodyware and control,” *Front Bioeng Biotechnol*, vol. 2, no. JAN, 2014, doi: 10.3389/fbioe.2014.00003.
[256] Y. Kim, G. A. Parada, S. Liu, and X. Zhao, “Ferromagnetic soft continuum robots,” 2019. [Online]. Available: https://www.science.org

[257] X. Dong *et al.*, “Continuum Robots Collaborate for Safe Manipulation of High-Temperature Flame to Enable Repairs in Challenging Environments,” *IEEE/ASME Transactions on Mechatronics*, vol. 27, no. 5, pp. 4217–4220, Oct. 2022, doi: 10.1109/TMECH.2021.3138222.
[258] M. Wooten, C. Frazelle, I. D. Walker, A. Kapadia, and J. H. Lee, “Exploration and Inspection with Vine-Inspired Continuum Robots,” in *2018 IEEE International Conference on Robotics and Automation (ICRA)*, Brisbane, Australia, May 2018, pp. 5526–5533.
[259] N. MA, “Design and modelling of a continuum robot with soft stiffness-adjustable elements for confined environments,” *TechRxiv.* , Mar. 2022, doi: 10.36227/techrxiv.19345547.v1.
[260] J. Burgner-Kahrs, D. C. Rucker, and H. Choset, “Continuum Robots for Medical Applications: A Survey,” *IEEE Transactions on Robotics*, vol. 31, no. 6. Institute of Electrical and Electronics Engineers Inc., pp. 1261–1280, Dec. 01, 2015. doi: 10.1109/TRO.2015.2489500.
[261] X. Dong *et al.*, “Development of a slender continuum robotic system for on-wing inspection/repair of gas turbine engines,” *Robot Comput Integr Manuf*, vol. 44, pp. 218–229, Apr. 2017, doi: 10.1016/j.rcim.2016.09.004.
[262] “Preprint”.
[263] M. Wang, X. Dong, W. Ba, A. Mohammad, D. Axinte, and A. Norton, “Design, modelling and validation of a novel extra slender continuum robot for in-situ inspection and repair in aeroengine,” *Robot Comput Integr Manuf*, vol. 67, Feb. 2021, doi: 10.1016/j.rcim.2020.102054.
[264] A. Jamoussi, “Robotic NDE: A New Solution for In-line Pipe Inspection,” in *3rd Middle East NDT Conference and Exhibition*, Bahrain, Manama, Nov. 2005. [Online]. Available: www.ndt.net